# Adsorption at Oil/Water Interface: Application in SAGD Operation

By

Maryam Razi

A thesis submitted in partial fulfillment of the requirements for the degree of

Doctor of Philosophy

in

Chemical Engineering

Department of Chemical and Materials Engineering

University of Alberta

# Abstract

Interfacial activity of SAGD PW endogenous surfactants, humic acids (HAs), and their interaction dynamics with naphtha-diluted Alberta oil sand bitumen (AOSB) present in model SAGD produced water has been addressed in the first part of this PhD thesis. Dynamic interfacial tension σ(t) between oil and water phases has been studied using a pendant drop tensiometer in the first part of this PhD thesis and its correlation to the properties of SAGD PW has been further investigated. The effect of AOSB dilution ratios, pH of model SAGD PW and surfactant concentrations on the dynamic interfacial tension (IFT) of naphtha-diluted bitumen/water interface has been monitored. A theoretical model of surfactant adsorption at the interface of naphtha-diluted bitumen/model SAGD produced water has been applied to the experimental curves.

In the next part of this PhD thesis, the oil/water (O/W) interface at nano-scale has been studied using a thin liquid film (TLF) set up. The interface of O/W has been monitored for different aqueous phases of surfactant solutions and ionic liquids. Later, a systematic study of TLF of n-dodecane as an intervening liquid phase in aqueous surfactant solution is performed using a 3D-printed modified Scheludko-cell (MSC). The effect of the ionic strength of the ionic liquid (IL) phase on the current–voltage characteristic curve of the system is monitored. It is found that TLF conductivity increases as the ionic strength of the IL phase increases. Moreover, the transient study of the TLF conductivity showed that the TLF conductivity increases over time until it reaches to a quasi-steady condition. We obtained an induced conductivity for the TLF formed for two cases of SDS as anionic surfactants and KCl as inorganic hydrophilic ions. We later developed a model for the adsorption of the ionic species at the perfect dielectric liquid (PDL)/IL interface in both cases of the anionic surfactants and inorganic hydrophilic ions. In

order to rule out the charge leakage effect within oil phase in the observed increase in the TLF conductivity, the oil film conductivity without the presence of any aqueous phase is measured under the current experimental conditions. The electric field applied to the TLF is also quantified by simultaneously solving the non-linear Poisson-Boltzmann equation for IL phase and Laplace equation for the PDL phase. Either studies rule out the evidence of charge leakage within the oil phase under the current experimental conditions. The validity of the surfactants adsorption at O/W interface is also examined by utilizing the pendant drop tensiometric study of the oil phase in aqueous solution. The adsorption time-scale of surfactants present in IL phase at O/W interface using this method was comparable to the electrical conductivity measurement done by MSC. In the last part of this PhD thesis work, a theoretical model has been developed to study the O/W interface electric potential at different applied voltages to the TLF.

We anticipate that the results of this study will bring about a better understanding of the interfacial film properties leading to the advancement of the design of the next generation SAGD W/O or O/W emulsion separation unit operations and the furtherance of the prediction of the coalescence mechanism in SAGD PW emulsions.

**Keywords**: SAGD, oil/water (O/W) interfacial tension, produced water (PW), separation, nano-tensiometer, thin liquid films (TLFs), modified Scheludko-cell (MSC), O/W interface, TLF conductivity, surfactant adsorption, ionic liquid, amphiphilic ions adsorption, O/W interface electric potential, O/W interface applied electric field

# Preface

This PhD thesis is original work by Maryam Razi. The literature review in this thesis was done by myself. The design and establishment of the experimental setups used throughout this work was done by myself. The concepts examined in Chapter 3 and Chapter 4 of this thesis and the experimental procedures were proposed by myself. The experiments were performed by myself. Data analysis and preparation of the final results were done by myself. In Chapter 3, some of the results has been published in the journal of Energy & Fuels, in which S. Sinha was responsible for the theoretical modeling adjustment of the system. P. R. Waghmare, S. Das and T. Thundat had an advisory role. Parts of the results of Chapter 4 has been published in Colloids and Surfaces A: Physicochemical and Engineering Aspects. H. Nazaripoor has helped in data interpretation. B. Sadri has help with the experimental procedure at the initial stage of the project. M. Sadrzadeh and T. Thundat had an advisory role. The preparation of the manuscripts reflecting the outcome of this PhD research work has been done solely by myself.

Some parts of this research, chapters 2, 3, 4 and 5 of this PhD thesis have been published or presented as:

1. M. Razi, H. Nazaripoor, B. Sadri, M. Sadrzadeh, T. Thundat, ‘’Development of a novel 3D-printed modified Scheludko-cell: Potential application for SAGD produced water de-oiling thin liquid film study”, Colloids and Surfaces A: Physicochemical and Engineering Aspects, October 2018
2. M. Razi, M. Sadrzadeh, T. Thundat, “SAGD produced water Oil/Water separation: A novel modified Sheludko-cell (MSC) for Oil/Water separation study” Poster presentation, 3rd International Conference on Desalination using Membrane Technology, Spain, 2-5 April 2017

3. M. Razi, B. Sadri, M. Sadrzadeh and T. Thundat, "Surfactants on oil/water interface studied by modified Scheludko-cell", The XVIth World Water Congress "Bridging Science and Policy"; is jointly organized by the International Water Resources Association (IWRA), the National Water Commission of Mexico (CONAGUA) and the National Association of Water and Sanitation Utilities (ANEAS), Cancun, Mexico, 29 May-2 June 2017. IWRA World Water Congress Publication.
4. M. Razi, S. Sinha, P. R. Waghmare, S. Das and Thomas Thundat, " Effect of Steam-Assisted Gravity Drainage (SAGD) produced water properties on Oil/Water Transient Interfacial Tension", Energy & Fuels (ACS Publications), American Chemical Society (ACS), DOI 10.1021/acs.energyfuels.6b01686
5. M. Razi, P. R. Waghmare, T. Thundat, "SAGD produced water emulsions interfacial studies" Oral presentation, the Seventh Annual Faculty of Engineering Graduate Research Symposium (FEGRS 2016), June 22-23, 2016 at the University of Alberta, Edmonton, Alberta, Canada.
6. M. Razi, P. R. Waghmare, T. Thundat, "Interfacial phenomena in oil sands industry: Effect of Steam-Assisted Gravity Drainage (SAGD) produced water properties on diluted bitumen/water transient interfacial tension " 2016, 90th Colloid and Surface Science Symposium (CSSS), ACS (American Chemical Society), Harvard university, Abstract accepted, held in Cambridge, MA, June 5-8, 2016.
7. M. Razi, Faheem Khan, Thomas Thundat, "A feasibility study on the application of microfluidic apparatus for the SAGD produced water treatment"; FEGSR 2014 Conference, University of Alberta, Edmonton, Alberta, June 19th, 2014

# Dedication

I would like to dedicate this PhD thesis to my lovely and supportive parents, Masoumeh and Yadollah, who offered their endless guidance and support throughout the period of this work. Also, I would like to dedicate this work to all the female researchers and scientists all over the globe whose everyday vision and dedication to knowledge and their leadership can change the way society perceives women in science and their even smallest attempt is appreciated and will be everlasting. I felt God's presence everyday along this amazing PhD journey. I thankful and extremely lucky to have this amazing opportunity in my life.

# Acknowledgements

This work was supported by Canada Excellence Research Chairs (CERC) program.

I would like to offer my sincerest gratitude to Prof. Thomas Thundat who supported me and my work throughout the period of this work. His continual guidance not has only made me a better researcher and critical thinker but also made me to be an individual thinker and a problem solver. I also would like to appreciate the support from Prof. Sadrzadeh which his guidance and support was essential in completeness and wholeness of the present PhD research work. I also appreciate the support from chemical engineering department at the university of Alberta and scholarship from Westmoreland Coal Company Graduate Scholarship for their help during the completion of this PhD work. I truly appreciate the help and guidance from Prof. Tony Yeung as my committee member for his friendly support. The support and guidance of Prof. Vinay Prasad was paramount during my PhD studies. I also acknowledge the Golden Key international honor society for their recognition during the course of this PhD research work. At the end, I would like to offer my sincerest gratitude to my group members and colleagues at Nano Interfaces and Molecular Engineering (NIME) Group and Advanced Water Research Laboratory (AWRL) and University of Alberta for providing me with their opinions and supports. Discussions with Dr. Hadi Nazaripoor and Dr. Behnam Khorshidi have proven to be very helpful. I really appreciate the help and support of my friends: Babak Vajdi, Ishita Biswas, Amin Karkooti, Farshad Mohammadtabar, Zayed Almansoori, Laleh Shmaei, Debanik Bhattacharjee and Asad Asad; thank you all. Finally, I appreciate the financial support from the following agencies: Natural Sciences and Engineering Research Council of Canada (NSERC), Canada's Oil Sands Innovation Alliance (COSIA), ConocoPhillips Corporation, Suncor Energy Company and Devon Energy Company.

# Table of Contents

1 Introduction ..... 1

1.1 Water demand ..... 2

1.2 Oil Sands ..... 2

1.3 Rheological properties of oil sand bitumen ..... 4

1.4 Overview of SAGD operation ..... 6

1.5 SAGD PW Demulsification (O/W emulsion separation) ..... 8

1.6 Literature Review ..... 9

1.7 Research objectives ..... 15

1.8 Thesis organization ..... 16

1.9 Thesis contributions ..... 17

2 Materials and Methods ..... 19

2.1 SAGD produced water interfacial studies using pendant drop tensiometer; Materials . 20

2.1.1 CHNS elemental analysis of the bitumen sample ..... 21

2.1.2 SAGD produced water interfacial studies using pendant drop tensiometer; Methods 22

2.1.2.1 Measurement of dynamic IFT ..... 26

2.1.2.2 Analysis of dynamic interfacial tension (IFT) ..... 27

2.2 Formation and analysis of thin liquid films (TLFs); Materials ..... 28

2.2.1 Formation of TLFs ..... 30

2.2.2 Formation and analysis of thin liquid films (TLFs); Methods ..... 33

3 Fundamentals of O/W separation at micro-scale: Effect of Steam Assisted Gravity Drainage (SAGD) Produced Water Properties on Oil/Water Transient Interfacial Tension ..... 36

3.1 Introduction ..... 37

3.2 Dynamic interfacial tension (IFT): different measurement techniques and analysis ..... 40
3.2.1 Capillary rise method (CRM) ..... 40
3.2.2 Wilhelmy plate method ..... 41
3.2.3 Stallagmometer method – drop weight method ..... 42
3.2.4 Maximum bubble pressure method (MBPM) ..... 43
3.2.5 Pendant drop tensiometer ..... 43
3.2.6 Oscillating jet method ..... 44
3.3 Interfacial tension measurement and surfactant adsorption analysis at the O/W interface 44
3.4 Results and Discussion ..... 48
3.5 Conclusions ..... 55
4 TLFs: Development of a 3D-printed modified Scheludko-cell (MSC): Potential application for adsorption and thin liquid film study ..... 56
4.1 Abstract ..... 57
4.2 Keywords ..... 57
4.3 Introduction ..... 58
4.4 Results and Discussion ..... 63
4.4.1 Conductivity measurements using resistors model ..... 63
4.4.2 TLF in SDS and KCL solutions ..... 64
4.4.3 TLF conductivity: Time-dependent measurement ..... 70
4.5 Concluding Remarks ..... 73
5 TLFs: O/W interface theoretical modeling in the presence of external applied electric fields; Calculation Basics of O/W interface electric potential and electric fields applied to the film ..... 74
5.1 Abstract ..... 75
5.2 Keywords ..... 75

5.3 Introduction ..... 76
5.4 Flat interface of IL/PDL in MSC under external electric fields ..... 77
5.5 Leaky Dielectric model; Flat interface of IL/LDL in MSC under electric field ..... 86
5.6 Concluding Remarks ..... 87
6 Concluding Remarks and Future Works ..... 89
6.1 Conclusions ..... 90
6.2 Recommendations for Future Works ..... 93

# Complete List of Tables

Table 1-1. Comparison of different industrial water, Oil-Field Produced Water (OFPW), Oil Sands Process-Affected Water (OSPW), SAGD Produced Water (PW), and SAGD boiler blow-down (BBD), the data taken from Thakurta et al. [25] ..... 13

Table 2-1. CHNS analysis of AOSB ..... 21

Table 2-2. Properties of WLS inlet water [34] ..... 23

Table 2-3. Properties of conventionally-treated SAGD-BFW (SAGD-Boiler Feed Water) [34]. 23

Table 5-1. Constants and parameters used in the theoretical modeling of the system ..... 81

# Complete List of Figures

Figure 1.1 : Schematic representation of oil sands composition [10] ..... 4
Figure 1.2. Hypothetical diagram representing the molecular characteristics of the asphaltenes precipitated from bitumen by n-alkane addition [12]. ..... 5
Figure 1.3. Schematic of Steam Assisted Gravity Drainage (SAGD) operation [16] ..... 7
Figure 2.1. (a) Steelink model of the humic acid monomer [35], (b) a portion of proposed "type" structure of humic acid (reproduced from [36], courtesy of Ray von Wandruszka). ..... 25
Figure 2.2. Schematic diagram of the method used for adsorption analysis of endogenous surfactants present in SAGD produced water (SAGD PW). ..... 27
Figure 2.3. Sodium dodecyl sulfate (SDS) chemical structure as the anionic surfactant ..... 29
Figure 2.4. (a) n-dodecane chemical structure as the anionic surfactant, b (i-iii). Computer-aided design (CAD) model and 3D-printed MSC for study of W/O emulsion TLF, (c) Schematic representation of a 3D-printed MSC set up for the study of TLFs of oil phase in surfactant solution (Ionic Liquid phase) ..... 29
Figure 2.5. Current density vs electric potential curve for the system composed of 0.1 wt% SDS in milli-Q water as aqueous phase and n-dodecane as oil phase (TLF phase). The black cubes and blue circles represent before and after the formation of TLF, respectively. The shaded error bands represent the error bars..... 31
Figure 2.6. (a-m) Sequential images of the formation of TLF. The diameter of the hole is 200μm. The last image (m), bottom right, shows the stable oil film formed in the experiment. After the formation of the film (image m), the highest contrast of the image is attainable, which can be distinguished from the no-film case (image a). The aqueous phase in this case is 0.1 wt% SDS in milli-Q water and the oil phase is n-dodecane. ..... 32
Figure 2.7. Electric potential vs current density for 0.1 wt% SDS as IL phase. Top view inset figures for (a) before, (b) film-forming stage and (c) after oil film formation. ..... 33
Figure 2.8. Schematic representation of a 3D-printed MSC set up for the study of TLFs of oil phase in surfactant solution (Ionic Liquid phase) ..... 34
Figure 3.1. Photomicrographs of emulsions which are produced from a SAGD well. (a) O/W emulsion; (b) W/O emulsion in which bitumen is the continuous phase [41]. ..... 40
Figure 3.2. CRM schematic representation [42]. ..... 41

Figure 3.3. Wilhelmy plate method schematic diagram [42]..... 42
Figure 3.4. (a) a schematic of pendant drop hanging from a needle. (b) a dilbit drop image which is captured by CCD camera in the experiments. ..... 46
Figure 3.5. Schematic diagram of the method used for adsorption analysis of endogenous surfactants present in SAGD produced water. ..... 47
Figure 3.6. Variations in Oil/Water dynamic interfacial tension: Effect of different dilution ratios of naphtha-diluted bitumen (dilbit) on Oil/Water dynamic interfacial tension (water in these sets of experiment is milli-Q water and pH of the aqueous solution has been measured as 5.74). ..... 50
Figure 3.7. Comparison of the Oil/Water dynamic interfacial tensions (IFT) obtained from the theoretical model, i.e., eqs. (1-3) (shown by continuous lines) with the experimental results (shown by markers) for two values (20% and 30%) of dilbit weight percentage. Parameters used in the theoretical model are D=3.5×10−10 $m^2s^{-1}$, $\Gamma_\infty$ =4 ×$10^{-6}$ mol $m^{-2}$ , KL=1838 $m^3mol^{-1}$ and r=0.001 m at T=298 K. The bulk concentrations are, $c_b$,30% =7×$10^{-4}$ and $c_b$, 20% =8×$10^{-4}$ mol $m^{-3}$. ... 51
Figure 3.8. IFT versus t for naphtha-diluted bitumen/SAGD synthetic brine at different pH values (7.1, 8.0 and 9.0) of SAGD synthetic brine. ..... 53
Figure 3.9. IFT versus t for naphtha-diluted bitumen/SAGD synthetic brine at increasing basic pH values (9.5 and 10) of SAGD synthetic brine. ..... 54
Figure 4.1. Current density vs. electric potential curve for the system composed of different concentrations of (a) SDS and (b) KCl in milli-Q water as aqueous phase and n-dodecane as oil phase film. (i) Before film formation (BFF) and (ii) after film formation (AFF) ..... 65
Figure 4.2. Current density vs electric potential curve for the system composed of 0.05 wt% KCl in milli-Q water as aqueous phase and n-dodecane as oil phase (TLF phase) which includes different regimes of current-voltage characteristics of the system (AFF condition) ..... 66
Figure 4.3. Nondimensional TLF conductivities, $\boldsymbol{\sigma}1$ and $\boldsymbol{\sigma}2$, vs (a) SDS and (b) KCl concentrations (C, wt%) using resistors-in-series modelling of the TLF. The results are normalized by the TLF base conductivity of deionized water and n-dodecane oil film..... 69
Figure 4.4. Nondimensional TLF conductivity ($\sigma1/\sigma0$) versus time for different surfactant concentrations ..... 72
Figure 5.1. Schematic diagram of PDL and IL interface in IL/PDL/IL system. n represents the outward normal vector which originates from the interface at x=0 towards the PDL. PDL represents the oil phase (film forming medium) and IL represents the surfactant solution ..... 78

Figure 5.2. (a) O/W interface electric potential versus film thickness (film thickness: 0-100 nm), (b) O/W interface electric potential versus film thickness (film thickness: 0-800 nm) in the IL/PDL/IL system. PDL represents the oil phase (film forming medium) and IL represents the surfactant solution. (c) O/W interface electric potential distribution at the IL/PDL interface versus film thickness ..... 82
Figure 5.3. O/W interface electric potential distribution versus film thickness for different surfactant concentrations (film thickness: 0-20 nm)..... 83
Figure 5.4. O/W interface electric potential distribution versus film thickness for different surfactant concentrations (molar concentrations of SDS) (film thickness: 0-100 nm)..... 84
Figure 5.5. Maxwell stress distribution vs film thickness for different surfactant concentrations (molar concentrations of SDS as IL phase) versus film thickness (film thickness: 0-100 nm).... 85

# Chapter One

## 1 Introduction

## 1.1 Water demand

According to the Global Risks Report by World Economic Forum in 2016, water crisis is the foremost global risk to environmental, social and economic development of many countries in the next ten years [1]. Demand for the usage of fresh water has drastically been increased due to the fast-growing world's population, industrialization advancement, growing scarcity of ground and surface water resources and the global climate change [2]. In today's world, more than one-fifth of the world's population has poor access to safe and clean drinking water. This fact happens to be one of the major causes of millions of deaths each year [3,4].

This is due to this fact that there has been an accelerated effort toward the development of novel and sustainable techniques for potable water production utilizing municipal and industrial waste waters reclamation and sea water desalination and other techniques [5]. As an example, Canada's oil sands industry consumes 0.5 to 0.9 barrel of fresh water per barrel of oil produced in SAGD operation [6] and there is an urgent need for novel and environmentally viable solutions for water management and water scarcity reduction.

## 1.2 Oil Sands

Oil sands are a combination of clay, sand, water, and bitumen. Oil sands can be mined and processed to extract the oil-rich bitumen, which is then refined into oil. The bitumen which is present in oil sands cannot be pumped from the ground in its natural state; instead oil sand deposits are mined conventionally, usually using strip mining or open pit techniques, or the oil is extracted unconventionally by underground heating via in situ methods with additional upgrading [7]. Oil sands recovery processes include extraction and separation systems to separate the bitumen from the clay, sand, and water that make up the oil sands. Bitumen also needs

additional upgrading before it can be refined. Due to bitumen high viscosity, it also requires dilution with lighter hydrocarbons to make it easy to transport via pipelines [8].

The raw bitumen, at the extraction plant, is separated from the sand, clay and water and is being prepared for upgrading. The tailings (water, clay, sand and residual bitumen) are pumped to holding ponds where they are treated and prepared for reclamation [8]. Alberta's oil sands deposits are regarded as the second largest reserves of oil in the world, with established reserves estimated at 28.3 billion cubic meters (178 billion barrels). These reservoirs are in the form of oil sands which are mainly consist of 55–80% inorganic materials (primarily quartz), 4–18% bitumen, and 2–15% water. The Athabasca oil sands clay mineralogy has been studied fairly extensively and most studies agree that the major minerals are kaolinite and illite [9]. Typically, Bitumen solids generally refer to the fine solids in bitumen froth, which are smaller than 44μm. According to Kaminsky, primary bitumen froth was enriched in chlorite, kaolinite, iron oxide-hydroxides, zircon, and titanium oxides compared with the other streams. On the other hand, the middling's stream was enriched in all the clay minerals, and especially in illite-smectite. He also experimentally observed that the majority of the titanium and iron in all streams was found in the <45μm size fraction (fines) [9].

Schematic representation of oil sands composition has been shown in Fig.1. 1. [10].

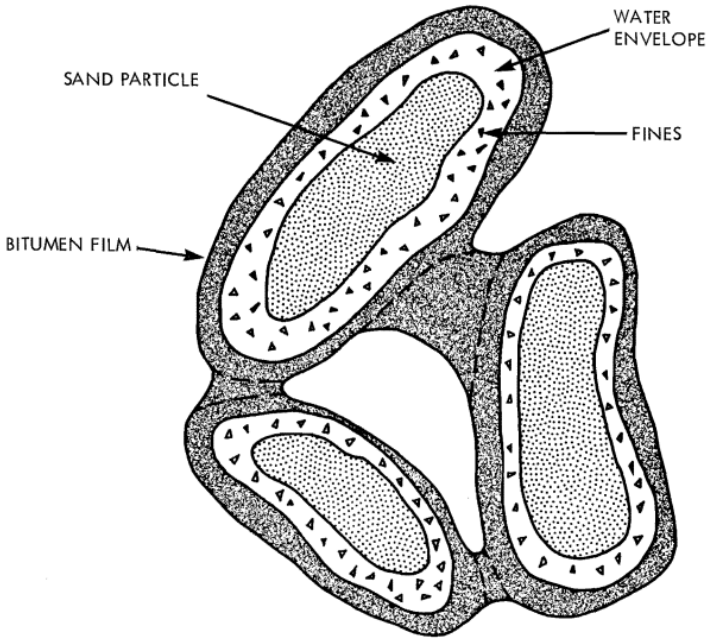


Figure 1.1 : Schematic representation of oil sands composition [10]

## 1.3 Rheological properties of oil sand bitumen

Bitumens are composed of many organic compounds which their detailed molecular structure is not well known yet. Bitumens are generally fractionated on the basis of solubility in a certain solvent, usually pentane. The constituents are generally divided into two categories, soluble “maltenes” and heavier, insoluble “asphaltenes.” In addition to these fractions, there is a light hydrocarbon fraction, some of which is lost if the bitumen is prepared by solvent extraction and drying or if it is degassed [11].

Asphaltenes correspond to the fraction of bitumen that is insoluble in an excess of low-molecular weight alkanes, usually pentane or heptane, but which is soluble in methylbenzene [12]. Recent studies consider that asphaltenes have a molar mass between (0.4 and 1.5) $kg.mol^{-1}$. They usually exhibit a condensed matrix containing aromatic rings associated with heteroatoms, which result in

some polarity, and some alkyl chains that provide a good match with the maltene, a polar fraction. Fig.1. 2. represents the range of heavy compounds precipitated by mixing bitumen with pentane and heptane [12].

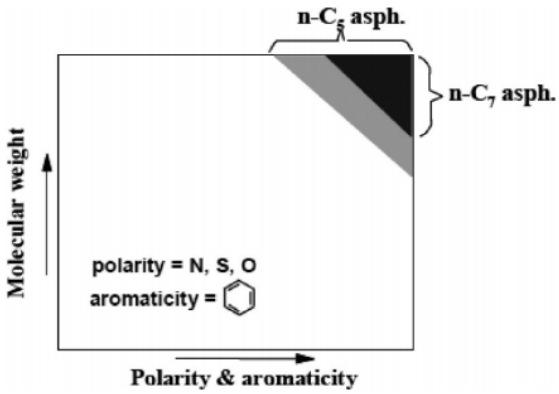


Figure 1.2. Hypothetical diagram representing the molecular characteristics of the asphaltenes precipitated from bitumen by n-alkane addition [12].

Dealy studied the bitumen extracted from oil sand taken from the Athabasca and Cold Lake regions of Alberta by means of a mechanical Spectrometer. He also studied heavy crude produced in the Lloydminster area. He measured the viscosity and first normal stress difference as well as viscoelastic functions. According to Dealy, the bitumens are mildly non-Newtonian in shear and viscoelastic [11]. According to him, it is the high-molecular-weight asphaltene fraction which is responsible for the presence of structure in bitumens and thus causes their non-Newtonian rheological behavior. Although the exact molecular structures of asphaltenes are not well known yet, it is thought to consist of a mixture of polycyclic aromatic and hetero aromatic molecules. The average molecular weight of asphaltenes is about 6000, and the polymeric linkages are based on carbon-carbon bonds or hetero-atom bonds such as the thio-ether bond [11].

## 1.4 Overview of SAGD operation

Recovery of oil sands bitumen utilizing SAGD process is a water intensive process. This technology which is a comparatively new one in the category of EOR invented by Roger Butler in the 1970s, is utilized to produce bitumen and heavy crude oil. This technology which is a kind of steam stimulation process consists of a pair of horizontal wells which are drilled into the oil reservoir. By using high pressure steam, the viscosity of the bitumen froth is decreased and causes the bitumen slurry which is a type of emulsion to drain into the lower wellbore. Afterwards, the slurry will be pumped out to reach the surface facilities [13].

SAGD offers several advantages in comparison with conventional surface mining extraction techniques and alternate thermal recovery methods; it provides significantly greater per well production rates, greater reservoir recoveries, reduced water treating costs, and dramatic reductions in the steam to oil ratio (SOR) [14].

SOR which is a key measure of efficiency for operations using SAGD technology is the amount of steam needed to produce a barrel of oil. According to Cenovus energy, the performance of their SAGD operation at Foster Creek and Christina Lake had a combined SOR of approximately 2.1 in 2012. This number means they used approximately 2.1 barrels of steam to produce one barrel of oil. The water which is converted to steam is primarily brackish water, which is not suitable for animal or human consumption, or agriculture, and is mostly recycled. This number is among the lowest SOR in the industry. A low SOR allows industry to grow and sustain production with comparatively smaller plants and lower energy usage and emissions, all of which results in a smaller environmental footprint [15].

In a typical SAGD process, two horizontal wells running parallel to one another about 5 m apart are employed, as represented in Fig.1. 3., Steam is injected into the upper injection well, causes a

reduction in the viscosity of the oil which drains into the lower production well along with condensed steam and is then pumped to the surface [15].

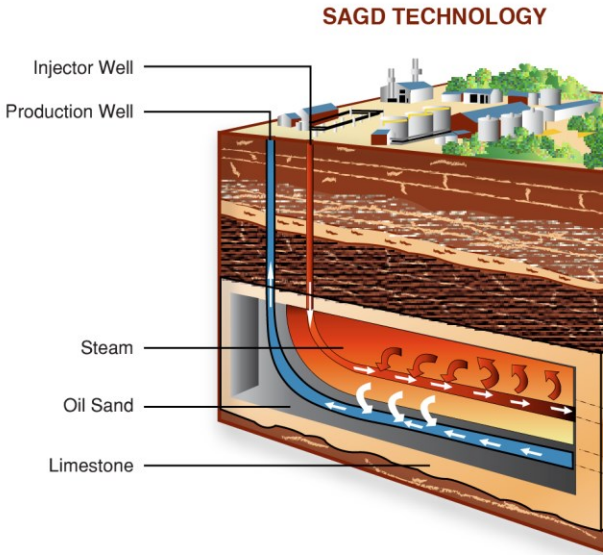


Figure 1.3. Schematic of Steam Assisted Gravity Drainage (SAGD) operation [16]

Due to the continuous injection of the steam, a steam chamber is formed and expanded in the reservoir and owing to this reason, the SAGD process performs better with bitumen and oils with low mobility, as steam channels are less likely to form [17]. SAGD operations are very sensitive to operational and geometrical properties of the reservoir porous medium in which high vertical permeability being inevitably vital to the process' success. Oil reservoir thickness, rock permeability, reservoir heterogeneity and operational conditions such as well separation and length and steam rate are also important [17]. For Canadian oil sands, it has been estimated that 57% of reservoirs are unable to be processed using SAGD operations due to the reservoirs of less than six meters in thickness [17].

SAGD operations consume large volumes of water with between two and ten barrels of water injected as steam per each barrel of oil produced. This water has to be later separated from the

produced oil along with any formation water [17]. It is the energy requirement that is the main limitation on the use of SAGD and other steam-based methods and this problem is enhanced by the creation of significant quantities of greenhouse gases, in particular carbon dioxide, during steam generation [17].

## 1.5 SAGD PW Demulsification (O/W emulsion separation)

Whether it is bitumen films in emulsions occurring in oil sands extractions techniques or bitumen droplets present in oil sands process-affected water (OSPW), the interfacial properties of O/W system play an important role in designing bitumen recovery techniques which promote environmental sustainability.

There are different types of emulsions which can be formed by two liquids. For example, water and oil can form different types of emulsions, water in oil and oil in water. In the former, water is considered the dispersed phase and oil is considered as the continuous phase. They also can form multiple emulsions which can be as the forms of water-in-oil-in-water and oil-in-water-in-oil emulsions. When it comes to emulsions in the oil and gas production and refinery, water in oil (W/O) and oil in water (O/W) emulsions play a significant role in this regard [18].

These kinds of emulsions are very stable due to the presence of highly surface-active endogenous molecular structures which are mainly composed of saturates, asphaltenes, resins, aromatics, solids, clays, endogenous naphthenic acids and waxes. The other components which are present in these emulsions, but they are less surface-active are petroleum-derived compounds and biodegraded materials [19]. The occurrence of these emulsions is not favorable due to the problem they cause in oil transportation or catalytic poisoning owing to their sticky natures. So, there is always a need to find efficient and reliable methods and techniques to resolve them [19].

One of the most common emulsions occurring during oil production process is the emulsion in which water is dispersed in the continuous phase of oil. In SAGD process, however, the extracted produced water is composed of water as the continuous phase, oil droplets which are dispersed in water, clay particles and dissolved organic matters (DOM). This type of emulsion is generally very difficult to treat due to high TDS (Total Dissolved Solids), TSS (Total Suspended Solids) and high oil content, but it is very important to apply reverse-emulsion breaking methods to treat these kinds of emulsions owing to the fact that there are limited numbers of disposal wells. There are also high steam demands of SAGD operations in which the need for reusing the produced water is crucial. Another important aspect of the necessity for treating these emulsions is that effectively treated reverse emulsions in SAGD process causes less unwanted depositions on heat exchangers downstream and thus it reduces the fouling which is a predominant issue in SAGD process [20]. Investigating the factors affecting the stability of these kinds of oil in water emulsions provides the opportunity to understand the underlying interfacial phenomena at a fundamental level and thus provides us the tools for efficient demulsification. There are several factors which affect the stability of these emulsions including the presence of endogenous surfactants, DOM, temperature, pH, salt content of the produced water, shearing, mixing and solid contents [20].

## 1.6 Literature Review

Razi et al. evaluated the effect of a different formulation of demulsifiers on the efficiency of chemical demulsification of heavy crude oil. They monitored the stability of these emulsions experimentally using bottle test method. They also examined the effect of dynamic IFT during emulsion formation using a spinning drop tensiometer. They concluded that the TLF which is formed between water droplets and the oil phase can be analyzed to give a better understanding of

the mechanism of water-in-oil emulsion separation at a molecular level [12]. Petrowski et al. examined the stability of an emulsion using microwave irradiation. They found that after 15 sec of microwave heating of the emulsions, which were visibly destabilized by means of creaming or coalescence, their surface temperature was lower than that of the stable emulsions. They used that methodology to quantitatively examine the stability of stable O/W emulsions. According to Petrowski et al., after microwave heating, the emulsions exhibiting the highest surface temperatures yielded the lowest amount of coalesced oil after centrifugation. They also found that the aqueous phase conductivity which is influenced by the oil concentration plays an important role in destabilization [21]. Song Gao studied the stability of water-in-diluted bitumen emulsion droplets. He used the bitumen which was extracted from the Athabasca region of Alberta. He used the Gibbs adsorption isotherm to monitor the interfacial tension characteristics of the interfacial film. The Langmuir-Blodgett film, Brewster angle microscopy, atomic force microscopy and Fourier transform infrared spectroscopy have been utilized by him to characterize the emulsion. He characterized the interfacial properties of asphaltenic films using a Langmuir trough. The other important aspect of the research done by Song Gao was the difference between IFT isotherms of maltene system and asphaltene system, which has been interpreted by him as the competitive adsorption among the asphaltenes and maltenes. He also quantitatively characterized the "skin formation" at the O/W interface using the crumpling ratio analysis [22]. In the other study by Poteau et al., the effect of pH on stability and dynamic properties of asphaltenes and other amphiphilic molecules at the O/W interface has been examined. According to them, crude oil endogenous surface-active components, asphaltenes and naphthenic acids, compete to reach the O/W interface. They studied the dynamic IFT between water and model oil (toluene). Different amounts of asphaltenes were solubilized in the model oil phase. They concluded that pH affects

the interfacial properties of the asphaltene molecules at the O/W interface drastically. Increase of pH enhances the asphaltene molecules surface activity which is due to the fact that its functional groups become charged. They also investigated the effect of lower-molecular-weight surface-active species present in the heavy oil phase which includes natural naphthenic acids contained in maltenes and found an interaction between asphaltenes and maltenes which causes a molecular rearrangement at the interface. According to this work, at high or low pH, very little coalescence of water droplets was observed. They found that interfacial microscopic properties and emulsion macroscopic behavior are correlated [23].

Angle et al., monitored the effect of the surface activity of simulated tailing ponds natural surfactants on dynamic IFT of toluene-diluted bitumen in simulated tailings water. They compared the effect of adsorption of two surfactants, hexanoic acid (HAA) and 3-cyclopentylpropionic acid (CPPA), with sodium naphthenates (SNs) at the toluene/water interface. They also measured the dynamic IFT for bitumen/water system at trace, saturated and near the critical micelle concentration (CMC) of each surfactant. According to them, each surfactant acts on and interacts with the interface differently, depending upon the concentration and pH of the solution. They concluded that SNs were the most effective ones in reducing IFT versus time at all concentrations. They observed that at low concentrations of surfactants, HAA and CPPA caused a reduction in interfacial activity of the bitumen/water while at benchmark-saturated concentrations they were ineffective in lowering the IFT of bitumen/water in which SNs were synergistically efficient. The benchmark-saturated concentration was representing interfacial saturation, low enough where changes in solution pH are small and it was measured to be equivalent in all three surfactants as 0.0087 mol $kg^{-1}$. In this case, the aqueous phase was composed of 0.0087 mol $kg^{-1}$ surfactant-in-buffer solutions and oil phase was composed of 10 wt % AOSB. According to them, at CMC, SNs

were exceptionally effective in increasing the surface activity of bitumen/water in comparison with HAA and CPPA which did not show much effectiveness in lowering the IFT [24]. Nguyen et al., examined the effect of diluents on interfacial rheology in SAGD emulsions and related that to its emulsion stability. They used the interfacial oscillating drop tensiometry to address the interfacial rheology of SAGD emulsions and related that to SAGD emulsion stability. They concluded that the aged interface of diluted O/W, when is close to its gelation points, behaves the same as a bidimensional gel. They found that the adsorbed amphihpilic molecules such as asphaltenes and resins which rearrange themselves at the interface form a gel-like network which acts as a stabilizing agent for produced emulsions. According to their work, all diluents contain surfactants which can add to the stability of the SAGD emulsions [14].

Thakurta et al., characterized the dissolved organic matter (DOM) in steam assisted gravity drainage (SAGD) boiler blow-down (BBD) water. According to their work, there are high concentrations of dissolved organic matter (DOM) and total dissolved solids (TDS) present in SAGD boiler blow-down (BBD) water. They fractionated the DOM in BBD water into hydrophilic and hydrophobic fractions of base, acid and neutral compounds. They also fractionated the DOM on a size basis using filtration method. Additionally, they utilized fluorescence excitation−emission matrix spectroscopy (EEMs), FTIR and specific UV absorbance (SUVA) to characterize the water samples. They concluded that there are high percentages of hydrophobic acids (39%) and hydrophilic neutrals (28.5%) present in DOM. According to Thakurta et al., the SAGD boiler blow-down water is remarkably concentrated in DOM in comparison with oil sands process-affected water (OSPW). The other conclusion by the aid of fluorescence excitation−emission mapping of the hydrophobic acid fraction was the fact that the fluorophores in DOM molecules are more representative of HAs other than naphthenic acids, which is a

distinctive characteristic of this water stream in SAGD operation from the mining OSPW present in oil sands tailings ponds. They also concluded that due to extremely high amounts of DOM (typically > 2000 mg/L) in BBD and lower solubility of naphthenic acids (NAs) in mining OSPW (at best of the order of 100 mg/L), a large fraction of DOM in SAGD BBW cannot be naphthenic acids [25]. A typical characteristic difference table for several industrial waters has been provided in Table.1-1.

Table 1-1. Comparison of different industrial water, Oil-Field Produced Water (OFPW), Oil Sands Process-Affected Water (OSPW), SAGD Produced Water (PW), and SAGD boiler blow-down (BBD), the data taken from Thakurta et al. [25]

| **Characteristics** | **OFPW** | **OSPW** | **SAGD PW** | **BBD** |
|---|---|---|---|---|
| **pH** | 7.4−8.5 | 8.6−9.12 | 7.11 | 10.6 |
| **Conductivity** | 1400−5000 | 2370−3459 | 1540 | 18000 |
| **TDS** | 700−2000 | 2477 | 1005 | 17000 |
| **TSS** | 90−180 | | | 65 |
| **COD** | 274−431 | 250 | | 4000 |
| **TOC** | 68−140 | 48.3−83 | 232 | 2400 |
| **Alkalinity** | 300−380 | 490−690 | 120 | 2700 |
| **$Ca^{2+}$** | 2−11 | 7.3−47.5 | 2.5 | 4.2 |
| **$Mg^{2+}$** | 0.01−1.3 | 4.2−24 | 0.05−0.15 | 0.68 |
| **iron (total)** | 0.1−0.5 | | 0.05 | 3.3 |
| **$SiO_2$ (soluble)** | 7−14 | | 102 | 90 |

All units in mg/L except conductivity ($\mu$S/cm) and pH

HAs are endogenous surface-active components which are naturally present in SAGD PW. It has been previously proven in the literature that the presence of HA in an alkaline, aqueous solution

causes the surface tension of the solution to decrease. It has been reported in the literature that by increasing the HA concentration in the solution, the surface tension will continue to decrease until the point when HA concentration reaches to its critical micelle CMC. According to Guetzloff et al., the similarities between the effect of surfactants which form micelles and HAs on the surface tension of aqueous solutions suggest that HAs form micelles in aqueous solutions. They examined the possibility of micelle formation for HAs in an alkaline aqueous solution. According to their work, humic acid at extremely high concentration form a micelle in an alkaline aqueous solution (7.4 g humic acid/L) [26].

Terashima et al., examined the effect of pH on the surface activity of HAs. They monitored micelle-like aggregate formation and interfacial adsorption of HAs at the air/water interface. According to their work, the surface tension for an HA solution decreases with increasing concentration of HA. They also concluded that as the pH was decreased, there was a shift in the surface tension versus HA concentration curve towards a lower HA concentration regime. Their results showed that acidic regime significantly facilitates the micelle-like aggregation and the interfacial adsorption of HAs [27].

Mamba et al., utilized humic acid as a model for natural organic matter (NOM), in the removal of odorants from water using cyclodextrin polyurethanes. According to them, NOM present in the produced water, can block the adsorption sites of activated carbon which results in lower geosmin and 2-methylisoborneol (2-MIB) removal and causes deficiencies in water-treatment facilities. They used HA as a model NOM to study the effect of presence of NOM on the removal efficiency of geosmin and 2-MIB as odor chemicals from wastewater. According to them, as odor removal is important for potable-water treatment by water supply companies and municipalities, the role of HAs as model NOM matter in wastewater should be further investigated since HAs accounts for

about 70% of NOM [28]. These natural surfactants have the capability to modify the interfacial properties of O/W emulsions encountered in SAGD operations. These studies signify the need for understanding the interfacial interactions of diluted bitumen with the endogenous surface-active components present in SAGD PW. These interactions are the basis for the bitumen film stability which is a predominant factor in SAGD PW emulsions stability.

Adsorption mechanism of these surface-active compounds at the O/W interface in SAGD operations is not well-understood. There are few publications which address the interaction effects of endogenous surfactants with diluted bitumen in tailing ponds and aquifers, whereas the effects of SAGD PW characteristics on dynamic interfacial properties of diluted bitumen drops affected by natural surfactants have not yet been reported. Therefore, in the first section of this study, the aim is to find the dynamic IFT effects, and in the second section of this work, the interaction dynamics of SDS surfactants as amphiphilic ions and inorganic ions like ($K^+$ or $Cl^-$) at nanoscale using the TLF apparatus that we developed in AWRL (Advanced Water Research Lab), has been studied.

## 1.7 Research objectives

The main goal of the present research is to understand the mechanism of SAGD PW emulsion separation at different scales of micrometer and nanometer. As there is a substantial lack of relevant literature on SAGD PW emulsion separation, we aimed to develop a systematic study to be able to understand the mechanism of surfactant adsorption at O/W interface. To reach this goal, the current research work is based on the following two themes:

(i) Studying the fundamentals of O/W separation at micro-scale. For this purpose, we monitored the effect of SAGD PW properties on O/W transient IFT. As it is generally accepted that the adsorption mechanism of surfactants at the O/W interface causes changes to the IFT of O/W and

alters the phase separation of two phases, in the first part of this thesis, the effect of SAGD PW properties on O/W transient IFT has been monitored.

(ii) In the second part of this PhD thesis, the fundamental structural elements of various dispersed systems widely spread in nature including foam and emulsions, TLFs, has been systematically studied. Developing robust and high-performance experimental techniques to study TLFs is of vital importance. In any emulsion system, rate of coalescence of dispersed phase droplets relates to the drainage of the intervening film. Since the rate of film drainage, thinning and rupture is a kinetic process which depends on the interfacial properties of the medium, studying TLFs is of paramount significance. Therefore, novel experimental techniques are aimed to be developed to impart advanced functionalities to the existing experimental techniques for TLF studies. In this regard, it is expected that the results of this study bring about a better understanding of interfacial film properties which leads to a predictable coalescence mechanism in SAGD PW emulsion separation studies and facilitate the design of next generation SAGD deoiling unit operations.

## 1.8 Thesis organization

The present dissertation is organized as follows: In chapter 1 of the present thesis, SAGD PW treatment methods has briefly been introduced along with the necessity of such a study due to the worldwide water crisis and shortage. Oil sands mineralogy, rheological properties of oil sand bitumen and SAGD PW Demulsification are also covered in this chapter. The research objectives, thesis organization and scope of the work and contributions are also described. In Chapter 2, materials and methods applied for the present work are described. This chapter has been divided into two main parts for the materials and methods employed for the main studies of SAGD PW O/W emulsion separation at micro and nanoscales. In the first part, the materials and methods for the SAGD PW interfacial studies using pendant drop tensiometer has been introduced and in the

second part, the materials and methods for the formation and analysis of TLFs has been reviewed in detail. In Chapter 3, fundamentals of O/W separation at micro-scale has been covered. Effect of SAGD PW properties on O/W transient IFT has been described.

Different measurement techniques and analysis of dynamic IFT and surfactant adsorption analysis at the O/W interface using these techniques is introduced. Chapter 4 is merely focused on the development of a 3D-printed MSC and its potential application for adsorption and TLF study in the context of the present work. In this chapter conductivity measurements using resistors model, TLF in SDS and KCL solutions and time-dependent measurements of TLF conductivity are presented. Chapter 5 includes O/W interface theoretical modeling in the presence of external applied electric fields with the application in the TLF introduced in the previous chapters. This chapter also covers the flat interface of IL/PDL in MSC under external electric fields, different models possible for the ions transfer in the IL phase which includes the leaky dielectric and perfect dielectric models and their application for the TLF under study of the present thesis. Chapter 6 concludes the previous chapters. This chapter also includes recommendations for the future works.

## 1.9 Thesis contributions

In the first part of this PhD thesis, the interfacial activity of SAGD PW endogenous surfactants, HAs, and their interaction dynamics with naphtha-diluted AOSB present in a model SAGD PW is introduced. O/W dynamic IFT has been studied using a pendant drop tensiometer in the first part of this PhD thesis and its correlation to the properties of SAGD PW has been further investigated. It is the first time that such a study for a model SAGD PW is performed as demonstrated in the present PhD thesis. The effect of AOSB dilution ratios, pH of model SAGD PW and surfactant concentrations on the dynamic IFT of naphtha-diluted bitumen/water interface has been reported

for the first time. No study to date has also examined the theoretical modeling of the adsorption of surfactants at the naphtha-diluted bitumen/model SAGD PW interface for the model SAGD PW which has been reported in the present thesis. The development of the 3D-printed MSC with the potential application for adsorption and TLF study is a novel approach for the adsorption of surfactants at nanoscale. Moreover, the electrical detection unit applied for the TLF formation detection and induced conductivity measurements using the developed technique is novel in the sense that methods for investigating such films are very limited and there is not such a detection method available in the literature for the detection of TLF formation and adsorption study using this technique.

# Chapter Two[†]

## 2 Materials and Methods

[†] Part of this chapter has been published or presented as; Energy Fuels, 2016, 30 (12), pp 10714–1072; M. Razi, H. Nazaripoor, B. Sadri, M. Sadrzadeh, T. Thundat, ‘’Development of a novel 3D-printed modified Scheludko-cell: Potential application for SAGD produced water de-oiling thin liquid film study”, Colloids and Surfaces A: Physicochemical and Engineering Aspects, October 2018

## 2.1 SAGD produced water interfacial studies using pendant drop tensiometer; Materials

AOSB provided by Syncrude Canada Ltd. has been used as received. The results of the SARA (Saturates, Aromatics, Resins and Asphaltenes) analysis of the sample are provided in Table 2-1. [29] TAN (total acid number, obtained by ASTM D664 method), sulphur content and ash content of the bitumen sample are known to be 3.5 mg of KOH/g of bitumen, 5.3, and 0.59 wt %, respectively [30,31]. The ASTM D664 method is according to the following procedure for the measurement of TAN; The sample is dissolved in Toluene and isopropanol and water and the resultant solution is titrated with alcoholic potassium hydroxide. Then, a glass electrode and reference electrode are placed in the solution and are connected to the potentiometer/ voltmeter. Afterwards, using a well-defined inflection point, the endpoint of the titration is identified, or when the meter reading corresponds to a pre-defined buffer solution. The details of the technique can be found in the literature [32]. CHNS elemental analysis of the bitumen sample, which has been done using Flash 2000 elemental analyzer (Thermo Fisher), is also provided in Table 2-1. The industrial produced water which has been used in the experiments was from a SAGD produced water treatment plant which was located in the Athabasca oil sands region of Alberta, Canada. As has been widely discussed in the first chapter, SAGD is a thermally enhanced heavy crude oil recovery method which is widely practiced for the extraction of bitumen from oil sands which are present mostly in Alberta, Canada.

Table 2-1. CHNS analysis of AOSB

| Elemental Analysis Results of AOSB sample | | | | |
|---|---|---|---|---|
| | Carbon | Hydrogen | Nitrogen | Sulfur |
| Average | 83.22608795 | 10.16238556 | 0.552172315 | 5.308692646 |
| Error (SD) | 0.586248542 | 0.467123537 | 0.015116601 | 0.13411086 |
| SARA analysis of AOSB sample [29] | | | | |
| Saturates, wt% | | 17.30 | | |
| Aromatics, wt% | | 39.70 | | |
| Resins, wt% | | 25.70 | | |
| Asphaltenes, wt% | | 17.30 | | |
| Properties of AOSB sample | | | | |
| Density, g/cc at 15.6°C | | 1.011 | | |
| API gravity | | 8.46 | | |
| Viscosity at 40°C, cP | | 26900 | | |
| Viscosity at 60 °C, cP | | 3070 | | |

### 2.1.1 CHNS elemental analysis of the bitumen sample

CHNS elemental analysis of the bitumen sample has been done using Flash 2000 elemental analyzer (Thermo Fisher). As the chemical characterization of the organic compounds plays a predominant role in all of the processes of purification, separation and synthesis and also the structural identification of the organic compounds present in bitumen samples plays a significant role in the properties that bitumen samples show once in the process, whether it is in an in-situ operation like SAGD operation or open-pit operations [33]. Organic elemental composition is periodically monitored for the characterization of the bitumen samples. As it is essential to have a precise and accurate technique which is reproducible as well, the Thermo Scientific™ FLASH 2000 CHNS analyzer has been chosen for the elemental analysis of the bitumen sample. This technique which is based on the dynamic combustion of the sample,

determines carbon, nitrogen, hydrogen and sulfur content of the bitumen sample quantitatively in a single run [33].

Another advantage of using this technique is the fact that this system is accurate, reproducible and has a low cost per analysis. To determine the CHNS content of the sample, the elemental analyzer operates on the basis of the dynamic flash combustion of the sample. In this technique, Samples are weighed in a capsule and are introduced into the combustion reactor through autosampler with a proper amount of oxygen. After the combustion happened, the produced gases are carried by a helium flow to a layer which is filled with copper, then swept through a GC column which separates the combustion gases and are detected by a thermal conductivity detector (TCD). The total run time in this section is 10 minutes, then a complete report is generated by the data handling software and the data is shown at the end of the analysis [33].

### 2.1.2 SAGD produced water interfacial studies using pendant drop tensiometer; Methods

Industrial treated Naphtha (SAN # 7764) provided by Syncrude Canada Ltd., has been used as diluent. Naphtha-diluted bitumen (or dilbit) solutions with different dilution ratios were prepared using the following method: Bitumen sample was weighed and added to graduated bottles containing pre-weighed naphtha, followed by agitating the prepared solution using a digital vortex mixer (Fisher Scientific) with a mixing speed of 3000 rpm for the duration of 15 minutes. Different dilution ratios of bitumen ranging from 20 wt% to 60 wt% were eventually prepared using this method. The water used in these experiments had the pH of 5.73 obtained from lab-scale Millipore purification process. pH of the aqueous solutions was measured using a Mettler Toledo pH-meter. SAGD PW samples, WLS (warm lime softening) inlet and BBD (boiler blowdown) water have been obtained from Suncor Energy. The properties of WLS inlet

water and conventionally-treated SAGD-BFW (SAGD-Boiler Feed Water) which has been used in the experiments are provided in Table 2. 2. and Table 2. 3., respectively.

Table 2-2. Properties of WLS inlet water [34]

| Parameter | Unit | Specification |
|---|---|---|
| pH | - | 10.0 |
| TOC | mg/L | 480 |
| TDS | mg/L | 1100 |
| Conductivity | µS/cm | 1750 |
| $Na^+$ | mg/L | 380 |
| $Cl^-$ | mg/L | 205 |
| $Mg^{2+}$ | mg/L | 0.70 |
| $Ca^{2+}$ | mg/L | 1.60 |
| Iron, Total | mg/L | 0.45 |
| $SiO_2$, dissolved | mg/L | 90 |

Table 2-3. Properties of conventionally-treated SAGD-BFW (SAGD-Boiler Feed Water) [34]

| Parameter | Unit | Specification |
|---|---|---|
| Conductivity | mS/cm | 1.8-2.2 |
| pH | - | 9.80-10.5 |
| TDS | mg/L | 1800-2000 |
| TOC | mg/L | 450-550 |
| Silica as $SiO_2$ | mg/L | 30-40 |
| Calcium | mg/L | 0.4-0.5 |
| Iron | mg/L | 0.2-0.3 |

Commercial humic acid (HA, Sigma-Aldrich, technical grade) was used as model natural surfactants present in SAGD produced water. The published chemical structures of these surfactants, the Steelink model of the humic acid monomer and a proposed typical structure of these surfactants are depicted in Figure.2. 1. (a) and Figure.2. 1. (b), respectively. Two sets of

experiments have been conducted; in the first set, dynamic and equilibrium IFT of dilbit samples with different dilution ratios has been studied in pure water. No surfactant was present in the buffer solution for this run. Temperature and pH of the aqueous phase remained constant in all of the experiments. In the second runs of experiments, dynamic IFT of dilbit in SAGD synthetic brine solutions with different pH values has been monitored.

(a)

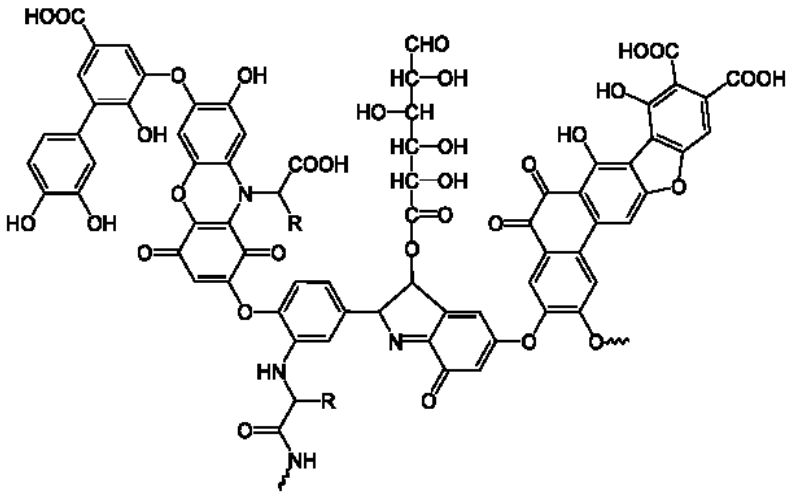


(b)

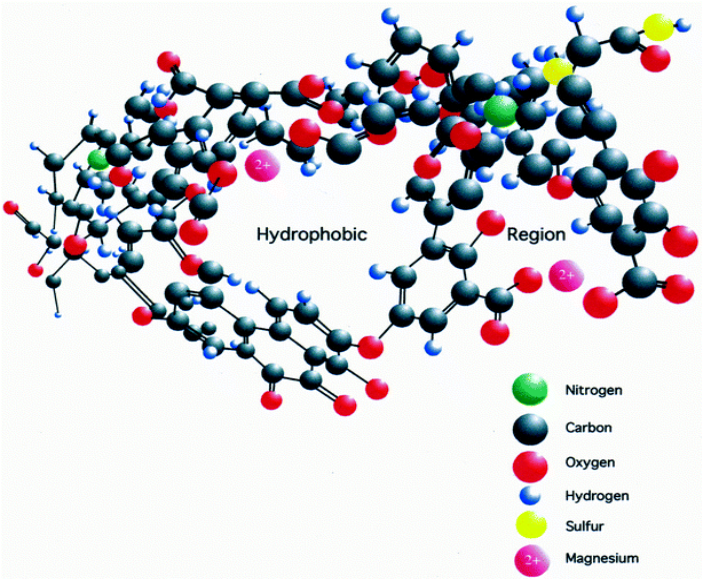


Figure 2.1. (a) Steelink model of the humic acid monomer [35], (b) a portion of proposed "type" structure of humic acid (reproduced from [36], courtesy of Ray von Wandruszka).

#### 2.1.2.1 Measurement of dynamic IFT

Adsorption analysis of endogenous surfactants present in SAGD PW at O/W interface has been carried out using different runs of interfacial tension measurement. The dynamic interfacial tension measurements were performed using a pendant drop tensiometer (KRÜSS GmbH Drop Shape Analyzer, DSA100) which employs time-dependent drop shape analysis (DSA) for the measurement of dynamic interfacial tension. The procedure for all sets of experiments was as follows. Different volumes of dilbit droplets (ranging from 15 μL-40 μL) depending on the dilution ratio, were generated at the tip of an inverted needle (20-gauge diameter) immersed in a cuvette filled with water. The needle was connected to a syringe (500 μL, Hamilton Co., USA). The syringe was mounted in a syringe holder positioned above a cuvette containing 25 mL of the aqueous phase. The needle was immersed in the cuvette aqueous phase by adjusting the syringe position. To obtain a clear visualization on the computer screen, the alignment adjustments were made in such a way that the drops were in line with the tensiometer charge-coupled device (CCD) camera. A schematic diagram of the method is depicted in Figure. 2. 2.

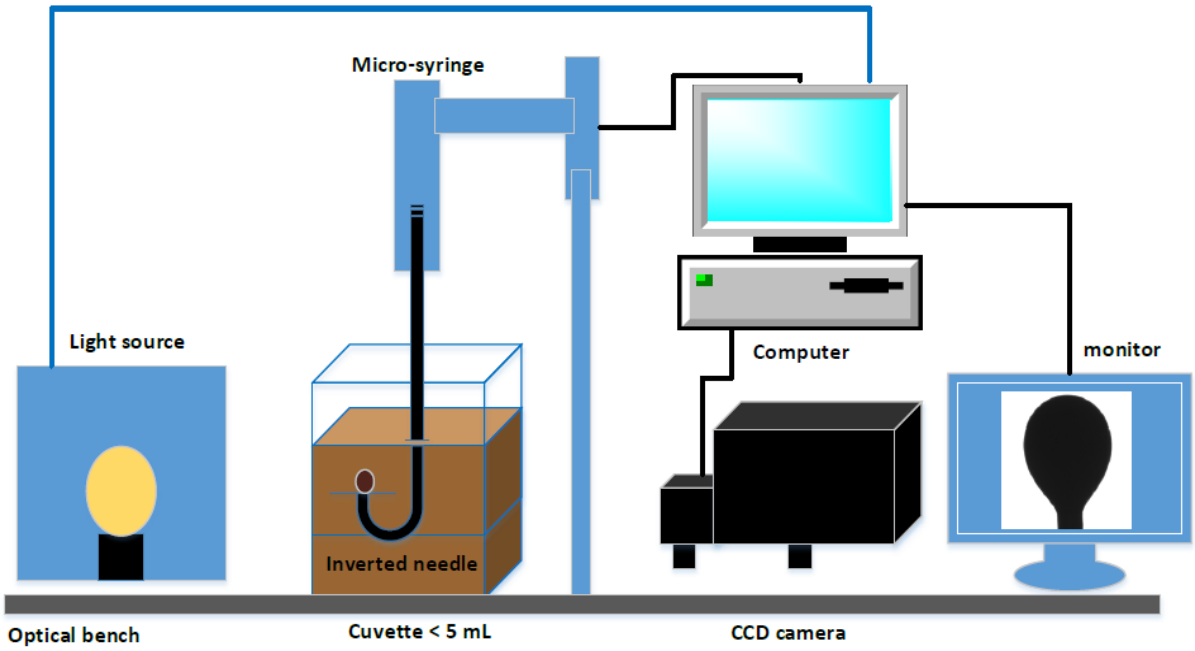


Figure 2.2. Schematic diagram of the method used for adsorption analysis of endogenous surfactants present in SAGD produced water (SAGD PW).

### 2.1.2.2 Analysis of dynamic interfacial tension (IFT)

The dynamic interfacial tension (IFT) between two liquids is determined using a drop shape analysis (DSA) system. The shape of the drop depends on the balance between two counteracting forces of gravity force which tends to elongate the drop and the interfacial tension which minimizes the interface area and tends to sphericalize the drop. The obtained drop profile is then related to the measured interfacial tension by means of Young-Laplace equation. More details about the measurement techniques of interfacial tensiometry are available in the literature; we intentionally include the main equation here for the sake of brevity. Using the following equation [37], the pressure difference (Laplace pressure) across a curved interface is related to the principal radii of curvature, $R_i$ and the interfacial tension $\gamma$;

$$\gamma\left(\frac{1}{R_1}+\frac{1}{R_2}\right)=\Delta P\equiv\Delta P_0-\Delta\rho gz \tag{2.1}$$

in which $R_1$ and $R_2$ are the curvature principal radii; $\Delta P = P_{in} - P_{out}$ is the Laplace pressure across the interface and $\Delta\rho = \rho_d - \rho$ is the density differences of two phases in which in our case is the oil and water phases.

## 2.2 Formation and analysis of thin liquid films (TLFs); Materials

Sodium dodecyl sulfate (SDS, $NaC_{12}H_{25}SO_4$, chromatographically pure, Fisher Scientific, CAS 151-21-3), has been used as surfactant in water phase. SDS chemical structure as the anionic surfactant has been depicted in Figure. 2. 3. Different aqueous surfactant concentrations have been prepared (0.02, 0.05, 0.1, 0.2 wt% of SDS). Water used in these experiments was the water sample (pH=5.73) obtained from lab-scale Millipore purification process. pH of the aqueous solutions was measured using a Mettler Toledo pH-meter. N-dodecane (Fisher Chemical, Laboratory grade, LOT 149004) has been used as oil phase. Different concentrations of KCl solutions have been prepared using the same supporting electrolyte (KCl, Fisher Scientific, Certified ACS). The chemical structure of n-dodecane used as oil phase film and MSC which has been designed using 3D CAD design software and has been 3D-printed using Form2 3D-printer, using GPCL02 resin material, is shown in Figure 2. 4. a and b(i-iii), respectively. Copper wires (Malin Co., .0253 PHOS. Bronze, LOT#25611) have been used as electrodes inserted in the pre-fabricated place for electrodes in the cell.

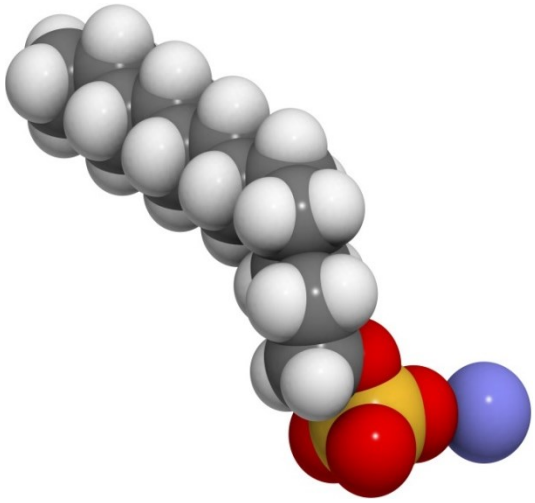

Figure 2.3. Sodium dodecyl sulfate (SDS) chemical structure as the anionic surfactant

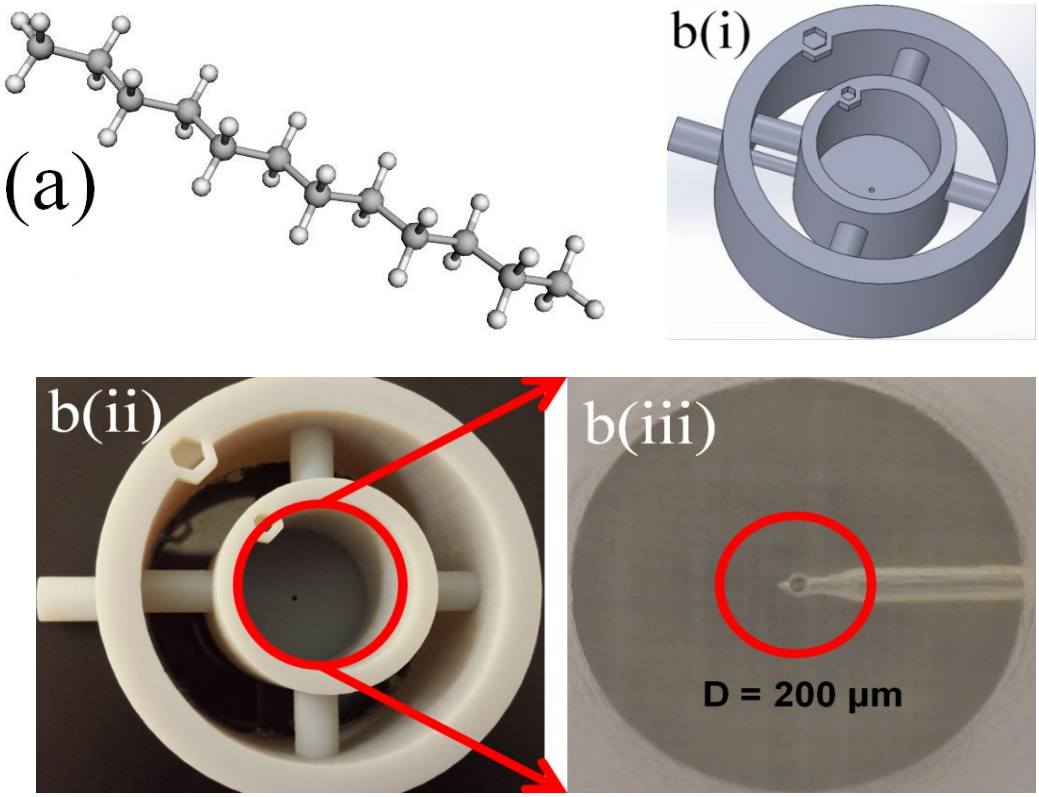


Figure 2.4. (a) n-dodecane chemical structure as the anionic surfactant, b (i-iii). Computer-aided design (CAD) model and 3D-printed MSC for study of W/O emulsion TLF, (c) Schematic

representation of a 3D-printed MSC set up for the study of TLFs of oil phase in surfactant solution (Ionic Liquid phase)

### 2.2.1 Formation of TLFs

**TLF formation**. The current density vs electric potential (*J*-*Ψ*) curve for the system composed of 0.1 wt% SDS in milli-Q water as aqueous phase and n-dodecane as oil phase is compared with no film case and presented in Figure. 2. 5. In both cases, the current density is linearly increasing when the applied voltage increases. We observed that the formation of TLF results in a decrease in the slope (inverse of resistance) of current density vs electric potential curve for the system. The significant change in current density (from $10^{-5}$ to $10^{-6}$ amp/cm$^2$), indicates the TLF formation is detected electrically. We hypothesize that this increase in total resistance of the system is caused by the addition of new resistance in the system, which we considered as the TLF resistance. Sequential images of the formation of TLF, is shown in Figure. 2. 6. The oil phase is pushed through the right-hand side (image (b)) in which the oil film is gradually formed as n-dodecane is slightly pumped to the hole. The last image, bottom right, shows the stable oil film formation and it remained stable in the first 30 minutes of the experiment. After the formation of the film (image m), the highest contrast of the image is attainable, which can be distinguished from the no-film case (image a).

Simultaneous monitoring of TLF formation and J- Ψ curve detection is presented in Figure. 2. 7. The electrical detection of the film formation shows an abrupt change in the current density by the formation of the film. Three distinct regions in the J- Ψ curve are obtained which elucidates before formation of film (image (a)), intermediate stage of TLF formation (image (b)) that is concurrent with abrupt change in J and after film formation (image (c)). The J- Ψ curve shows linear increase in current density with increase in applied voltage for both before

and after TLF formation. However, the difference in slope of these two stages confirms the addition of resistance in the system due to TLF formation. We correlated the detection of the film formation by means of D.C. electric potential to the optical observation of the stages of the film formation in Figure. 2. 6.

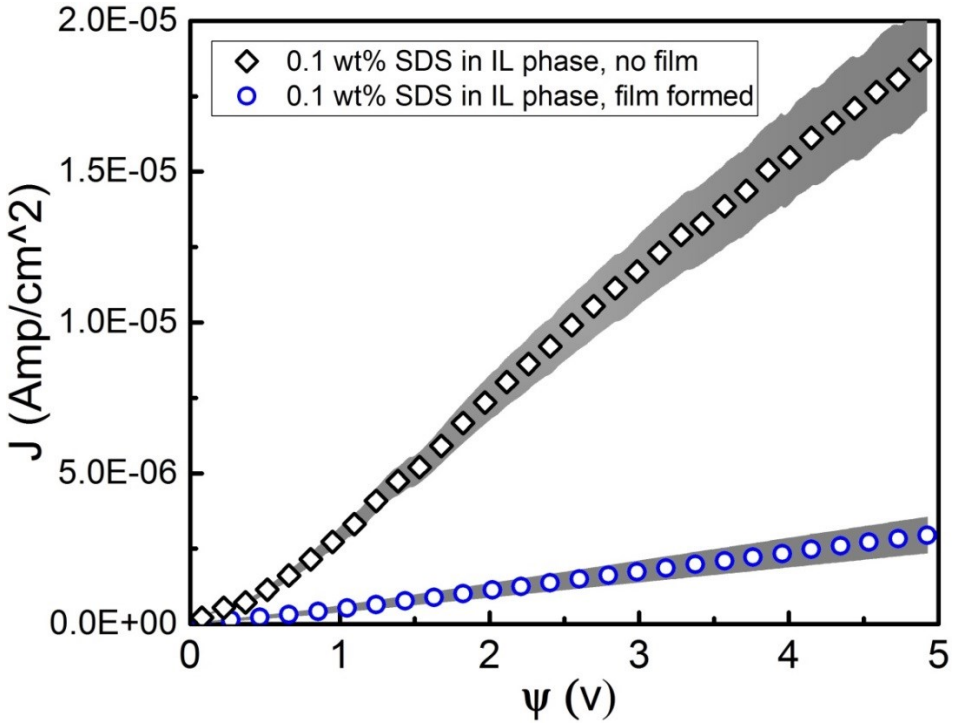


Figure 2.5. Current density vs electric potential curve for the system composed of 0.1 wt% SDS in milli-Q water as aqueous phase and n-dodecane as oil phase (TLF phase). The black cubes and blue circles represent before and after the formation of TLF, respectively. The shaded error bands represent the error bars.

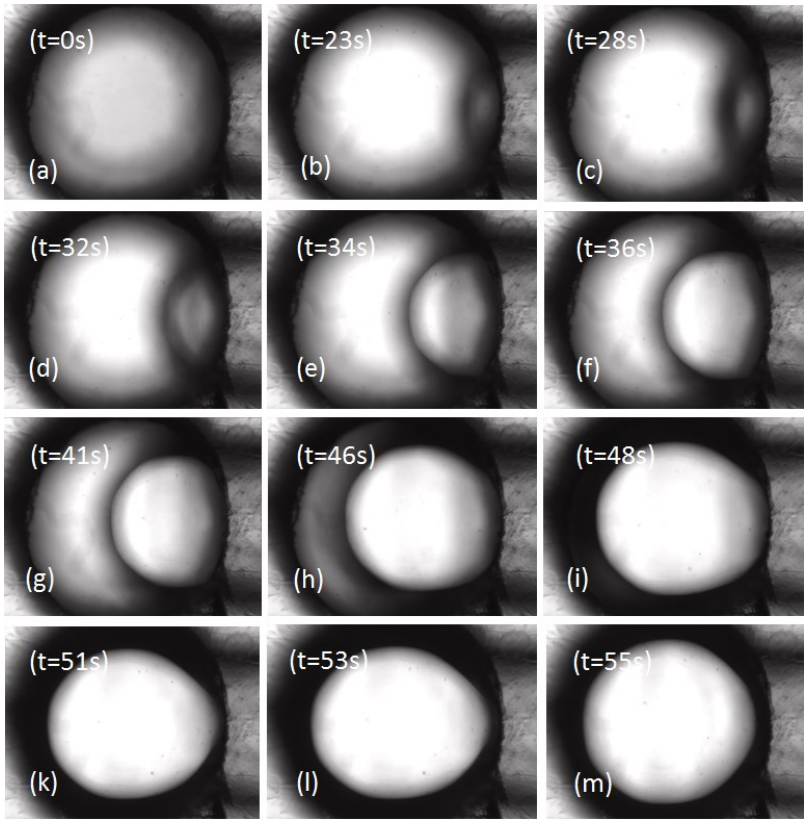


Figure 2.6. (a-m) Sequential images of the formation of TLF. The diameter of the hole is 200µm. The last image (m), bottom right, shows the stable oil film formed in the experiment. After the formation of the film (image m), the highest contrast of the image is attainable, which can be distinguished from the no-film case (image a). The aqueous phase in this case is 0.1 wt% SDS in milli-Q water and the oil phase is n-dodecane.

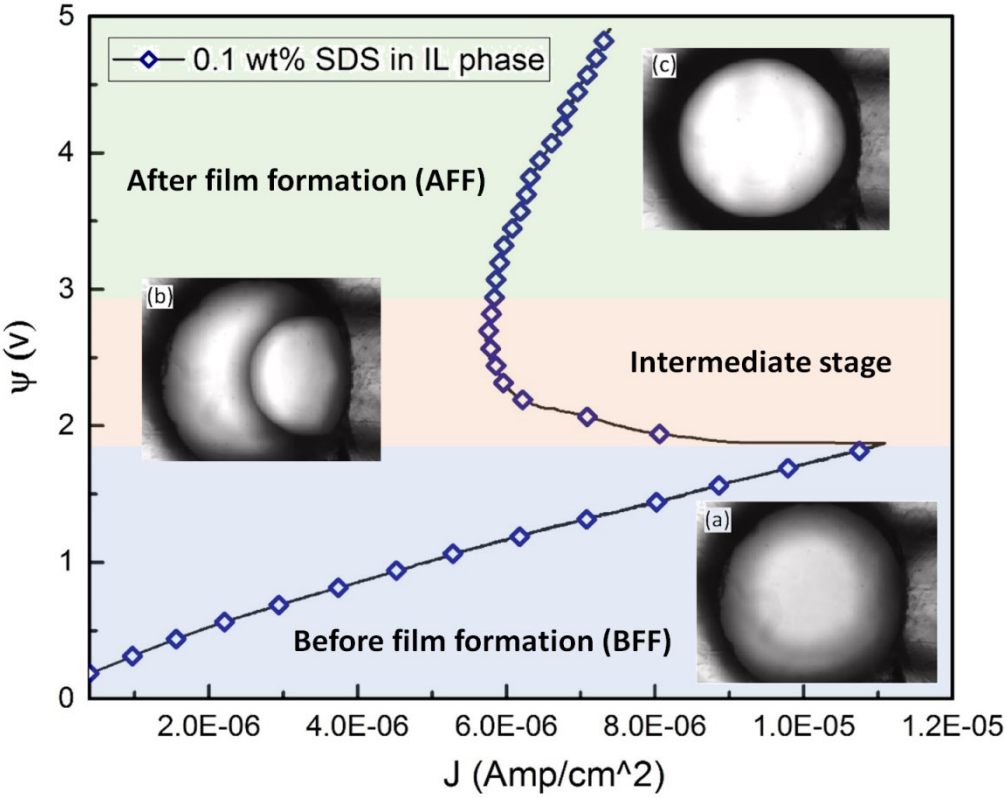


Figure 2.7. Electric potential vs current density for 0.1 wt% SDS as IL phase. Top view inset figures for (a) before, (b) film-forming stage and (c) after oil film formation.

### 2.2.2 Formation and analysis of thin liquid films (TLFs); Methods

The experimental setup used in the present work for electrical detection and visual observation of the formation of TLFs of oil phase is composed of the following parts. Hamilton micro-syringe (10000 µL, Hamilton Co., USA) has been used for the injection of the oil phase through the system. The electrical conductance of the system has been measured using a Princeton Applied Research Potensiostat/Galvanostat model 263A. CorrWare software has been used for data acquisition. The TLF formation was visualized using a ZEISS Axiovert 40 CFL, inverted

microscope. A Hitachi Kokusai Electric CCD camera model KP-M22AN was used for digital imaging of the films formed as shown in Fig. 2. 8. The film thickness has been measured using the known volume of the oil injected from the Hamilton micro syringe and the known film diameter. The MSC is filled with the surfactant solution and the oil phase is injected into the system using the Hamilton micro-syringe and syringe pump. The oil film is formed in the hole with 200 µm diameter as the intervening media between the upper and lower aqueous phases. Electrodes are adjusted in the cell to have the same height in both upper and lower reservoirs.

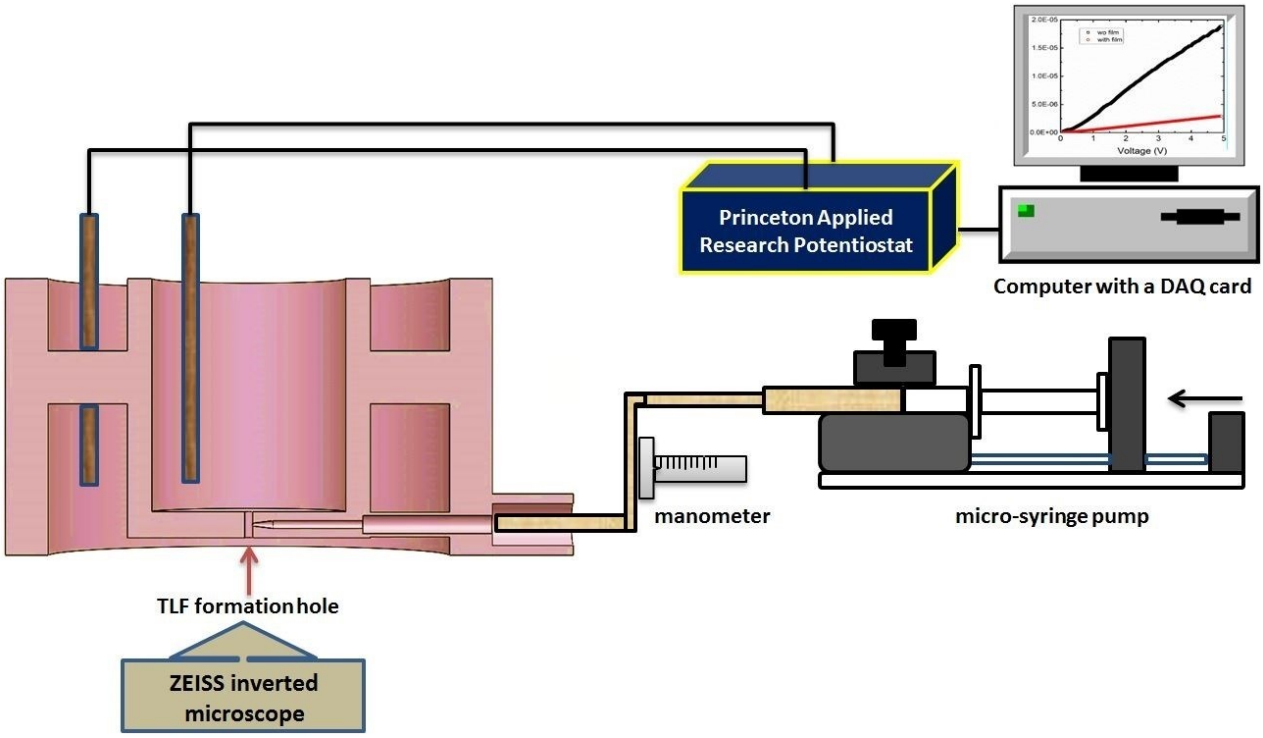


Figure 2.8. Schematic representation of a 3D-printed MSC set up for the study of TLFs of oil phase in surfactant solution (Ionic Liquid phase)

The electrical conductance of the system is monitored using the Princeton Applied Research Potensiostat/Galvanostat in either potentiostatic or potentiodynamic mode. Oil-phase TLF formation is detected using the system resistance measurement. Using MSC depicted in Fig.

2. 4. b (i-iii), and using the experimental set up shown in Fig. 2. 8, we were able to generate the TLFs of oil phase (n-dodecane) in dispersed phase of SDS solution. To prepare the dispersed phase, we prepared different concentrations of SDS in Milli-Q water. SDS CMC value in water (no other additives or salts) at 25 °C, atmospheric pressure, is 8.1-8.4 mM and we ensured to work with SDS concentrations ≤8.1 mM in our experiments (Mukerjee et al., 1970, Aniansson et al., 1976) [38,39].

# Chapter Three[†]

---

# 3 Fundamentals of O/W separation at micro-scale: Effect of Steam Assisted Gravity Drainage (SAGD) Produced Water Properties on Oil/Water Transient Interfacial Tension

[†]Parts of this chapter has been published in Energy Fuels, 2016, 30 (12), pp 10714–1072

## 3.1 Introduction

There are many factors which affect the SAGD operation recovery rates. From these factors one can name the permeability and heterogeneity of the reservoir, which are influencing both non-uniform heat transfer through the formation and propagation of the steam chamber and also phenomena such as viscous coupling and steam fingering which are related to the emulsion formation. These emulsions are composed of the steam (high temperature water) and oil phases. These factors exemplify one of the predominant factors of any system based on gravity drainage which is draining fluid viscosity. From various mathematical treatment methods which are based on the Butler's original SAGD concept for the rate of oil production, q, this is evident that [25]

$$q = L\sqrt{\frac{B\varphi\Delta S_0 kg\alpha h}{m v_s}} \tag{3.1}$$

in which φ is the porosity of the reservoir, $\Delta S_0$ is the difference between initial and residual oil saturation levels, L is the length of the production well, α is the thermal diffusivity of the rock, the height of the steam chamber is denoted by h, k is the effective oil permeability, $v_s$ is the kinematic oil viscosity in reservoir conditions, m is a constant relating to the temperature dependence of viscosity and B is a constant which is related to the configuration of the system. As some parameters of this equation are related to the reservoir characteristics and are not easy to be influenced. As seen from this equation, the drainage or recovery of a SAGD well is proportional to the viscosity so it is evident that to optimize the SAGD process, one need to minimize the oil viscosity. Other factors which are effective in SAGD process recovery enhancement are minimizing the residual oil saturation and increasing the porosity. As these properties can be related to the effectiveness of oil removal from the porous structure of the

reservoir, thus it is necessary to understand the effect of the size of the steam chamber and other reservoir properties for the improved steam chamber propagation which is related to the more efficient displacement of the oil within the reservoir in SAGD operation. Due to the natural tendency of bitumen and heavy oils to form W/O and O/W emulsions due to the presence of surface-active components, possibly also favored due to the oil and water viscosity ratio. In this case, the flow rate restrictions are expected to develop from the W/O emulsions which are formed in situ. These emulsions are more viscous than the bitumen or heavy oil at any given temperature. The viscosity of these emulsions is dependant on the volume fraction of the dispersed water phase (volume fraction, $\phi$) which are available in literature and given by Krieger and Dougherty [40]

$$\eta = \eta_0 \left(1 - \frac{\varphi}{\varphi_{max}}\right)^{-2.5\varphi_{max}} \tag{3.2}$$

As seen in this empirical equation, such as the empirical relationship which is given by the Krieger and Dougherty [40], in the case of W/O emulsions present in SAGD operation, the volume fraction of the disperse phase plays an important role in the viscosity determination of these emulsions. In this equation, $\varphi_{max}$ and $\eta_0$ , are the maximum close-packed phase volume and the (shear) viscosity of the oil phase, respectively. The factor 2.5 is the spheres intrinsic viscosity. According to this equation, in the case of increase in the water phase by 10%, the resultant increase in the viscosity would be 30%. In the case of 30% water incorporation, the resultant viscosity will be increased by 160%. In this case, we assume that

$\varphi_{max}$ is equal to 0.74 which is the maximum packing fraction for monodisperse spherical droplets. As we consider the gravity drainage of a mixture of condensed water, bitumen and steam under high shear, pressure and temperature with a water/bitumen ratio of at least 3 at the periphery of the steam chamber, the bitumen emulsification in water to form (O/W emulsions)

and the presence of water phase in oil (O/W emulsions) are inevitable. The produced fluids are composed of different types or mixtures of W/O, O/W and multiple emulsions of water-in-oil-in-water (W/O/W). O/W emulsions which are formed during SAGD operations are considered to be more favorable due to the ability to lower the viscosity of the fluid and drain more efficiently than the corresponding W/O emulsions. As seen in Figure 3.1 of this chapter, the produced emulsions from the Athabasca oil sands SAGD operations, are mainly O/W and W/O emulsions in which the droplet sizes of water and bitumen phases are less than 20 microns. A major portion of these droplets are less than 5 microns in diameter for either O/W or W/O emulsion types [41]. O/W emulsion images with higher magnification shows that bitumen droplets can contain water droplets which are finely dispersed and form different types of W/O/W emulsions [41]. As it has been suggested in the literature, the predominant emulsion types present in SAGD operation will be influenced by the water/bitumen ratio which is varying over the production lifetime of the SAGD operation. Photomicrographs of emulsions which are produced from a SAGD well are depicted in Fig.3. 1.

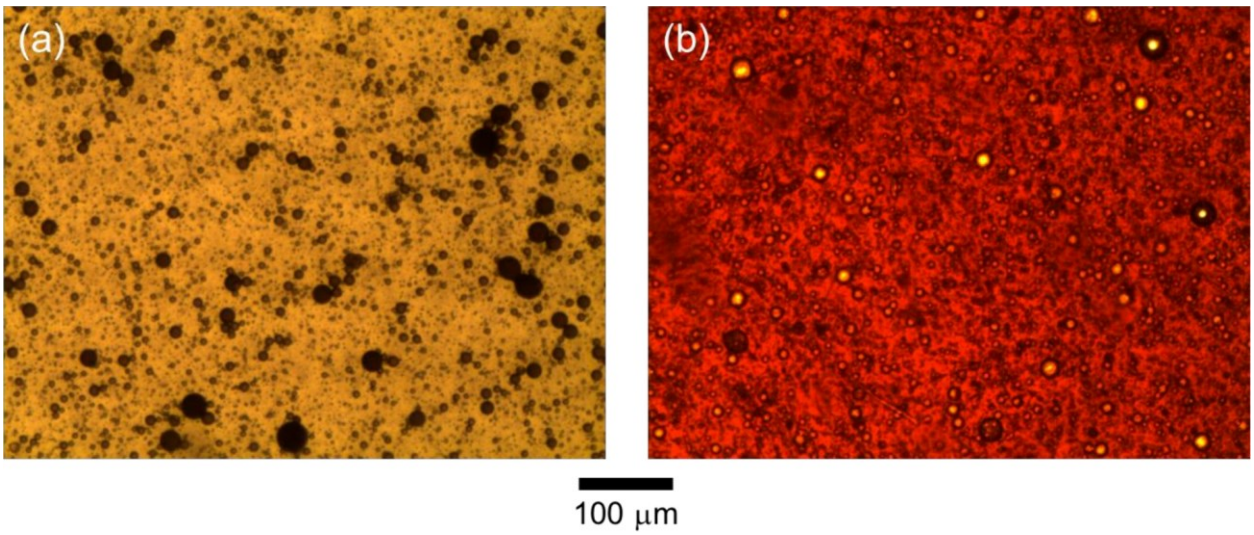


Figure 3.1. Photomicrographs of emulsions which are produced from a SAGD well. (a) O/W emulsion; (b) W/O emulsion in which bitumen is the continuous phase [41].

## 3.2 Dynamic interfacial tension (IFT): different measurement techniques and analysis

### 3.2.1 Capillary rise method (CRM)

Capillary rise method (CRM) is one of the most ancient methods for the measurement of the surface and interfacial tensions. Using this technique, the surface/interfacial tension of two phases of gas/liquid or liquid/liquid is measured using a capillary tube which is usually made of glass. This method is used for determination of the interfacial tension (IFT) in general. For determination of the liquid surface tension, a thin circular capillary is dipped into the liquid in which the gas/liquid surface tension is measured. In the case of higher interaction forces of the liquid with the capillary walls (adhesion) in comparison with the interaction forces between the liquid molecules (cohesion), the liquid can wet the wall of the capillary tube and rise in the capillary. In this case the meniscus is hemi-spherically concave. A schematic of this method is depicted in Figure.3. 2.

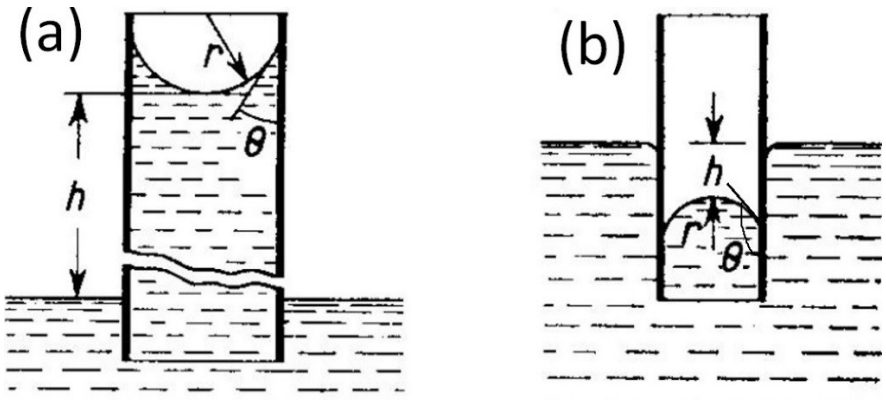


Figure 3.2. CRM schematic representation [42].

### 3.2.2 Wilhelmy plate method

Wilhelmy plate method is another method for the measurement of the equilibrium surface tension (SFT) of a liquid in which the meniscus is formed only on the perimeter of the plate. In this method, the plate does not need to be pulled above the surface to form the meniscus, rather needs to be placed right at the surface of the liquid being measured and kept stationary while the SFT is being measured. In this method, the plate is touched to the surface (Plate of roughened Pt is typically dipped into the liquid and brought back, then held within 1.0 microns of the position of the surface) and then the surface of the liquid is permitted to relax and be in the equilibrium condition with the plate. Afterwards, an acting force of F is exerted on the plate when this vertical plate touches the liquid surface which is measured in this technique. The equation governing this method is the following equation;

$$\sigma = \frac{F}{L.\cos(\theta)} \tag{3.3}$$

a schematic of the method is depicted in Figure.3. 3. [42]. As seen in this figure, the plate perimeter is equal to the wetted length (L) of the plate.

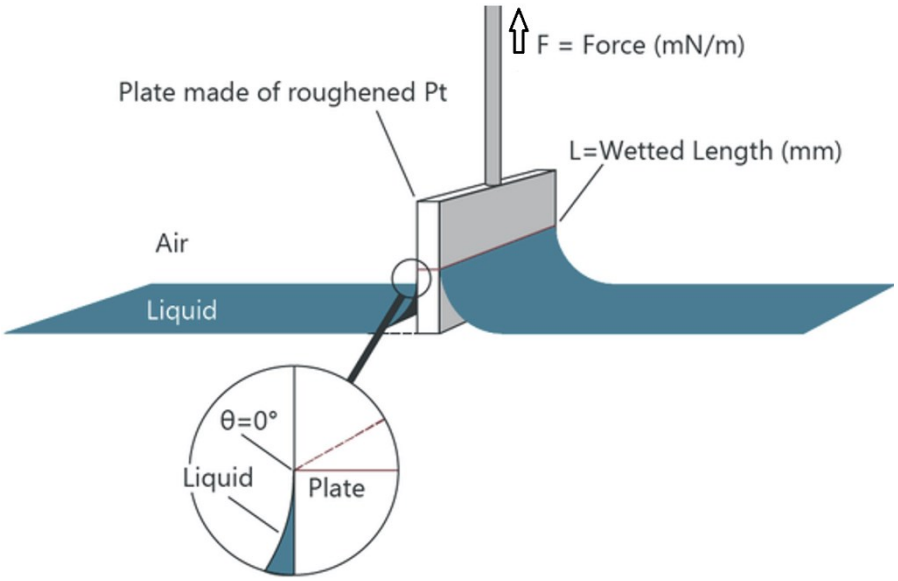


Figure 3.3. Wilhelmy plate method schematic diagram [42]

### 3.2.3 Stallagmometer method – drop weight method

Surface tension or interfacial tension can be developed using the accurate technique of drop weight method. This method has been developed as a standard method for the analysis of surface and interfacial tension. This method also known as drop volume method, is one of the preferred method due to its simplicity of handling, small sample size, easy temperature control, its applicability for either liquid/liquid or liquid/air systems and also good reproducibility of the results it provides. In this method a precision of $\pm$ 0.01 mN/m is achievable under specific conditions [43].

### 3.2.4 Maximum bubble pressure method (MBPM)

Precise and accurate values of the equilibrium surface tension as well as of the dynamic surface tension can be obtained using maximum bubble pressure method [44]. In this method, using gas bubble generation, as each bubble samples a clean and fresh surface with the sensitivity of [mdyn. $Cm^{-1}$], the dynamic surface tension of a liquid is easily measured. The method of dynamic measurement using this technique is a way of measuring the evolution of the surface tension and thus the adsorption dynamics can be obtained using this technique [44].

### 3.2.5 Pendant drop tensiometer

One of the methods for the measurement of the surface and interfacial tension is the use of drop shape analysis (DSA) techniques. The accuracy of using this method for the measurement of surface and interfacial tension depends predominantly on the shape of the droplet. This is due to this fact that generation of stable drop has a huge effect on the accuracy of the measurement using this technique. When the pendant drop shape is close to spherical, this measurement technique is at its lowest accuracy level. In this case it is important to optimize the design of the pendant drop technique and evaluate the accuracy of the measurement using this technique. Generally speaking, the shape of the pendant drop depends on the gravity and surface tension force balances which is mathematically represented by Laplace equation of capillarity. In the case when surface tension and gravitational effect are comparable, the surface tension force can be obtained using the shape analysis of the pendant drop tensiometry technique [45]. This is due to the fact that the surface tension causes the drop to maintain its spherical shape, while the gravity force causes the drop to elongate as a pendant drop. In the case of higher surface tension effects in comparison with the gravitational force, the droplet shape is closer to spherical [45]. Theoretically, the shape of the droplet is evaluated using

image analysis and a CCD camera and it corresponds to a specific surface tension value. A slight change in the surface tension of the droplets causes a paramount change in the surface/interfacial tension of the droplet in the case of droplets which are formed accurately. In the case that droplets are not well-formed (nearly spherical drop shapes), a remarkable surface tension change can only cause a negligible change in the drop shape which causes the surface tension measurement to be less sensitive [45].

### 3.2.6 Oscillating jet method

The method of the oscillating jet is based on the fact that in the case of the flow of a liquid jet out of a thin orifice of an elliptical cross-section, the oscillation of the jet cross-section happens (harmonically) which is due to the action of the surface tension forces. The action of the stationary oscillations continues till the point that they discontinue due to the jet break ups or due to the action of the liquid viscosity. These flows are important in fiber spinning, polymer extrusion and spray formation. The age of the surface is estimated using the measured flow rate and also from the position on the surface [46].

## 3.3 Interfacial tension measurement and surfactant adsorption analysis at the O/W interface

Adsorption analysis of endogenous surfactants present in SAGD PW at O/W interface has been carried out using different runs of interfacial tension measurement. The dynamic interfacial tension measurements were performed using a pendant drop tensiometer (KRÜSS GmbH Drop Shape Analyzer, DSA100) which employs time-dependent drop shape analysis for the measurement of dynamic interfacial tension. A drop shape analysis system can be used to determine the dynamic interfacial tension between two liquids. The pendant drop shape is

determined in particular by surface tension and gravitational forces. These two counteracting forces, the former seeks to minimize the surface area and get the drop into a spherical shape and the latter stretches the drop from its spherical shape, act together to determine the drop shape. The drop shape analysis is based on the Young-Laplace equation. This equation relates the pressure difference (Laplace pressure) across a curved interface to the principal radii of curvature $R_i$ and the interfacial tension $\gamma$ using the following equation [47–51],[52–58].

$$\gamma\left(\frac{1}{R_1}+\frac{1}{R_2}\right)=\Delta P\equiv\Delta P_0-\Delta\rho gz \tag{3.4}$$

where $R_1$ and $R_2$ are the principal radii of curvature; $\Delta P\equiv P_{in}-P_{out}$ is the Laplace pressure across the interface and $\Delta\rho=\rho_d-\rho$ is the density difference of two medium (see Fig. 2). Drop phase density and continuous phase density are denoted by $\rho_d$ and $\rho$, respectively. This pressure gradient can be written in terms of a reference pressure $\Delta P_0$ at $z=0$ and a hydrostatic pressure of $\Delta\rho gz$. To obtain principal radii of curvature for a pendant drop, one can consider drop radius $R_0$ at the apex in which $R_1=R_2=R_0$. So, if one put the reference plane in this point (at the apex), for each point above it holds $R_2=x/sin\,\varphi$ (see Fig. 3. 2). Considering the aforementioned equations one can obtain:

$$\frac{1}{R_1}+\frac{\sin\varphi}{x}=\frac{2}{R}\mp\frac{\Delta\rho gz}{\gamma} \tag{3.5}$$

Eq. (1) can be expressed in terms of the cylindrical coordinates $r$, $z$ and the tangent angle $\varphi$, using axisymmetry, as it is depicted in Fig.3. 4. In this case, the Young–Laplace equation can be obtained as a coupled set of three first-order differential equations with three boundary values in terms of the arc length *s* measured from the drop apex, which is solvable by numerical procedures and results in:

$$\frac{d\varphi}{ds}=-\frac{sin\,\varphi}{x}+\frac{2}{R}\mp\frac{\Delta\rho gz}{\gamma} \tag{3.6a}$$

$$\frac{dx}{ds} = \cos\varphi \tag{3.6b}$$

$$\frac{dz}{ds} = \sin\varphi \tag{3.6c}$$

$$0 = x(s=0) = z(s=0) = \varphi(s=0) \tag{3.6d}$$

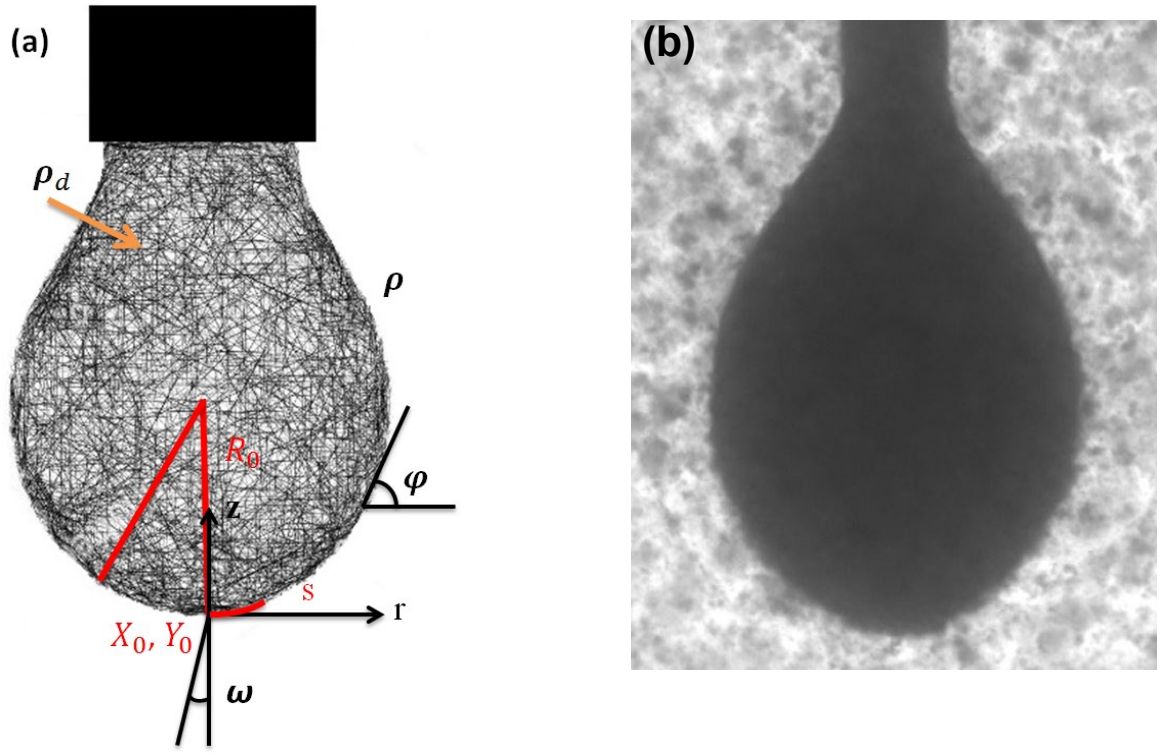


Figure 3.4. (a) a schematic of pendant drop hanging from a needle. (b) a dilbit drop image which is captured by CCD camera in the experiments.

Drop shape is recorded by the camera and the numerical fit of the theoretical drop shape to that finally yields the interfacial tension of two phases. This is the essence of pendant drop technique's analysis procedure. The fitted Young–Laplace solution then can be used further to give additional information such as drop surface area $A_d$ and drop volume $V_d$ which are defined using the following equations:

$$A_d = 2\pi \int r\, ds, \qquad V_d = \pi \int r^2 \sin\varphi\, ds, \tag{3.7}$$

This can be used to extract further interfacial data. For example, by monitoring the drop volume change over time, one can quantify the drop evaporation rate. In our study, the procedure for all sets of experiments was as follows.

Different volumes of dilbit droplets (ranging from 15 µL-40 µL) depending on the dilution ratio, were generated at the tip of an inverted needle (20-gauge diameter) immersed in a cuvette filled with water. The needle was connected to a syringe (500 µL, Hamilton Co., USA). The syringe was mounted in a syringe holder positioned above a cuvette containing 25 mL of the aqueous phase. The needle was immersed in the cuvette aqueous phase by adjusting the syringe position. To obtain a clear visualization on the computer screen, the alignment adjustments were made in such a way that the drops were in line with the tensiometer charge-coupled device (CCD) camera [45–49], [50–56]. A schematic diagram of the method is depicted in Fig.3. 5.

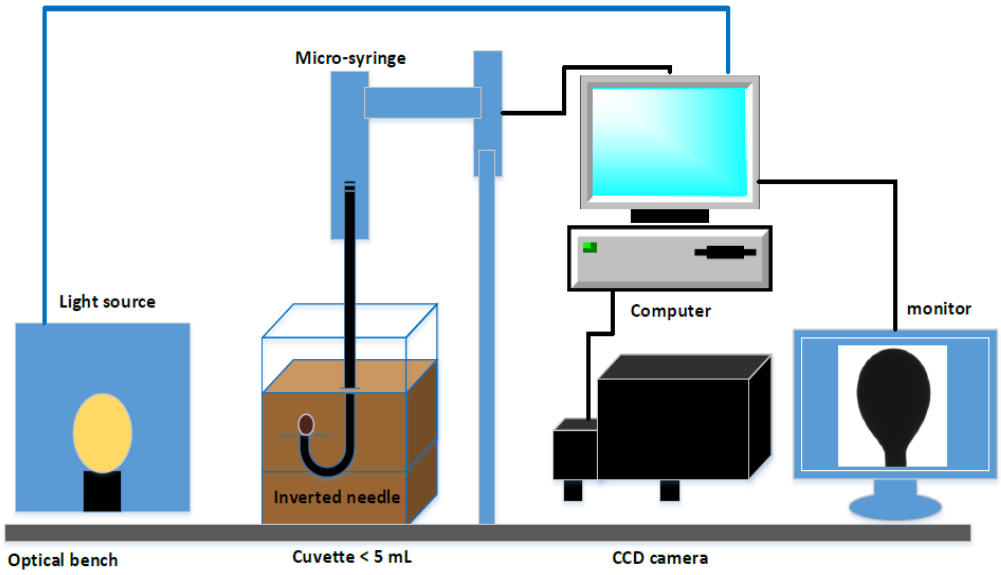


Figure 3.5. Schematic diagram of the method used for adsorption analysis of endogenous surfactants present in SAGD produced water.

Dynamic interfacial tension $\gamma_{i(t)}$ measurements were initiated immediately as the droplet generated to record images at the rate of 1 frame/s for the whole duration of the experiment. The recordings continued until the dilbit drop detached from the needle.

The dilbit drop volume was kept constant for the total aging time of the droplet. Each experiment has been repeated five times to ensure the reproducibility of the interfacial tension measurements. Temperature for all the experiments was kept constant at 23 °C.

## 3.4 Results and Discussion

In Figure 3.6., we show the dynamic interfacial tension (IFT) of dilbit in the water sample without the presence of any additives and surfactants (pH=5.74), for different dilution ratios ranging from 20 to 60 wt%, plotted as a function of time (see Figure 3.6.). We observe that increasing the dilution ratio causes an increase in the IFT at t=0. By definition, x wt% of a dilbit drop implies (100-x) % of bitumen in x% of naphtha solvent. Consequently, smaller wt% of dilbit drop implies a larger amount of bitumen in a smaller amount of the naphtha solvent. Accordingly, such smaller wt% of the dilbit drop will also imply larger concentration of asphaltene within the drop. This can explain smaller value of the IFT at t=0 for smaller wt% of the dilbit drop, given that larger aphaltene concentration in a dilbit drop has been known to cause a larger reduction in the IFT [59]. The central finding expressed in Figure 3.6. is the temporal variation of the IFT for different wt% of the dilbit drop. In fact, for 20 wt% of dilbit drop in pure water, we observe that the IFT curve reaches near-equilibrium values, which is consistent with the finding of Zakar et al. [59]. We hypothesize that this dynamic lowering of the surface tension of the dilbit drop is caused by the gradual adsorption of the asphaltene present within the dilbit drop on the oil-water interface. We employ a combination of the Ward-Tordai surface adsorption model and the Langmuir isotherm

to theoretically explain this time-dependent asphaltene adsorption from the bulk phase (within the dilbit drop) to the oil-water interface and the corresponding time-dependent lowering of the IFT. Following Mysels [60], we can express the Ward-Tordai equation as [61]:

$$\Gamma(t) = 2\sqrt{\frac{D}{\pi}}\left\{c_b\sqrt{t} - \int_0^t c(\tau)\,d\sqrt{t-\tau}\right\} + \frac{D}{r}\left\{c_b t - \int_0^t c(\tau)\,d(t-\tau)\right\}, \tag{3.8}$$

where $D$ is the average diffusivity of asphaltene migrating from the dilbit drop bulk phase to the oil-water interface, $r$ is the drop radius, $\Gamma(t)$ is the surface concentration of asphaltene adsorbed at the oil-water interface, and $c_b$ is the bulk concentration of asphaltene within the oil drop and $c(\tau)$ is the sub-surface asphaltene concentration. Langmuir isotherm provides the equations of state (EOS) relating this sub-surface concentration with the surface concentration as well as the surface concentration with the surface pressure. Surface and sub-surface concentration definitions are according to the terms used by Ward and Tordai [61]. Full derivation from Fick's law to Ward-Tordai equation can be found elsewhere in the literature [61]. The combined model does not account for any reversibility in the surfactant adsorption which is a good fit the adsorption of asphaltenes [62].

Therefore:

$$c = \frac{1}{K_L}\frac{\Gamma}{\Gamma_\infty - \Gamma}, \tag{3.9}$$

$$\Pi = \gamma_0 - \gamma = -nRT\Gamma_\infty \ln\left(1 - \frac{\Gamma}{\Gamma_\infty}\right), \tag{3.10}$$

where $K_L$ is a constant, $\Gamma_\infty$ is the saturation surface excess, R is the universal gas constant, T is the absolute temperature, n is an integer (takes a value of 1 for non-ionic surfactants or 2 for ionic surfactants) which represents the number of species produced by the surfactant in the solution. For

an ionic surfactant that produces two ions in the solutions (e.g., cetyltrimethylammonium bromide or sodium dodecyl sulfate), n=2 and for a nonionic surfactant (e.g., Tween 20) n=1 [63].

$\Pi$ is the surface pressure, and $\gamma_0$ and $\gamma$ are the bulk value (or value at t=0) and the dynamic value of the surface tension of the oil-water interface. In Fig. 3.7., we compare the result from this theoretical model with the experiments for two chosen values of dilbit weight percentage (see the caption of Fig. 3.7. for the parameter values). In this figure, $\Gamma_\infty$ has been obtained from the fitting, $D$ and $K_L$ are obtained from literature [64,65].

We get reasonably acceptable match for the experimental trend using our theoretical predictions. Of course, our theoretical predictions yield similar acceptable match for experimental results corresponding to other dilbit weight percentage; we intentionally do not show them here for the sake of brevity.

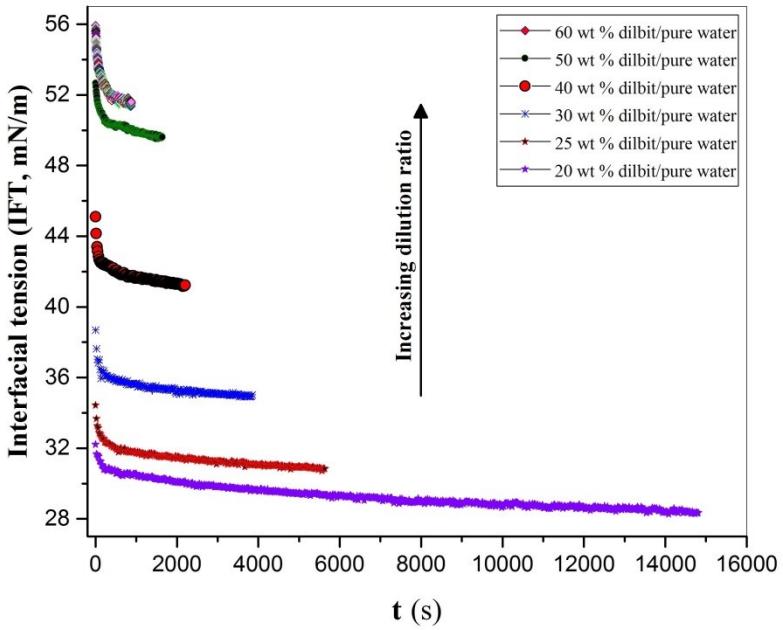


Figure 3.6. Variations in Oil/Water dynamic interfacial tension: Effect of different dilution ratios of naphtha-diluted bitumen (dilbit) on Oil/Water dynamic interfacial tension (water in these sets of experiment is milli-Q water and pH of the aqueous solution has been measured as 5.74).

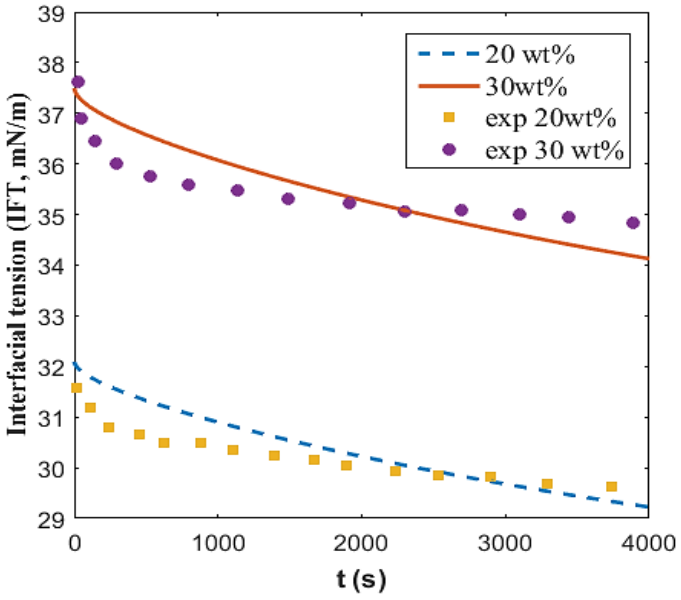


Figure 3.7. Comparison of the Oil/Water dynamic interfacial tensions (IFT) obtained from the theoretical model, i.e., eqs. (1-3) (shown by continuous lines) with the experimental results (shown by markers) for two values (20% and 30%) of dilbit weight percentage. Parameters used in the theoretical model are $D=3.5\times10^{-10}$ $m^2s^{-1}$ [64], $\Gamma_\infty=4\times10^{-6}$ mol $m^{-2}$ , $K_L=1838$ $m^3mol^{-1}$ [65] and r=0.001 m at T=298 K. The bulk concentrations are, $c_b$,30% $=7\times10^{-4}$ and $c_b$, 20% $=8\times10^{-4}$ mol $m^{-3}$ [64,65].

Fig.3. 8 depicts IFT versus t for dilbit/SAGD synthetic brine interface at different pH values of the aqueous phase for 40 wt% dilbit ratios. As seen in this figure, in pH values of 7-9, the dynamic interfacial tension of naphtha-diluted bitumen/SAGD synthetic brine is decreasing. However, towards the basic spectrum of the pH values (pH=9), which is relevant for SAGD operation (pH 9 to 11), the instability of the dilbit drop is observed. The fluctuations in dynamic interfacial tension in this case can be related to the frequent adsorption and desorption of indigenous surfactants present in the oil phase. Observed increase in interfacial activity of surfactants at higher pH values,

responsible for such frequent adsorption-desorption dynamics, is consistent with the work reported by Angle et al. [66] The initial IFT (i.e., IFT value at t=0) is almost the same for all of pH values. The detachment time of dilbit drop from the needle is different for different pH values. As seen in this figure as pH goes toward basic pH values, the detachment time of dilbit drop from the needle reduces from 1800 sec to 100 sec. This can be related to the increase in the rate of reaction of surfactants at the neck of droplet at higher pH values.

In Fig.3. 9, we depict the variation of the IFT of the dilbit-SAGD (synthetic brine) interface for pH values 9.5 and 10. Most remarkably, we find that the IFT increases with time. While at pH=9.5, the dynamic IFT does decrease with time for the first 415 sec (see inset of Fig.3. 9), this temporal enhancement of the IFT is prevalent for the rest of the cases (for larger time for pH=9.5 and for all time for pH=10). It is expected that larger the increase in pH values, greater will be the interfacial activity of the surfactants. The fact that by increasing pH from 7 to 9 there is a reduction in IFT (see Fig.3. 9) is due to the increased saponification of indigenous surfactants present in bitumen (asphaltenes) at basic pH values which causes the enhanced interfacial activity of these surfactants and a lower IFT is expected. It has been previously shown by earlier publications [66,67] that indigenous surfactants present in bitumen reorganized as nanoclusters at these bitumen concentrations. It can be concluded that at higher pH values, transport, rearrangement, and reordering of surfactants occur over larger timescales. It is also concluded that at higher pH values, the complexity of nature of dilbit/SAGD brine interfaces is much higher, paving the way for such highly non-intuitive IFT versus t variation. At higher pH values of SAGD synthetic brine, the consumption of free $OH^-$ ions in SAGD brine is lower and causes a decrease in the $H^+$ ions in solution.

This is the same as the response associated with the saponification of carboxylic groups in higher pH values of SAGD brine solution. The interaction of indigenous surfactants present in bitumen with HAs present in SAGD synthetic brine at dilbit/SAGD brine interface is evident from the reductions in IFTs which is an indicator of elevated interfacial activity of surfactants. These results are in accordance with the work done by Angle et al. [24] in which they concluded that IFTs of heavy crude oils interfaces are less at high pH values in comparison with lower pH values.

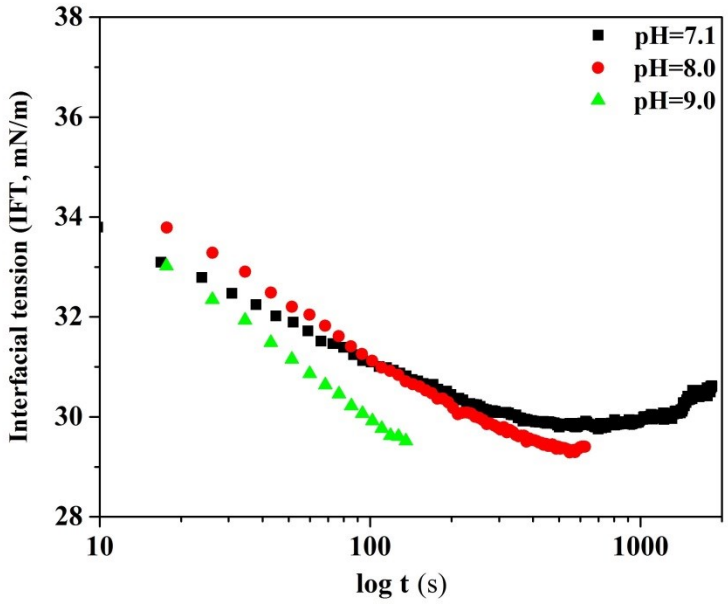


Figure 3.8. IFT versus t for naphtha-diluted bitumen/SAGD synthetic brine at different pH values (7.1, 8.0 and 9.0) of SAGD synthetic brine.

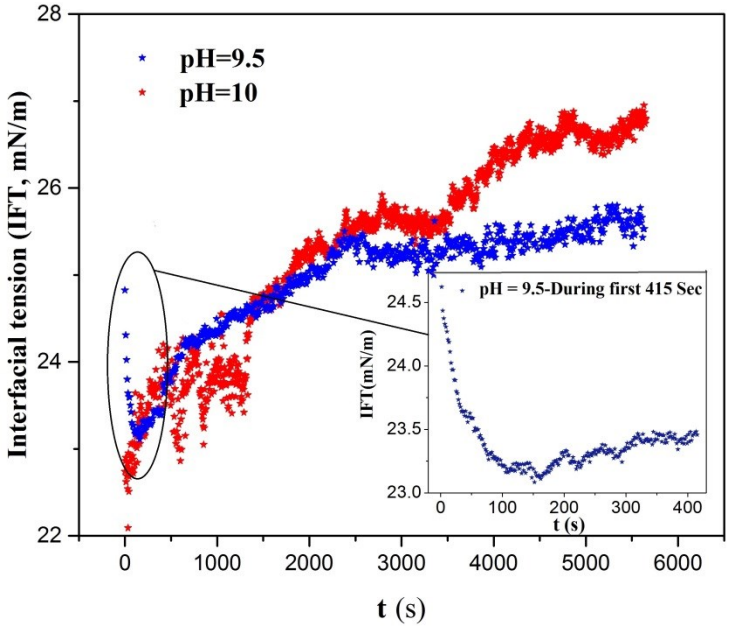


Figure 3.9. IFT versus t for naphtha-diluted bitumen/SAGD synthetic brine at increasing basic pH values (9.5 and 10) of SAGD synthetic brine.

## 3.5 Conclusions

In this study the effect of bitumen dilution ratios and pH of model SAGD produced water on dynamic interfacial tension of naphtha-diluted bitumen/SAGD synthetic brine interface has been monitored. A theory based on the combination of Ward-Tordai model (for surface concentration) and Langmuir isotherm has been applied to explain the experimental trends. Dynamic IFT of naphtha-diluted bitumen in SAGD synthetic brine solutions with different pH values has been monitored and it has been concluded that as pH goes towards basic pH which is the case for SAGD operations (pH range 9-11), there is no exponential reduction in interfacial tension between O/W interface. To the best of our knowledge, it is the first time that such a study has been done for SAGD PW. The results of this study can usher in a better quantification of interfacial film properties, thereby paving the way for a controllable de-emulsification mechanism for emulsions in SAGD PW, which in turn will be vital for designing next generation SAGD de-oiling unit operations.

# Chapter Four[†]

---

# 4 TLFs: Development of a 3D-printed modified Scheludko-cell (MSC): Potential application for adsorption and thin liquid film study

[†]This chapter has been published or presented as;
M. Razi, H. Nazaripoor, B. Sadri, M. Sadrzadeh, T. Thundat, "Development of a novel 3D-printed modified Scheludko-cell: Potential application for SAGD produced water de-oiling

thin liquid film study", Colloids and Surfaces A: Physicochemical and Engineering Aspects, 2018

## 4.1 Abstract

A systematic study on the formation of TLFs of n-dodecane, as an intervening liquid phase in aqueous surfactant solution, was performed using a modified 3D-printed Scheludko-cell (MSC). The formation and stability of TLFs are electrically detected using the current density-voltage (J-Ψ) characteristics of the system, and it is confirmed by in-situ visualization of TLFs. The conductivity of the TLFs is measured using the J-Ψ curve and resistors in a series model of the system. The induced conductivity of the film is measured for different concentrations of potassium chloride (KCl) and sodium dodecyl sulfate (SDS) aqueous solutions. We monitored an increase in TLF conductivity due to the accumulation of inorganic hydrophilic ions like ($K^+$ or $Cl^-$) and adsorption of amphiphilic anion of dodecyl sulfate to the interface. The higher rate of increase in the TLF conductivity in the case of SDS is attributed to the ability of amphiphilic ions to pass through a so-called unscreened potential in the vicinity of oil-aqueous solution interface leading to an unscreenable potential at the boundary of the TLF. The predicted adsorption time-scale of surfactants using the MSC cell in ionic liquid (IL) phase, at O/W interface, is found to be in good agreement with the dynamic interfacial tension test results.

## 4.2 Keywords

Thin liquid film (TLF), modified Scheludko-cell (MSC), oil/water interface (O/W interface), TLF conductivity, surfactant adsorption, ionic liquid, amphiphilic ions adsorption

## 4.3 Introduction

Interfacial properties in oil/water systems play a vital role in designing bitumen recovery techniques, either for oil sands extraction, where bitumen films are generated in emulsions, or water treatment, where bitumen droplets form in oil sands process-affected water (OSPW) [68]. The presence of surfactants is a necessity for emulsion stability, whether the emulsion be formed by water in oil (W/O), oil in water (O/W) or oil in water in oil (O/W/O) multiple emulsions [69]. These emulsions, commonly present in oil and gas production processes and refineries, are very stable, due to the presence of highly surface-active indigenous molecular structures that are mainly composed of asphaltenes and resins and also the presence of aromatics, solids, clays, indigenous naphthenic acids and waxes [41]. However, owing to their sticky characteristics, the occurrence of these emulsions causes problems in oil transportation or catalytic poisoning, so there is always a need to find efficient and reliable methods and techniques to resolve these problematic emulsions [19].

In any emulsion system, the rate at which dispersed phase droplets coalesce is related to the drainage of the intervening film. Since film drainage, thinning, and rupture are dynamic processes which depend on the interfacial properties of the medium, studying TLFs is of paramount significance [70–72]. TLFs are indeed the fundamental structural element of widespread and various, dispersed systems in nature, including foam and emulsions. To date, the research on W/O emulsion films is inadequate and provide limited information on the TLF structure and stability. A common approach is to experimentally monitor these emulsions using the bottle test method and to examine the effect of dynamic interfacial tension (IFT) during emulsion formation employing a spinning drop tensiometer [73]. To provide more insight regarding the thin film properties efforts have been primarily focused on applying sophisticated

micro-interferometric TLF-pressure balance technique (PBT) [74–76]. Application of external disturbances on TLFs is yet another approach to further elucidate the role of TLF hydrodynamics in the coalescence of emulsion systems.

To date, a few studies has gone in to the study of the formation of TLF and its hydrodynamics under external disturbances [77–80]. Several recent investigations studied the electrical behavior of TLFs in aqueous solutions, as well as electric-field-induced adsorption of surfactants at O/W interface. Wu et al., used the second harmonic generation (SHG) imaging method to show that, due to the adsorption of typical ionic surfactants, such as, cetyltrimethylammonium bromide (CTAB), sodium dodecyl sulfate (SDS), and other amphiphilic long-chain molecules, there are notable changes in the SHG intensity at the O/W interface. Accordingly, this change can be correlated to the change of the interfacial potential induced by adsorption of the charged molecules [81]. Bumajdad et al., studied the effect of $D_2O$ content, surfactant concentration, and the composition of the surfactant on the electrical conductivity of $D_2O$/n-heptane micro-emulsions, stabilized by cationic/nonionic surfactant mixtures. In agreement with the theoretical micro-emulsion conductivity models, they showed that the micro-emulsion's conductivity is independent of the concentration of cationic surfactant [82]. In another study, Rennell et al., measured the permittivity, loss factor, and DC conductivity of TLFs of n-heptanol in both purified and non-purified states. They found clear evidence of interfacial polarization effects, which can be fitted to a single mobile charge carrier model [83]. Tchoukov et al., studied TLF formation for the stability of petroleum emulsions using the micro-interferometric method and utilizing the Scheludko-Exerowa cell. They measured the lifetime, thickness and thinning rates of different emulsions of water in diluted bitumen. The different film properties were found to depend on the solvent-to-bitumen (S/B)

ratio and solvent aromaticity. They observed rigid W/O interface and formation of small asphaltene aggregates at critical S/B ratio [84]. One of the advantages of monitoring TLFs using the Scheludko-Exerowa cell was the ability to observe the film directly (using the optical microscopy) and also measuring the disjoining pressure and film thickness as a function of time by TLF-PBT [85]. All these studies provide valuable insight into the hydrodynamics of TLFs under an external electric field. However, there is a significant lack of experimental work on real-time "electrical" detection of the formation of liquid films in aqueous solution. Anklam et al., have conducted dynamic studies on application of DC polarization to W/O emulsions [70]. They used supported decane film as a simulation of polymeric surfactant stabilized W/O emulsions and studied its electrical behavior over time. Panchev et al., developed a method based on the micro-interferometric TLF-PBT to study TLFs in W/O emulsion. They found a strong correlation between film drainage and the bitumen to toluene dilution ratio for the most concentrated solution (toluene-diluted bitumen, 50% bitumen). The critical voltage of film rupture (with the diameter was being maintained at 200 μm) was measured as a function of film thickness under the applied DC voltages of 25 mV/s with the electric field of 125 V/m, [76] and the critical voltage found was in accordance with results of Khristov et al. and Taylor [74,86]. Nguyen et al. developed a new theoretical dual-ellipsoid Laplace model for the electro-orientation of submerged layered micro-particles in order to correct the effect of the non-uniform layer thickness around the ellipsoid in submerged lipid-coated graphitic micro-particles as subjected to an alternating current (AC) electric field. Such a model can generate correct quantitative electric torque predictions. Results showed how the overall electrical properties of the micro-flakes changes due to the lipid shell thickness, conductivity of the solution and the particle shape [87].

Silva et al. spread the poly(3-alkylthiophene)s, regioregular poly(3-butylthiophene), poly(3-hexylthiophene) and poly(3-octylthiophene) polymers at the interface of air and water (A/W) and formed the Langmuir monolayers. Using the surface pressure-area isotherms and polarization-modulation infrared reflection–absorption spectroscopy (PM-IRRAS), they concluded stable films form when it is mixed with Stearic Acids (SAs). These monolayers have been transferred from the liquid interface to solid supports using the Langmuir-Schaeffer (LS) and Langmuir-Blodgett (LB) techniques. The SA monolayers were expanded due to the polymer incorporation, changing the rheological properties of the monolayer using the surface pressure-area isotherms. Benefiting from the PM-IRRAS, they found that at the molecular level, the organization of the film is affected due to the chemical structure of the chosen polymer. These conformational change of the films when transferred to a solid support is dependent on the deposition type (LB or LS) [88].

The electric-field-induced alignment characteristics of high structure carbon black (HSCB) nanoparticles in silicone oil base fluids is studied by Knite et al. [89]. It was shown that the resistivity changes versus time for HSCB/silicone oil fluids at different electric field strengths with different HSCB filler concentrations and different viscosities of the silicone oil. The percolation theory was used to analyze the results. The decrease in electrical resistance versus time is steeper for lower silicone oil viscosities and more substantial electric field strengths. A decrease from 0.6 wt% to to 0.01 wt% for the percolation threshold of HSCB/silicone oil fluid observed when an aligning electric field of 250 V/cm is applied [89].

Er et al., monitored the effects of dissolution modes of the silver (I) ions in the ionic liquids (ILs). They prepared silver nanoparticles (AgNPs) from ILs of silver(I) N-alkyl ethylenediamine complexes and from protic ionic liquids (PILs) of N-alkylethylenediamines.

They concluded that there is a drastic effect of the ethyl-branch of the alkyl chains on the physicochemical properties of the AgILs [90].

Nevertheless, there is no easily-implemented method that allows investigation of electrical properties of TLFs in W/O and O/W emulsions.

The adsorption of surfactants on TLFs is a significant parameter in their stability, and there is, therefore, a substantial need to understand the interfacial interactions of surfactant medium and oil phase at scales representative of the real emulsion films. In this regard, the development of advanced techniques that can detect the interfacial film characteristics at micro and submicron scales, is of vital importance. Although the effect of the adsorption of surfactants on the thermal and electrical conductivity and mechanical properties of solid films has been widely reported [91], to the best of our knowledge the effect of the adsorption of surfactants on the electrical conductivity of TLFs has not yet been reported.

We conducted a systematic study of oil TLF formation at different concentrations of SDS and KCl in deionized water solutions. A 3D-printed modified Scheludko-cell (MSC) was employed due to its simplicity and the feasibility of obtaining real-time optical responses during the experiment. In the first section, we present the formation of TLF of the oil phase (n-dodecane) and its detection using DC electric potential. Then, the effect of surfactants adsorption dynamics on TLF electrical behavior was examined. By considering different layers of electrolyte/oil TLF/electrolyte as ionic liquid (IL)/perfect dielectric (PDL)/IL resistors-in-series, the TLF conductivity is quantified, and the effect of surfactant concentration on the electrical conductivity of TLF is monitored. We anticipate that the results of this study will bring about a better understanding of the interfacial film properties and will advance the study of liquid film rupture. The results can potentially lead to a predictable coalescence mechanism

for W/O and O/W emulsion separation studies whether electrically or using other separation techniques.

## 4.4 Results and Discussion

### 4.4.1 Conductivity measurements using resistors model

To demonstrate the effect of the adsorption of surfactants at O/W interface, verifying experiments were conducted using two different electrolytes with multiple concentrations of electrolyte solutions, and the results were compared with the base case TLF in deionized water. The slope of the current-voltage characteristic curves was calculated for two different conditions of BFF and AFF for each concentration of electrolytes. The resulting net resistance was used to find the TLF conductivity due to the adsorption onto the film of free ions inside the electrolyte solution. TLF formation is also characterized electrically using potentiostatic measurements mode where a constant applied voltage of 1 V is applied to the system and the current density is measured over time. The J-t curve for TLF formation is available in section 1 of appendix A of this dissertation. The *J-t* curve shows a decreasing trend in the current as the film is forming and reaches a constant value after the TLF is completely formed.

Conductivity measurements were performed using resistance-in-series analyses. To evaluate the induced conductivity to the TLF, three layers of IL phase/n-dodecane/IL phase were each treated like a resistor, connected in a series. The electrical behavior of the TLF is modeled in a circuit where all three phases are connected in series to an electric potential source [81,92]. Details about the calculation of the induced conductivity using a resistance-in-series model are available in section 3 of appendix A of this dissertation.

In order to examine the effect of the type of the ions present in IL phase on the TLF formation and the current-voltage characteristic curves of the system, different types of ions, including inorganic ions ($K^+$ and $Cl^-$) and amphiphilic ions (SDS as a typical representative of amphiphilic ions), were studied. The KCl solution has also been studied to see the different mechanisms involved in the cases of the inorganic hydrophilic ions other than the amphiphilic SDS moieties in IL phase. KCl has a crystalline structure, similar to sodium chloride (NaCl), and was chosen for the sake of simplicity of its ionic structure and the fact that it possesses the same mobility of the cationic and anionic parts due to the similar sizes of $K^+$ and $Cl^-$ ions. To investigate the TLF conductivity and the effect of adsorption of ionic moieties on the TLF conductivity, three cases were studied in the present work: (i) TLF in SDS surfactant solution; (ii) TLF in KCl solution; and (iii) TLF in deionized water as a base case.

### 4.4.2 TLF in SDS and KCL solutions

Current density vs. electric potential curves for different concentrations of SDS solution are shown in Figure 4.1.(a). As can be observed, by increasing the surfactant concentration (higher conductivity of aqueous solution) the slope of J-Ψ curve increased for both BFF and AFF. However, the current density values decreased significantly (one order of magnitude) after the formation of the film. This is expected because of the presence of highly resistive oil layer acting as a barrier in the system. To compare the effect of the adsorption and ions accumulation on the measured TLF conductivity, the J-Ψ curves for the TLF formed in KCl solutions (0.02 wt%, 0.05 wt%, 0.1 wt%, 0.2 wt%) were obtained and presented in Figure 4.1.(b). Similar to the SDS surfactant solutions, an increasing trend was observed in the current density vs. the applied potential as KCl concentration increased for both BFF and AFF cases.

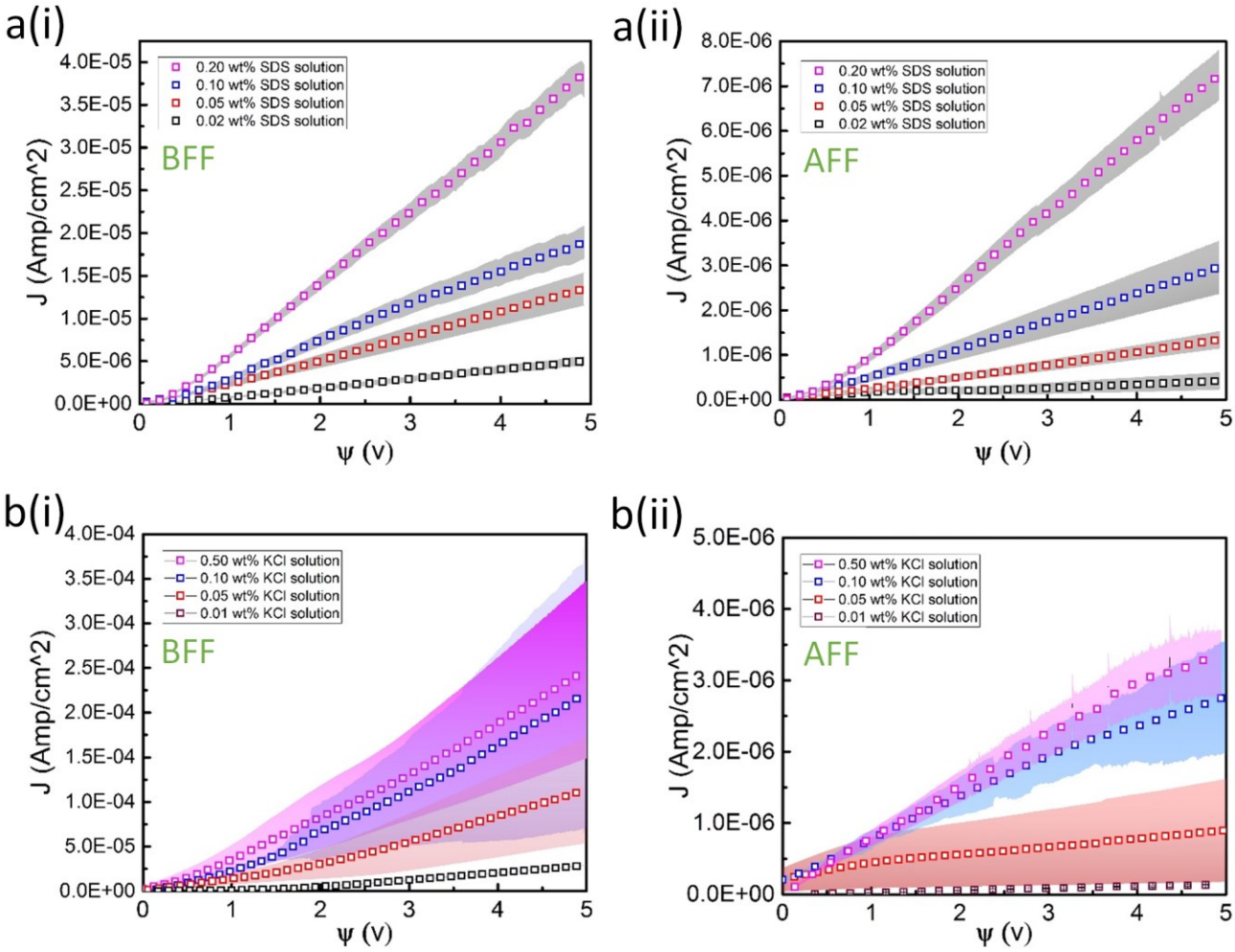


Figure 4.1. Current density vs. electric potential curve for the system composed of different concentrations of (a) SDS and (b) KCl in milli-Q water as aqueous phase and n-dodecane as oil phase film. (i) Before film formation (BFF) and (ii) after film formation (AFF)

Taking a closer look at J-Ψ curves in Fig.4.1., two Ohmic regimes (linear current density vs. electric potential relation) were distinguished. These two regimes are more clearly presented in Fig.4.2. for 0.05 wt% KCl case. Given that, the conductivity of the formed TLF was calculated using two different slopes of the J-Ψ curve, from 0 to 1.5 volts and 1.5 to 5.0 volts, as $\boldsymbol{\sigma}_1$, (S/m) and $\boldsymbol{\sigma}_2$, (S/m), respectively.

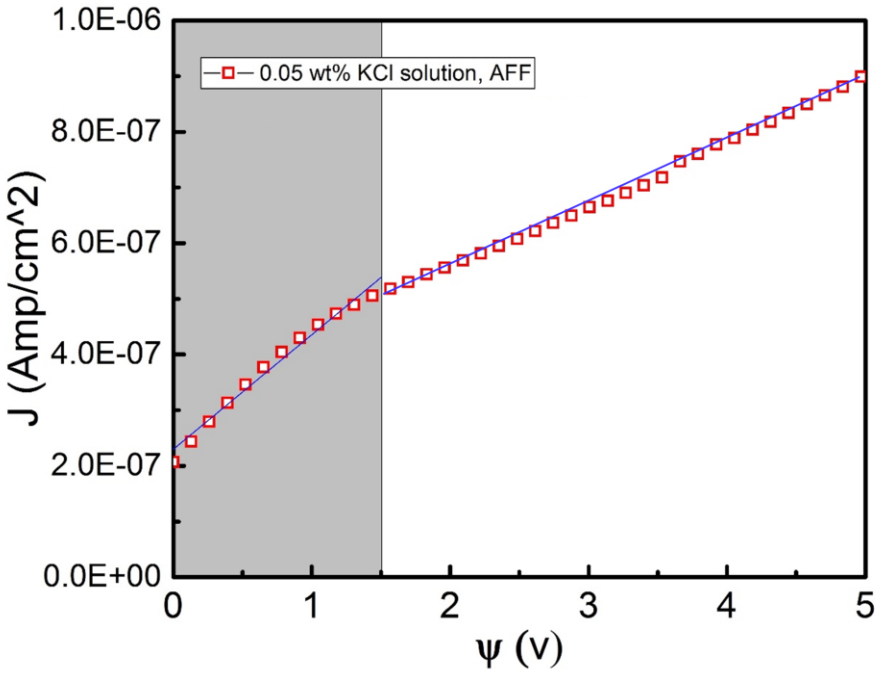


Figure 4.2. Current density vs electric potential curve for the system composed of 0.05 wt% KCl in milli-Q water as aqueous phase and n-dodecane as oil phase (TLF phase) which includes different regimes of current-voltage characteristics of the system (AFF condition)

To explore the role of adsorption/accumulation of ions in the measured TLF conductivity, the conductivity values were normalized with the base case, where there are no additives present in the aqueous phase and its pH was measured to be 7, and the results are presented in Fig 4.3. As can be seen, the TLF conductivity increased with an increase in the concentration of both SDS (KCl) in aqueous solutions, which means higher adsorption/accumulation of ions at the IL/PDL interface. The accumulation of the counterions at the interface causes a reduction in surfactant dissociation and, hence, shifts the HLB to be more lipophilic. As lipophilic surfactants dissolve in the oil phase more readily in this case, transferring the ion (counterion) to the other side of the liquid film which results in higher conductivity of TLF. A quantitative comparison of the normalized conductivity values for two cases showed that the adsorption of SDS to the TLF surface is considerably higher than of KCl ions. This could be explained by the different mechanisms by

which SDS and KCl adsorb onto the TLF interface. The ions with amphiphilic topology adsorb with the hydrophilic polar head solvated in water and the hydrophobic tail mostly dissolved in the oil phase. It has been shown that the adsorption of amphiphilic ions at the oil/water interface creates more interfacial potential than $Cl^-$ [93].

The amphiphilic ions can pass through a so-called unscreened potential in the vicinity of PDL/IL interface towards the oil phase, causing an unscreenable potential at the boundary of the TLF. The existence of such an unscreenable potential drop was discovered by other researchers when boundary potential variations have been measured for the adsorption of different salt ions in bilayer lipid membrane (BLM) [94,95]. It was shown that, due to the adsorption of the inorganic hydrophilic ions (like $K^+$ and $Cl^-$) in BLM, the boundary potential drop is located only in the electrolyte diffuse double layer and no unscreenable component of the potential drop exist. Therefore, we hypothesize that the amphiphilic ions can quickly pass through the unscreenable potential layer in the vicinity of PDL/IL interface towards the oil phase and manifest themselves by an increase in the conductivity of TLF. Investigating the kinetics of the ion transport through the IL phase and the qualitatively accepted adsorption dynamic stages (diffusion, barrier overcoming, adsorption acts, reorientation, rearrangement or conformational changes) of the hydrophilic ions and amphiphilic anion of dodecyl sulfate is out of the scope of this study and is the topic of our current research.

Fig.4. 3. also shows that the increase in conductivity is linear for SDS while it is nonlinear for KCl (marked with black dash-lines). Based on the theory developed by Debye and Huckel [96] and later modified by Onsager and Fuoss [97], this nonlinear effect in conductivity can be attributed to the concentration-dependent mobility of the ionic species. As the mobility of the ions changes by an increase in the concentration of ions present in IL phase, the adsorption dynamics of the

ionic species also changes. An increasing the ionic concentration leads to lower mobility of ions present in the IL phase.

Furthermore, at lower concentrations, the electrical conductivities ($\boldsymbol{\sigma}_1$ and $\boldsymbol{\sigma}_2$) were found to be close to each other, whereas, at higher concentrations the deviation between these two measured conductivities increases. A likely explanation is having dissimilar electrical response at higher concentrations where lower mobility of ions results in their lower adsorption. Although the TLF is dynamically stable over the range of 0 to 5 V applied potential, the IL phase response was found to be more sensitive in higher applied potentials and higher concentrations. At higher surfactant and salt concentrations, the produced films were unstable and data acquisition at higher voltages and higher surfactant concentration was not applicable. The TLF was considered stable when it did not break-up in the first 30 min of the experiment. The film instability at higher surfactant concentration was due to a significant reduction of the interfacial tension of oil-water interface leading to TLF rupture.

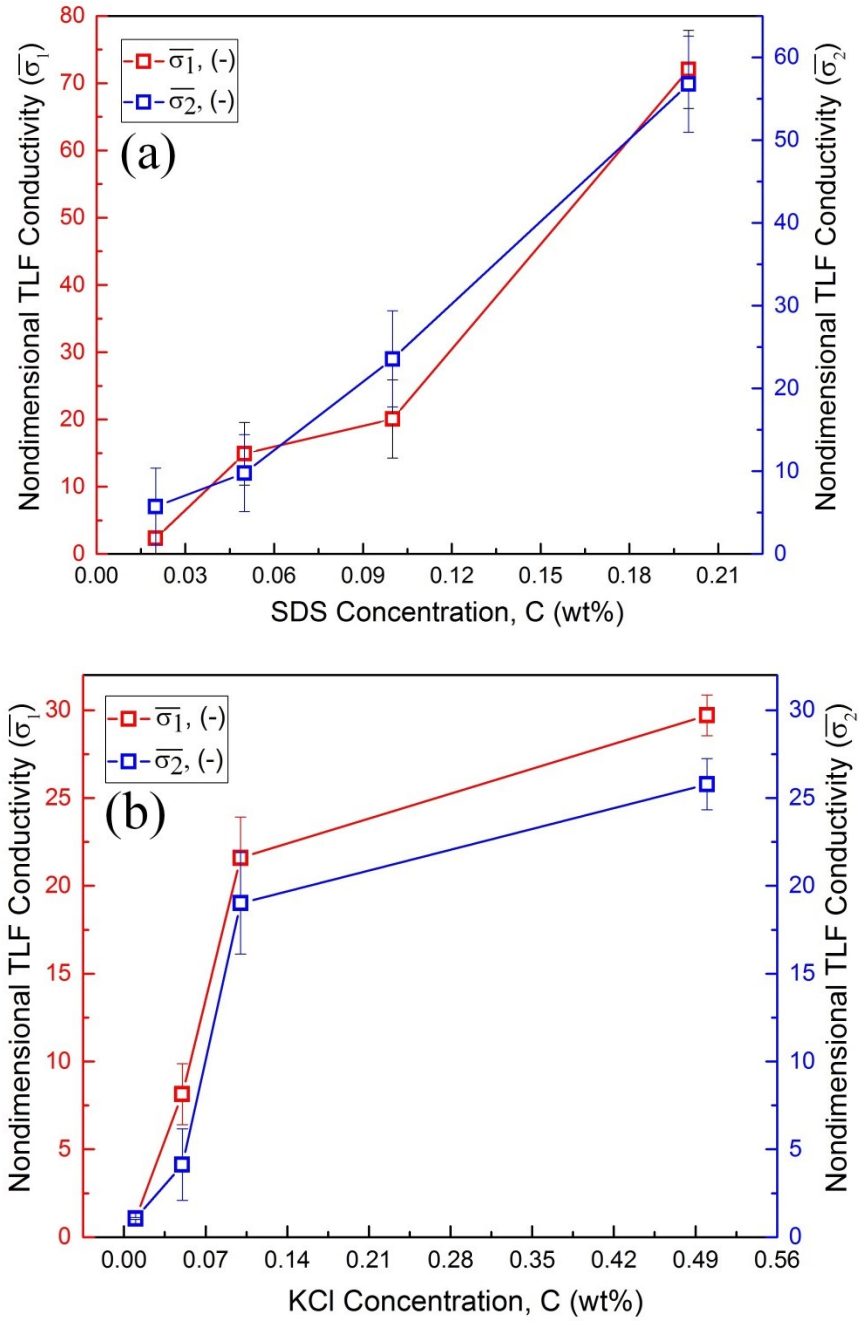


Figure 4.3. Nondimensional TLF conductivities, $\overline{\boldsymbol{\sigma}}_1$ and $\overline{\boldsymbol{\sigma}}_2$, vs (a) SDS and (b) KCl concentrations (C, wt%) using resistors-in-series modelling of the TLF. The results are normalized by the TLF base conductivity of deionized water and n-dodecane oil film

Since n-dodecane can be considered as a leaky dielectric medium in different electrical conditions [92], the charge leakage in the oil phase is evaluated to rule out the effect of charge leakage on the measured induced conductivity to the TLF. The film-forming hole is filled with TLF medium, and the current density of the system is monitored as a function of electric potential. Experimental details and results are presented in section 4 of the electronic supporting document. Current density of n-dodecane in the experimental condition remained constant as the applied potential increased. This ruled out the charge leackage in the TLF due to an applied electric potential.

This completed the study of the effect of different types and concentrations of additives on the TLF conductivity.

### 4.4.3 TLF conductivity: Time-dependent measurement

The time-dependent measurement of the TLF conductivity was performed for different surfactant concentrations (0.08, 0.10, 0.13 and 0.20 wt%), to investigate the TLF aging (Fig.4. 4.). The J-Ψ data was collected 5 times for a total period of 30 min, after the film formation (t=0). The voltage range of the measurement was set to as low as 0 to 1 volt to ensure that the TLF conductivity was not affected by the applied potential. The Nondimensional TLF conductivity $\bar{\sigma}_1$ for each concentration was re-scaled with the TLF conductivity at time zero ($\bar{\sigma}_0$) and the results are plotted versus the experiment time. The results show that the induced conductivity increased over time, and eventually reached a saturation point where the change in TLF conductivity was insignificant. For lower surfactant concentrations (≤0.1 wt%), the saturation time was about 10 min. To verify the obtained results of SDS adsorption by the developed MSC, the interfacial tension (IFT) measurement was performed for the 0.1 wt% SDS aqueous solution, as water phase, and n-dodecane, as the oil phase, using pendant drop tensiometry. The IFT experiment methodology and

results are presented in section 5 of the electronic supporting information. The results showed no significant reduction in IFT after around 600 sec (10 min) of the experiment, implying an excellent agreement between IFT and MSC measurements. As seen in Fig.4. 4., an increase in the SDS concentration resulted in a delayed saturation time. For example, for 0.13 wt% it was increased to about 20 minutes, and for 0.20 wt%, it exceeded the 30 minutes measurement times. Significantly, the relative conductivity was about 12 times more than the measured conductivity at t=0 for 0.2 wt% SDS. The saturation time of the surfactant adsorption was increased in the case of increase in SDS concentration due to the fact that at higher surfactant concentration, the mobility of the surfactants decreases, which resulted in a delayed saturation time of the surfactant at IL/PDL interface. The lower mobility of the surfactant at higher concentration is balanced by the likely shorter diffusion path of adsorption and/or larger concentration gradient. The more rapid mass transfer at higher surfactant concentration can be contributed to these two factors. We suggest that the change in nondimensional TLF conductivity is due to the surfactant adsorption, as discussed above.

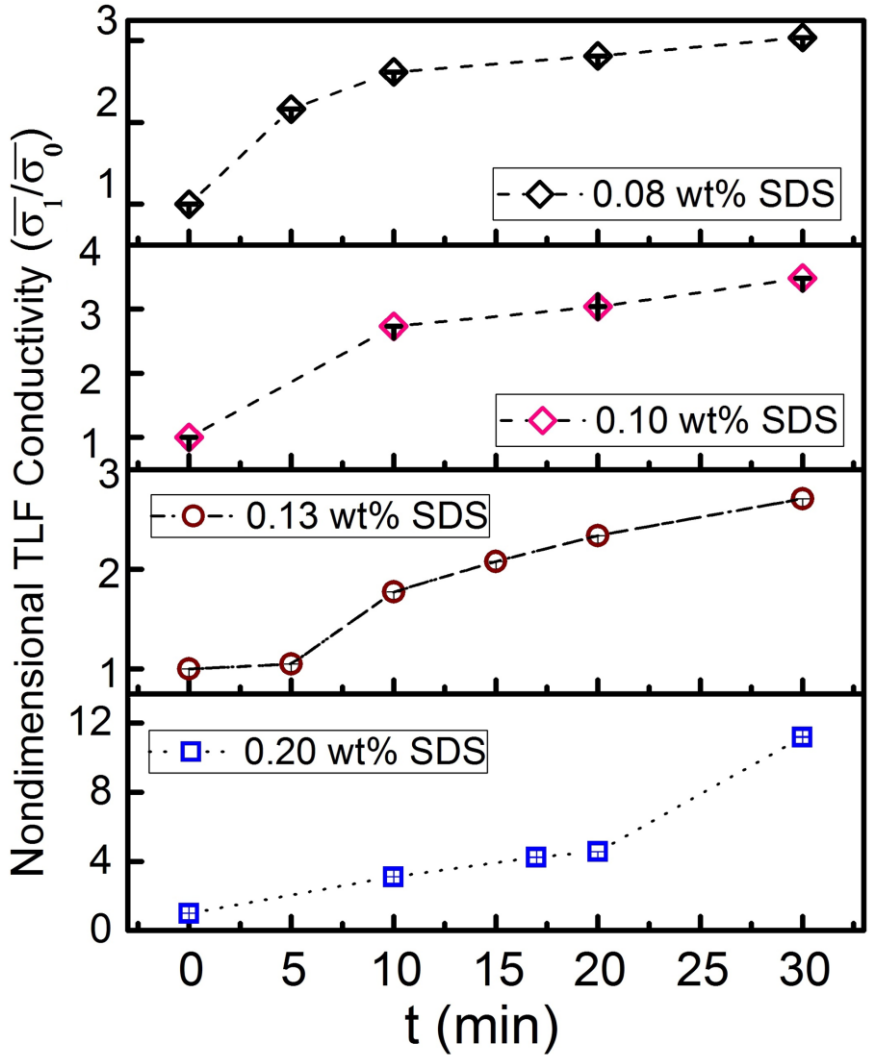


Figure 4.4. Nondimensional TLF conductivity ($\bar{\sigma}_1/\bar{\sigma}_0$) versus time for different surfactant concentrations

## 4.5 Concluding Remarks

In this study, a 3D-printed MSC was developed and used to study TLF formation and the change in TLF conductivity due to the adsorption/accumulation of amphiphilic/inorganic ions. Different stages of film formation were correlated to the electrical behavior of the system using the simultaneous monitoring of TLF formation and J-Ψ curve detection. The electrical detection of the film formation showed an abrupt change in the current density as a TLF of oil phase was formed. To demonstrate the effect of the type and concentration of ions on their adsorption/accumulation onto the TLF and thus its conductivity, two different electrolytes, SDS and KCl aqueous solutions, with multiple concentrations, were utilized. A resistance-in-series model was used to evaluate the conductivity of the TLF. Quantitative comparison of the normalized conductivity with concentration showed significantly higher adsorption of SDS to the interface than for inorganic KCl ions. This result was attributed to a different adsorption mechanism for SDS and KCl ions. The time-dependent measurement of the TLF conductivity was performed for different SDS concentrations to investigate the effect of TLF aging on measured conductivity. Results for the relative TLF conductivity showed that the induced conductivity increased over time, up to critical point (e.g., relative conductivity of 2 after 10 min), after which it remained unchanged. IFT measurements, using pendant drop tensiometry, demonstrated an excellent agreement between MSC and IFT results.

# Chapter Five

## 5 TLFs: O/W interface theoretical modeling in the presence of external applied electric fields; Calculation Basics of O/W interface electric potential and electric fields applied to the film

## 5.1 Abstract

Generally, the coalescence behavior in demulsification can be described in three stages: droplets approaching each other, the process of film thinning/drainage, and film rupture leading to droplet–droplet coalescence. This chapter presents the O/W interface theoretical modeling and the calculation basics of the O/W interface electric potential in the presence of external applied electric fields, highlighting particularly the mechanisms proposed for the PDL and IL interface electric field-change in the IL/PDL/IL system under the influence of an external applied electric field, as well as various factors influencing the film electric field. Film thickness effect on the O/W interface electric potential and O/W interface electric potential distribution at the IL/PDL interface has been obtained. The O/W interface electric potential versus film thickness for different surfactant concentrations and for different film thicknesses (film thickness: 0-20 nm, 0-100 nm and 0-800 nm) has been obtained. Maxwell stress distribution vs film thickness for different surfactant concentrations has also been demonstrated using the theoretical models. We adopt the theoretical models considering the oil phase to behave as a PDL medium. Nevertheless, the models considering the TLF to behave as LDL has also been presented at the end of this chapter for the sake of comparison and future works.

## 5.2 Keywords

Thin films, electrohydrodynamic, electrokinetic, perfect dielectric liquids (PDLs), leaky dielectric liquids (LDLs), ionic liquids (ILs), thin film instability, thin liquid film (TLF) dynamics, Poisson-Nernst-Planck (PNP)

## 5.3 Introduction

In recent years, there has been an increased interest in the study of IL/dielectric liquid (DL) interface under the applied electric field due to the increased application in many microfluidic systems, conventional processes and lab-on-a-chip (LOC) devices, namely electrophoretic actuation of a charged ionic liquid droplet in a dielectric liquid, jet formation from a Taylor cone of ionic liquid, and electrowetting of an ionic liquid droplet on a dielectric layer, etc. The IL/DL interface deforms when the electrical stress and the osmotic pressure overcome the Laplace pressure and viscous damping forces [98–103]. Dielectric liquids can be categorized into two types of PDLs and leaky dielectric liquids (LDL). PDLs have no free charges whereas the LDLs, have infinitesimal amount of charges. Under applied electric field, PDLs tend to polarize while in LDLs charges move and accumulate on the charged interfaces and interfaces [104]. In ILs, the applied electric fields cause the free ionic species present within the ILs redistribute and rearrange themselves at the charged interface. The diffuse layer of ions formed within the ionic liquids is called the electric double layer (EDL) [105,106]. Free ions dynamic within ILs is governed by the Poisson-Nernst-Planck (PNP) equation. According to Lee et al. [105], the IL phase behaves like a perfect conductor when subjected to a strong electric field (over O ($10^8$) V/m) . The ionic strength of the IL phase is determined by its molarity and EDL thickness is inversely related to the molarity of solution. Given that, the PDLs and LDLs considered as ILs with very large and small EDL, respectively [107]. When an external electric field is applied at the film interface, it causes instabilities on the deformable film interface. These instabilities are the basis for demulsification. The structure of the film interface changes under a homogeneous electric field based on the difference in the electric permittivity of the layers which film is formed of, and in this case this

change determines the direction of the net electric force imposed on the film [108]. When ILs are adjacent to the interface, redistribution and migration of the free ions result in the formation of EDL in the vicinity of the interface. The accumulation of the ions at the interface causes the change in electric potential distribution within the IL layer and alters the electric field on the TLF. As the molarity of the IL phase increases, the conductivity of the IL phase is increased which causes the lower Debye length. As has already been known, the presence of ILs with higher molarity (M = 1 mmol/L) causes the IL phase to act as perfect conductors and causes the lower change of the interfacial electric potential in comparison with the significant potential drop in the case of the lower ionic strength of the IL phase (M = 0.01 mmol/L, higher Debye length) [104]. It has been previously known by other researchers that the higher ionic strength of the IL phase causes the lower electric potential drop within the IL layer, thus the lower film in bilayer films experiences a higher electric field [108]. The theoretical modeling of the present work proves that by increasing the ionic strength of the IL phase, the electric potential drop is lower within the IL phase, at the vicinity of the TLF. In this chapter of the present thesis the analytical solutions are examined for the case of IL/PDL/IL system for different values of the molarity of IL phase and different film thicknesses of the TLF. The electric potential distribution has been obtained for the IL phase for different TLF thicknesses to show the effect of the film thickness on the device design variables.

## 5.4 Flat interface of IL/PDL in MSC under external electric fields

As in our current experimental condition, the surfactant solution which contains different concentrations of SDS moieties is considered as IL phase and we did apply different electric potentials at the IL/PDL interface, obtaining a comprehensive electrostatic model is crucial to predict the applied electric field to the TLF at the micro and nanoscales. An analytical model based

on the coupled nonlinear Poisson-Boltzmann and Laplace equations is developed for IL/PDL/IL system under the current experimental conditions (shown in Fig. 5.1.).

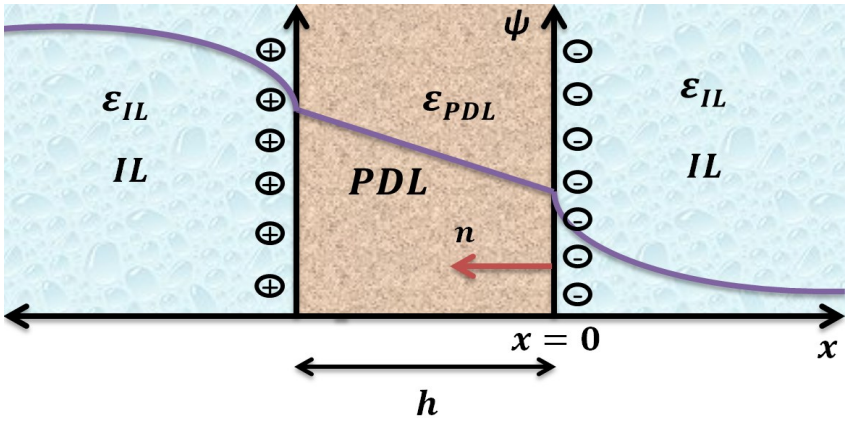


Figure 5.1. Schematic diagram of PDL and IL interface in IL/PDL/IL system. n represents the outward normal vector which originates from the interface at x=0 towards the PDL. PDL represents the oil phase (film forming medium) and IL represents the surfactant solution

We consider the interface region of IL/DL as shown in Fig. 5.1. and we are interested in the IL/PDL interface electric potential and electric potential distribution within PDL and IL layers. The interface is set at x = 0, the PDL phase is in the middle and the ILs are in the right and left side of the oil film. An electric field is related to the electric potential, ψ as $E = -\partial\psi/\partial x$. For the films of n-dodecane as PDL phase with no free charge, Laplace equation governs the electric potential in the layer [109].

$$\varepsilon_i \varepsilon_0 \nabla^2 \psi_i = 0 \qquad (5.1)$$

The PNP equation governs the electric potential distribution within the IL phase. Under the current experimental conditions, equilibrium condition, this equation is reduced to the Poisson–Boltzmann (PB) equation, [109]

$$\varepsilon_i \varepsilon_0 \nabla^2 \psi_i = -\rho_f \tag{5.2}$$

in which, $\rho_f$ is the free ions distribution within the IL phase which can be related to the ionic number concentration using the following formula; $\rho_f = \sum_{i=1}^{N} \overline{z_i}\, e n_i$, where $\overline{z_i}$ is the valence of the $i^{th}$ species in the electrolyte, N numbers of species, $e$ is the electron charge and $n$ is the ion number concentration which is given by the Boltzmann distribution at equilibrium condition [109];

$$n_i = n_{i\infty}\, exp\left[-\frac{\overline{z_i} e(\psi - \psi_{ref})}{k_B T}\right] \tag{5.3}$$

In which $n_{i\infty}$ and $\psi_{ref}$ are bulk ion number concentration and reference potential, respectively. We set the reference potential $\psi_{ref}$ as the applied voltage. Boltzmann constant and temperature in K, are denoted by $k_B$ and T, respectively. In our analysis, the bulk ion number concentration which depends on the molarity of the electrolyte is calculated using the following relation; $n_\infty = 1000\, N_A\, M$, in which $M$ is the molar concentration and $N_A$ is the Avogadro number. By using a Boltzmann distribution, the free ions dynamics become negligible and the electro-neutrality condition within the IL layer is satisfied. The constants and parameters used in the theoretical modeling of the system are shown in Table 5.1.

In the system shown in Figure 5.1., it is assumed the PDL/IL interface to be a planar interface and considering the SDS surfactants within the IL phase as symmetric monovalent electrolyte ($z_+ = -z_- = z$), the governing equation is given by [109],

$$\varepsilon \frac{d^2\psi}{dx^2} = 2zen_\infty sinh\left(\frac{ze\psi}{k_B T}\right) \tag{5.4}$$

where $n_{+\infty} = n_{-\infty} = n_\infty$, is the ionic number concentration in the bulk where $\psi = 0$. Using the appropriate boundary conditions for equation (5.4), $at\ x = 0\ \psi = \psi_s\ and\ x \to \infty\ \psi = 0$, the solution of equation (5.4) is obtained as [109]

$$\Psi = 2\ln\left[\frac{1+exp\ (-\kappa x)\tanh\ (^{\Psi_s}/_{4})}{1-exp\ (-\kappa x)\tanh\ (^{\Psi_s}/_{4})}\right] \tag{5.5}$$

in which $\Psi$ is the dimensionless potential which is defined as the following; $\Psi = \frac{ze\psi}{k_B T}$ and $\Psi_s = \frac{ze\psi}{k_B T}$ is the interface electric potential. In equation (5.5), $\kappa$ is the inverse of the Debye screening length while Debye screening length is defined as $\kappa^{-1} = (\frac{\varepsilon k_B T}{2e^2 z^2 n_\infty})^{1/2}$ [109].

Considering half of the IL/PDL/IL system ( $-h/2 \leq x \leq \infty$) in which h is TLF thickness and following boundary conditions,

$$\begin{cases} (i)\ @\ x = 0: \quad \psi_1 = \psi_1 = \Psi_s \\ (ii)\ @\ x = 0: \quad \varepsilon_{PDL}\varepsilon_0 \frac{\partial \psi_1}{\partial x} - \varepsilon_{IL}\varepsilon_0 \frac{\partial \psi_2}{\partial x} = 0 \\ (iii)\ @\ x = -{}^{h}/_{2}: \quad \psi_1 = \frac{\psi_{ref}}{2} = \frac{|\psi_{up}|+|\psi_{low}|}{2} \\ (iv)\ \ x \to \infty: \frac{\partial \psi_2}{\partial x} = 0,\ \psi_2 = 0 \end{cases} \tag{5.6}$$

the electric potential distribution within each layer is given by [109],

$$\Psi_{PDL} = ax + b \qquad\qquad -h/2 \leq x \leq 0 \tag{5.7}$$

$$\Psi_{IL} = 2\ V_T\ \ln\left[\frac{1+exp\ (-\kappa x)\tanh\ (^{\Psi_s}/_{4V_T})}{1-exp\ (-\kappa x)\tanh\ (^{\Psi_s}/_{4V_T})}\right] \qquad 0 \leq x < \infty \tag{5.8}$$

in which $V_T$ is defined as the thermal voltage, $V_T = \frac{k_B T}{ze}$. Term $\Psi_s$ is the interface electric potential and is given by the following nonlinear equation [109];

$$\varepsilon_{PDL}\varepsilon_0\left(\frac{2\Psi_s - \Psi_{ref}}{h}\right) + 2\varepsilon_{IL}\varepsilon_0 V_T\,\kappa\ sinh\ \left(\frac{\Psi_s}{2\ V_T}\right) = 0 \tag{5.9}$$

Table 5-1. Constants and parameters used in the theoretical modeling of the system

| **parameter** | **value** |
|---|---|
| Electron charge magnitude ($e$) | $1.602 \times 10^{-19}$ C |
| Boltzmann constant ($k_B$) | $1.378 \times 10^{-23}$ J/K |
| Avogadro number ($N_A$) | $6.022 \times 10^{23}$ 1/mol |
| free space electric permittivity ($\varepsilon_0$) | $8.85 \times 10^{-12}$ C/V.m |
| effective Hamaker constant ($A$) | $-1.5 \times 10^{-21}$ J |
| surface tension of film phase | 25.35 @ 20 °C in mN/m |
| electric permittivity of the PDL phase ($\varepsilon_{PDL}$) | 1.7708375634e-11 F/m |
| Relative electric permittivity of the PDL phase ($\varepsilon_{PDLr}$) | 2 |
| electric permittivity of the IL phase ($\varepsilon_{IL}$) | 710e-12 F/m |
| relative electric permittivity of the IL phase ($\varepsilon_{ILr}$) | 80 |
| molarity ($M$) of surfactant solutions (IL phase) | 0.69 mM, 1.7 mM, 3.50 mM, 6.93 mM |
| applied voltage ($\psi_{up}$) | 0−5 V |

The O/W interface electric potential versus film thickness for different surfactant concentrations and for different film thicknesses has been depicted in Figs. 5.2-5.4. Maxwell stress distribution vs film thickness for different surfactant concentrations (molar concentrations of SDS as IL phase) versus film thickness (film thicknesses: 0-100 nm) has been shown in Fig. 5.5.

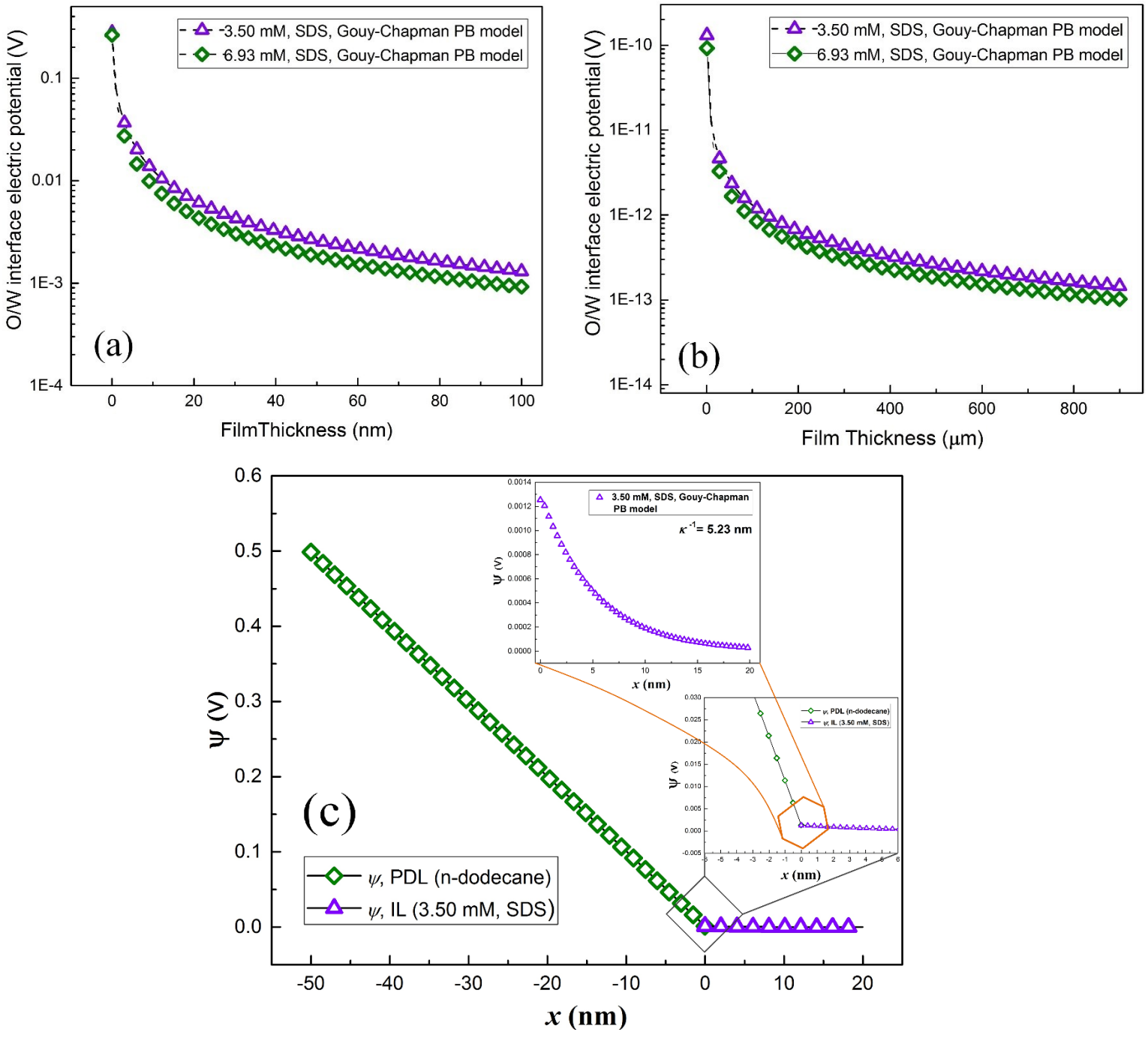


Figure 5.2. (a) O/W interface electric potential versus film thickness (film thickness: 0-100 nm), (b) O/W interface electric potential versus film thickness (film thickness: 0-800 nm) in the IL/PDL/IL system. PDL represents the oil phase (film forming medium) and IL represents the surfactant solution. (c) O/W interface electric potential distribution at the IL/PDL interface versus film thickness

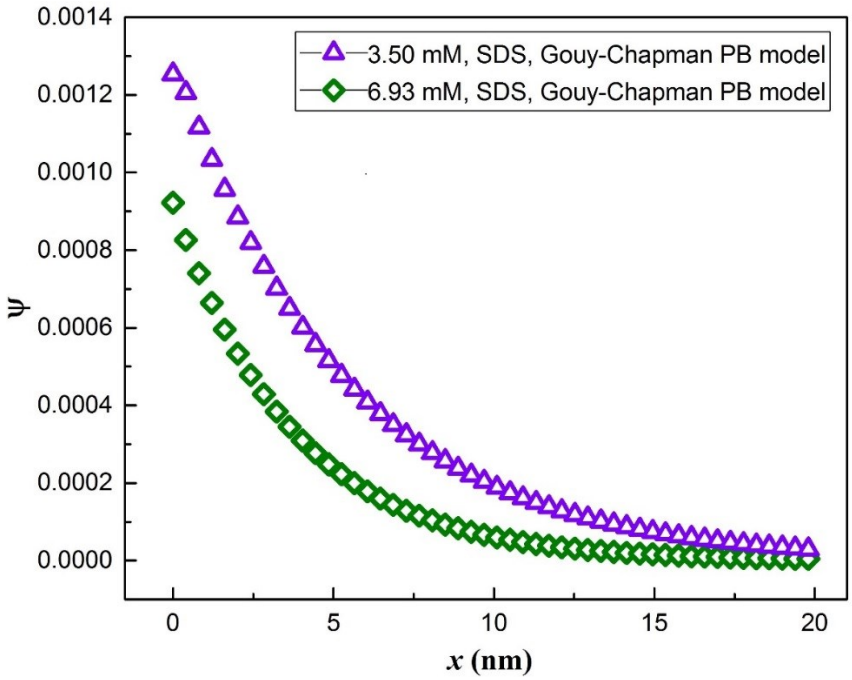


Figure 5.3. O/W interface electric potential distribution versus film thickness for different surfactant concentrations (film thickness: 0-20 nm)

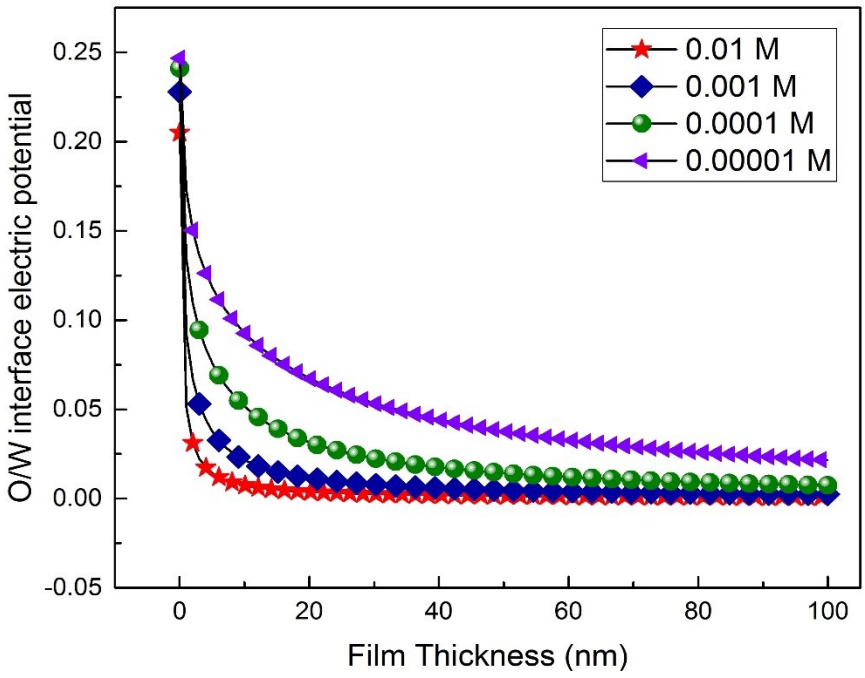


Figure 5.4. O/W interface electric potential distribution versus film thickness for different surfactant concentrations (molar concentrations of SDS) (film thickness: 0-100 nm)

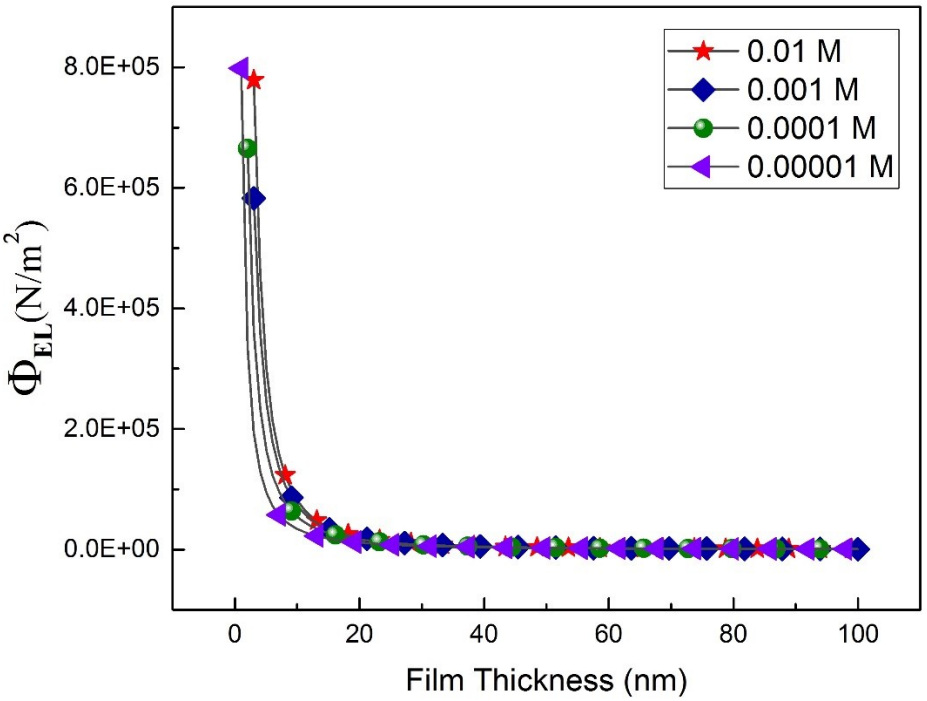


Figure 5.5. Maxwell stress distribution vs film thickness for different surfactant concentrations (molar concentrations of SDS as IL phase) versus film thickness (film thickness: 0-100 nm)

## 5.5 Leaky Dielectric model; Flat interface of IL/LDL in MSC under electric field

The electrohydrodynamic phenomena in poorly conducting liquids is described by the Taylor–Melcher leaky dielectric model. According to this model, there is no volumetric charge. This model is based on the Taylor's realization (1966) that poorly conducting liquids are basically different from PDLs and their conductivities are small. As has been mentioned by the review of the model by Schnitzer et al., the presence of these charges within the LDLs causes the occurrence of the infinitesimal liquid conductivities in the LDLs. In this case the Taylor–Melcher model avoids considering the ionic transport, which is a nonlinear mechanism and the primary mechanism involved in electrokinetic phenomena [110]. As the charge carriers in LDLs are typically ions [111], there are different challenges using the Taylor–Melcher model. This is due to the presence of the charged interfaces in the ILs that causes the formation of the diffuse ('Debye') layers, of charge opposite to that on the interface, within the IL phase. As this model doesn't count for the volumetric charges, there is not such a layer in this model. This is due to this fact that different approaches have been tried to unify the electrohydrodynamic models. In this part of the theoretical modeling of the current system we used Saville model of Taylor-Melcher leaky dielectric model [111]. A schematic of the model (IL/LDL/IL system) in the case of oil film behaving as LDL has been depicted in Fig. 5.6. Using Gouy-Chapman approximation [109] and considering crowding effect and neglecting the over-screening effect of ILs, the 1-D problem governing equations are as follows [110] ;

$$\frac{\partial^2 \psi_1}{\partial x^2} = 0 \qquad -\frac{h}{2} < x \leq 0 \tag{5.10}$$

$$\frac{\partial \psi_2}{\partial x} = 2V_T \left[\frac{-2\kappa * tanh\left(b/4V_T\right) * \exp(-\kappa x)}{1-\left[tanh^2\left(b/4V_T\right) * \exp^2(-\kappa x)\right]}\right], \qquad 0 \leq x < \infty \tag{5.11}$$

$$\frac{\partial q}{\partial t} = q\mathrm{n}.(\mathrm{n}.\nabla)\mathrm{v} - \mathrm{v}.\nabla_s\mathrm{q} + \sigma E_1.n + D_S{\nabla_s}^2 q \tag{5.12}$$

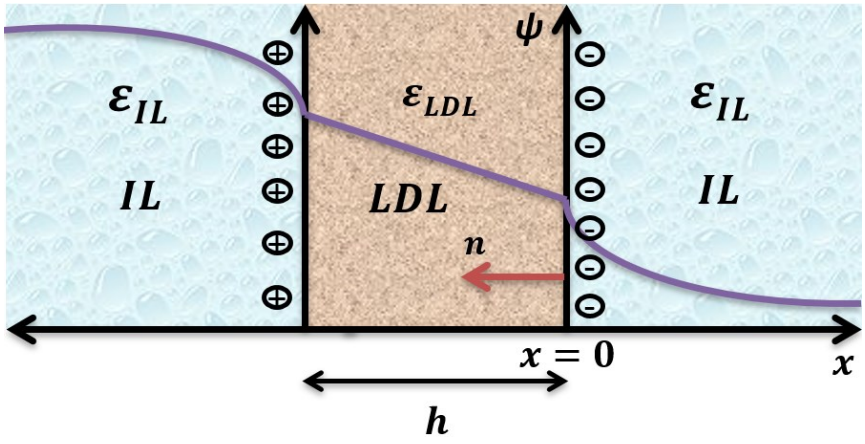


Figure 5.6. Schematic diagram of LDL and IL interface in IL/LDL/IL system. n represents the outward normal vector which originates from the interface at x=0 towards the LDL. LDL represents the oil phase (film forming medium) and IL represents the surfactant solution

## 5.6 Concluding Remarks

In this chapter of the present thesis, we worked with the electrostatics of the charges at the O/W interface. We considered the interface of the PDL and IL using the developed MSC in the presence of external electric fields. We theoretically modeled the IL/PDL interface and considered the effect of the applied electric field and film thickness on the IL/PDL electric potential. As has been confirmed by the model, we had huge electric fields applied to the film at nanoscale film thickness and at higher film thicknesses the effect of the electric field was less compared to the real experimentally monitored film thicknesses in the context of the present thesis using the MSC developed. We adopt the theoretical models considering the oil phase to behave as a PDL medium, as has been confirmed using the experimental procedures presented in section 4 of the appendix A of TLF supporting information of the thesis. Nevertheless, the models considering the TLF to

behave as LDL has also been presented at the end of this chapter for the sake of comparison and the future works in the case of TLFs behaving as LDL.

# Chapter Six

---

# 6 Concluding Remarks and Future Works

## 6.1 Conclusions

SAGD PW emulsions separation is of vital importance due to the current water crisis worldwide and the negligence of SAGD PW emulsion separation techniques specifically due to the fact that SAGD wells are not internationally spread out all over the globe. In this regard, the indigenous surfactants present in SAGD PW has received little attention in the literature. To overcome these challenges, systematic studies were conducted in this research to study the SAGD PW endogenous surfactants, HAs, and their interaction dynamics with naphtha-diluted AOSB present in a model SAGD PW and to develop advanced techniques to study the adsorption of surfactants at O/W interface. Initially, effect of SAGD PW properties on O/W transient interfacial tension has been studied. The dynamic IFT of dilbit in the water sample without any additive or surfactant (pH=5.74), for different dilution ratios ranging from 20 to 60 wt% has been demonstrated. It has been observed that, increasing the dilution ratio causes an increase in the IFT at t=0. As the smaller wt% of the dilbit drop will also imply larger concentrations of asphaltene within the drop, this can contribute to the smaller value of the IFT at t=0 for smaller wt% of the dilbit drop, given that larger aphaltene concentrations in a dilbit drop have been known to cause a larger reduction in the IFT. We hypothesized that this dynamic lowering of the IFT of the dilbit drop is caused by the gradual adsorption of the asphaltenes present within the dilbit drop on the O/W interface. A theory based on the combination of Ward-Tordai model (for surface concentration) and Langmuir isotherm has been applied to explain the experimental trends. The results from this theoretical model with the experiments for two chosen values of dilbit weight percentage has been demonstrated. The developed theoretical model was reasonably matched with the corresponding experimental results. In the other part of the study, IFT versus t for different pH values of the aqueous phase

for 40 wt% dilbit ratios has been obtained. The experimental results showed that at pH values of 7-9, the dynamic IFT of naphtha-diluted bitumen/SAGD synthetic brine was decreasing. However, towards the basic spectrum of the pH values (pH=9), which is relevant for SAGD operation (pH 9 to 11), the instability of the dilbit drop was observed. We hypothesized that the fluctuations in dynamic IFT in this case can be related to the frequent adsorption and desorption of indigenous surfactants present in the oil phase. Most remarkably, we find that IFT increases with time for pH values 9.5 and 10 for dilbit/SAGD (synthetic brine) interface. This is the same as the response associated with the saponification of carboxylic groups in higher pH values of SAGD brine solution. The interaction of indigenous surfactants present in bitumen with HAs present in SAGD synthetic brine at dilbit/SAGD brine interface is evident from the reductions in IFTs. This observation in the IFT results is an indicator of elevated interfacial activity of surfactants. As we increased the surfactant concentration of synthetic SAGD brine, we were unable to use pendant drop tensiometer used for the lower surfactant concentrations and the water samples without the presence of any surfactant and additive. As the surfactant concentration was increasing, the technique (IFT measurement for the adsorption study of the indigenous surfactants present in the aqueous phase) was unable to give reproducible results and the software was unable to detect the edge of the pendant drop in the aqueous solution due to the adsorption/desorption of the surfactants at the O/W interface. This limitation of the detection technique led us to think of a technique not to be visual to detect the adsorption of surfactants at O/W interface. As has been demonstrated in the 4$^{th}$ chapter, a 3D-printed MSC has been developed to electrically detect the surfactants adsorption at O/W interface. Its potential application for adsorption and TLF study has been demonstrated. The effect of the adsorption of surfactants at O/W interface has been shown using two different

electrolytes with multiple concentrations of electrolyte solutions as IL phase, surrounding a TLF formed in the developed device. The electrical behavior of the formed TLF was modeled in a circuit where all three phases were connected in series to an electric potential source. To examine the effect of the type of the ions present in IL phase on the TLF formation and the current-voltage characteristic curves of the system, different types of ions, including inorganic ions ($K^+$ and $Cl^-$) and amphiphilic ions such as SDS, as a typical representative of amphiphilic ion, were studied. TLF conductivity and the effect of adsorption of ionic moieties on the TLF conductivity has been examined for three cases of (i) TLF in SDS surfactant solution; (ii) TLF in KCl solution; and (iii) TLF in deionized water as a base case. It was observed that by increasing the surfactant concentration, the slope of J-Ψ curve increased for both BFF and AFF. The current density values decreased significantly after the formation of the film. The TLF conductivity increased with an increase in the concentration of both SDS (KCl) in aqueous solutions, which means higher adsorption/accumulation of ions at the IL/PDL interface. We also observed that the adsorption of SDS to the TLF surface is considerably higher than of KCl ions. We concluded that the amphiphilic ions can pass through a so-called unscreened potential in the vicinity of PDL/IL interface towards the oil phase, causing an unscreenable potential at the boundary of the TLF. We also theoretically modeled the O/W interface in the presence of external applied electric fields in the last part of the present thesis. An analytical model based on the coupled nonlinear Poisson-Boltzmann and Laplace equations was developed for IL/PDL/IL system under the current experimental conditions. As has been confirmed by the model, we had huge electric fields applied to the film at nanoscale film thicknesses and at higher film thicknesses the effect of the electric field was less compared to the real experimentally monitored film thicknesses.

## 6.2 Recommendations for Future Works

Further studies that can be performed as a continuation of the present study can be listed as follows;

- Examining the effect of different types of organic matters present in SAGD PW emulsions and development of theoretical models for the adsorption of different organic matters present in SAGD PW emulsions.
- Implementing different IFT measurement techniques to examine the adsorption of different indigenous surfactants present in SAGD PW emulsions.
- Using different bitumen related to different SAGD oil wells which results in different adsorption mechanisms and different theoretical models applied to the experimental results. In the present work, we utilized a specific bitumen related to a specific SAGD oil well and diluted it with specific solvent as applied in SAGD operations.
- Applying different polymeric resins used for 3D-printing of the cell developed in chapter 4 of the present thesis.
- Implementing other innovative methods of formation of TLFs and adsorption mechanism study using such a method.
- Type and concentration of surface-active components have been demonstrated to impart considerably stability and rheological property changes to the interfacial films, thus implementing different salts and ions present in IL phase and considering their effect on the induced conductivity of the formed films, can be of paramount importance for future considerations.
- Generating TLFs with different film thicknesses and monitoring the effect of surfactant adsorption/accumulation on the TLF.

- Electric field applied to the TLF under AC/DC current can be further studied to enhance the knowledge in the field of adsorption of surfactants in the presence of external electric fields.

# Complete List of References


[1] I. Report, The Global Risks Report 2016 11th Edition, (2016).

[2] N. Armaroli, V. Balzani, The Energy Challenge, Energy a Sustain. World. 452 (2011) 1–10. doi:10.1002/9783527633593.ch1.

[3] WHO (World Health Organization); UNICEF (United Nations International Children's Emergency Fund), 2015 Update and MDG Assessment, World Heal. Organ. (2015) 90. doi:10.1007/s13398-014-0173-7.2.

[4] J. Blackwell, Water: a shared responsibility UNESCO: World Water Development Report, 2006. doi:10.7748/nm.21.4.12.s12.

[5] M.A. Shannon, P.W. Bohn, M. Elimelech, J.G. Georgiadis, B.J. Marinas, A.M. Mayes, Science and technology for water purification in the coming decades, Nature. (2008). doi:10.1038/nature06599.

[6] Water Usage | Oil Sands Magazine, Oil Sands Mag. (2018).

[7] J. Farmer, Tar Sands or Scar Sands, Bournemouth University, 2017. http://eprints.bournemouth.ac.uk/29631/1/FARMER%2C Jennie Anne_M.Res._2017.pdf.

[8] K.L. Kaspersky, A Review of Properties and Treatment of Oil Sands Tailings, AOSTRA J. Res. (1992).

[9] H.A.W. Kaminsky, Characterization of an Athabasca oil sand ore and process streams, Alberta, 2008. http://login.ezproxy.library.ualberta.ca/login?url=http://search.ebscohost.com/login.aspx?direct=true&db=pta&AN=1073720&site=eds-live&scope=site.

[10] J.H. Cottrell, Development of an anhydrous process for oil-sand extraction Athabasca Oil Sands, (1963) 193–206.

[11] J.M. Dealy, Rheological properties of oil sand bitumens, Can. J. Chem. Eng. 57 (1979) 677–683. doi:10.1002/cjce.5450570604.

[12] M. Razi, M.R. Rahimpour, A. Jahanmiri, F. Azad, Effect of a different formulation of demulsifiers on the efficiency of chemical demulsification of heavy crude oil, J. Chem. Eng. Data. 56 (2011). doi:10.1021/je2001733.

[13] S. Thomas, Enhanced Oil Recovery – An Overview, Oil Gas Sci. Technol. …. 63 (2008) 9–19. doi:10.2516/ogst.

[14] D. Nguyen, V. Balsamo, J. Phan, Effect of diluents and asphaltenes on interfacial properties and steam-assisted gravity drainage emulsion stability: Interfacial rheology and wettability, Energy and Fuels. 28 (2014) 1641–1651. doi:10.1021/ef401880y.

[15] http://www.cenovus.com/operations/technology/sor.html, (2019) 8–9.

[16] https://surmontenergy.com/operations/, (2019) 2–4.

[17] A. Shah, R. Fishwick, J. Wood, G. Leeke, S. Rigby, M. Greaves, A review of novel techniques for heavy oil and bitumen extraction and upgrading, Energy Environ. Sci. (2010). doi:10.1039/b918960b.

[18] S.L. Kokal, Crude Oil Emulsions: A State-Of-The-Art Review, SPE Prod. Facil. (2006). doi:10.2118/77497-pa.

[19] J. Peng, Q. Liu, Z. Xu, J. Masliyah, Novel magnetic demulsifier for water removal from diluted bitumen emulsion, Energy and Fuels. 26 (2012) 2705–2710. doi:10.1021/ef2014259.

[20] R. Bosch, E. Axcell, V. Little, R. Cleary, S. Wang, R. Gabel, B. Moreland, A Novel Approach for Resolving Reverse Emulsions in SAGD Production Systems, Can. J. Chem. Eng. 82 (2004) 836–839. doi:10.1002/cjce.5450820424.

[21] G.E. Petrowski, J.R. Vanatta, Gas chromatographic determination of hydrophile-lipophile balance of nonionic emulsifiers, J. Am. Oil Chem. Soc. (1973). doi:10.1007/BF02641356.

[22] S. Gao, Stability of Water-in-Diluted Bitumen Emulsion Droplets, University of Alberta, 2010.

[23] S. Poteau, J.F. Argillier, D. Langevin, F. Pincet, E. Perez, Influence of pH on stability and dynamic properties of asphaltenes and other amphiphilic molecules at the oil-water interface, Energy and Fuels. (2005). doi:10.1021/ef0497560.

[24] C.W. Angle, Y. Hua, Tailings pond surfactant analogues: Effects on toluene-diluted bitumen drops in NaHCO3/K2CO3 solution. part 1: Dynamic interfacial tension, Energy and Fuels. 27 (2013) 3603–3612. doi:10.1021/ef400376v.

[25] S.E. Taylor, Interfacial Chemistry in Steam-Based Thermal Recovery of Oil Sands Bitumen with Emphasis on Steam-Assisted Gravity Drainage and the Role of Chemical Additives, Colloids and Interfaces. 2 (2018) 1–27. doi:10.3390/colloids2020016.

[26] T.F. Guetzloff, J.A. Rice, Does humic acid form a micelle?, Sci. Total Environ. (1994). doi:10.1016/0048-9697(94)90548-7.

[27] M. Terashima, M. Fukushima, S. Tanaka, Influence of pH on the surface activity of humic acid: Micelle-like aggregate formation and interfacial adsorption, Colloids Surfaces A Physicochem. Eng. Asp. 247 (2004) 77–83. doi:10.1016/j.colsurfa.2004.08.028.

[28] B. Mamba, R. Krause, T. Sithole, SPMalefetse, T. Nkambule, Humic acid as a model for natural organic matter (NOM) in the removal of odorants from water by cyclodextrin polyurethanes, Water SA. 35 (2016) 117–120. doi:10.4314/wsa.v35i1.76648.

[29] S. Bhattacharjee, A bridge between conventional oil and a sustainable energy future, in: Oil Sands, 2010.

[30] G. Bakker, The corrosive nature of diluted bitumen and crude oil literature review, (2011) 12.

[31] J.S. Clark, S.M. DeCorso, Stationary Gas Turbine Alternative Fuels, ASTM International, 1983. doi:10.1520/stp809-eb.

[32] C.C. Titration, Headquarters, M. International, Determination of the total acid number in petroleum products, n.d.

[33] L. Krotz, G. Giazzi, Thermo Scientific FLASH 2000 CHNS Analyzer : Stability , Linearity , Repeatability and Accuracy, (2000).

[34] B.K. Mianaee, Advanced Thin Film Composite and Nanocomposite Polyamide Membrane for Water Treatment, University of Alberta, 2017.

[35] C. Hagiopol, D. Atkinson, USA Patent Pub . No . US 2016/0032104 A1, 2016.

[36] R. von Wandruszka, Humic acids: Their detergent qualities and potential uses in pollution remediation, Geochem. Trans. 1 (2000) 10–15. doi:10.1039/b001869o.

[37] N. Bagalkot, A.A. Hamouda, O.M. Isdahl, Dynamic interfacial tension measurement method using axisymmetric drop shape analysis, MethodsX. 5 (2018) 676–683. doi:10.1016/j.mex.2018.06.012.

[38] P. Mukerjee, K.J. Mysels, NSRDS-NBS 36 -- Critical Micelle Concentrations of Aqueous Surfactant Systems, Natl. Stand. Ref. Data Syst. (1971). doi:10.1002/jps.2600610254.

[39] E.A.G. Aniansson, S.N. Wall, M. Almgren, H. Hoffmann, I. Kielmann, W. Ulbricht, R. Zana, J. Lang, C. Tondre, Theory of the kinetics of micellar equilibria and quantitative interpretation of chemical relaxation studies of micellar solutions of ionic surfactants, J. Phys. Chem. 80 (1976) 905–922. doi:10.1021/j100550a001.

[40] I.M. Krieger, T.J. Dougherty, A Mechanism for Non-Newtonian Flow in Suspensions of

Rigid Spheres, Trans. Soc. Rheol. 3 (2002) 137–152. doi:10.1122/1.548848.

[41] S. Kokal, Crude Oil Emulsions: A State-Of-The-Art Review, SPE Prod. Facil. 20 (2005) 5–13. doi:10.2118/77497-PA.

[42] E.-S.C. Boon-Beng Lee, Pogaku Ravindra, Methods of surface tension measurements, (2009). http://www.umcs.pl/pl/.

[43] D.M. Gans, W.D. Harkins, The drop weight method for the determination of surface tension. The effect of an inclination of the tip upon the drop weight, J. Am. Chem. Soc. 52 (1930) 2287–2289. doi:10.1021/ja01369a014.

[44] K.J. Mysels, The maximum bubble pressure method of measuring surface tension, revisited, Colloids and Surfaces. 43 (1990) 241–262. doi:10.1016/0166-6622(90)80291-B.

[45] S.M.I. Saad, Z. Policova, A.W. Neumann, Design and accuracy of pendant drop methods for surface tension measurement, Colloids Surfaces A Physicochem. Eng. Asp. 384 (2011) 442–452. doi:10.1016/j.colsurfa.2011.05.002.

[46] E.I. Franses, O.A. Basaran, C.-H. Chang, Techniques to measure dynamic surface tension, Curr. Opin. Colloid Interface Sci. 1 (2010) 296–303. doi:10.1016/s1359-0294(96)80018-5.

[47] J.S. Buckley, T. Fan, Crude oil/brine interfacial tensions, Petrophysics. 48 (2007) 175–185. https://www.scopus.com/inward/record.uri?eid=2-s2.0-34250780417&partnerID=40&md5=11c1270c2c895cf34d860d0fb2dcbeed.

[48] Y. Yang, C. Dicko, C.D. Bain, Z. Gong, R.M.J. Jacobs, Z. Shao, A.E. Terry, F. Vollrath, Behavior of silk protein at the air-water interface, Soft Matter. 8 (2012) 9705–9712. doi:10.1039/c2sm26054a.

[49] B. Trip, J. Magda, Adsorption of Globular Proteins at the Air-Water Interface as

Measured via Dynamic Surface Tension: Concentration Dependence, Mass-Transfer-Consideration and adsorption Kinetic, Colloid Interface Sci. 173 (1995) 16–27.

[50] S.Y. Lin, T.L. Lu, W.B. Hwang, Adsorption Kinetics of Decanol at the Air-Water Interface, Langmuir. 11 (1995) 555–562. doi:10.1021/la00002a033.

[51] Y. Rotenberg, L. Boruvka, A.W. Neumann, Determination of surface tension and contact angle from the shapes of axisymmetric fluid interfaces, J. Colloid Interface Sci. 93 (1983) 169–183. doi:10.1016/0021-9797(83)90396-X.

[52] J.D. Berry, M.J. Neeson, R.R. Dagastine, D.Y.C. Chan, R.F. Tabor, Measurement of surface and interfacial tension using pendant drop tensiometry, J. Colloid Interface Sci. 454 (2015) 226–237. doi:10.1016/j.jcis.2015.05.012.

[53] J. Lucassen, M.G.B. Drew, The crystal structure of sodium diheptylsulphosuccinate dihydrate and comparison with phospholipids, J. Chem. Soc. Faraday Trans. 1 Phys. Chem. Condens. Phases. 83 (1987) 3093–3106. doi:10.1039/F19878303093.

[54] P. Joos, J.P. Fang, G. Serrien, Comments on some dynamic surface tension measurements by the dynamic bubble pressure method, J. Colloid Interface Sci. 151 (1992) 144–149. doi:10.1016/0021-9797(92)90245-H.

[55] G. Serrien, P. Joos, Dynamic surface properties of aqueous sodium dioctyl sulfosuccinate solutions, J. Colloid Interface Sci. 139 (1990) 149–159. doi:10.1016/0021-9797(90)90452-T.

[56] P. Joos, J. Van Hunsel, Adsorption kinetics of micellar Brij 58 solutions, Colloids and Surfaces. 33 (1988) 99–108. doi:10.1016/0166-6622(88)80052-0.

[57] M. Jeribi, B. Almir-Assad, D. Langevin, I. Hénaut, J.F. Argillier, Adsorption kinetics of asphaltenes at liquid interfaces, J. Colloid Interface Sci. 256 (2002) 268–272.

doi:10.1006/jcis.2002.8660.

[58] S. Keleşoğlu, P. Meakin, J. Sjöblom, Effect of aqueous phase ph on the dynamic interfacial tension of acidic crude oils and myristic acid in Dodecane, J. Dispers. Sci. Technol. 32 (2011) 1682–1691. doi:10.1080/01932691.2010.516416.

[59] S. Zarkar, V. Pauchard, U. Farooq, A. Couzis, S. Banerjee, Interfacial properties of asphaltenes at toluene-water interfaces, Langmuir. 31 (2015) 4878–4886. doi:10.1021/acs.langmuir.5b00393.

[60] K.J. Mysels, Diffusion-controlled adsorption kinetics. General solution and some applications, J. Phys. Chem. 86 (1982) 4648–4651. doi:10.1021/j100220a036.

[61] J. Hristov, ORIGINAL ARTICLE A unified nonlinear fractional equation of the diffusion-controlled surfactant adsorption : Reappraisal and new solution of the Ward – Tordai problem, J. King Saud Univ. - Sci. 28 (2016) 7–13. doi:10.1016/j.jksus.2015.03.008.

[62] S. Acevedo, M.A. Ranaudo, C. García, J. Castillo, A. Fernández, Adsorption of asphaltenes at the toluene-silica interface: A kinetic study, Energy and Fuels. 17 (2003) 257–261. doi:10.1021/ef020104q.

[63] P. Ghosh, Adsorption at Fluid – Fluid Interfaces : Part III, Chem. Eng. (n.d.) 1–17.

[64] A.B. Andrews, R.E. Guerra, O.C. Mullins, P.N. Sen, Diffusivity of asphaltene molecules by fluorescence correlation spectroscopy, J. Phys. Chem. A. 110 (2006) 8093–8097. doi:10.1021/jp062099n.

[65] A. Rudrake, K. Karan, J.H. Horton, A combined QCM and XPS investigation of asphaltene adsorption on metal surfaces, J. Colloid Interface Sci. 332 (2009) 22–31. doi:10.1016/j.jcis.2008.12.052.

[66] C.W. Angle, Y. Hua, Tailings pond surfactant analogues: Effects on toluene-diluted

bitumen drops in NaHCO3/K2CO3 solution. part 2: Dilational interfacial viscoelasticity, Energy and Fuels. 27 (2013) 3613–3621. doi:10.1021/ef4003928.

[67] O.C. Mullins, The modified yen model, Energy and Fuels. 24 (2010) 2179–2207. doi:10.1021/ef900975e.

[68] M. Razi, S. Sinha, P.R. Waghmare, S. Das, T. Thundat, Effect of Steam-Assisted Gravity Drainage Produced Water Properties on Oil/Water Transient Interfacial Tension, Energy & Fuels. 30 (2016) 10714–10720. doi:10.1021/acs.energyfuels.6b01686.

[69] T.F. Tadros, Emulsion Science and Technology, 2009. doi:10.1002/9783527626564.

[70] M. Anklam, D. Saville, R. Prud, Disjoining Pressure and Film Tension in Comb-Graft Copolymer-Stabilized Oil Films, Langmuir. 15 (1999) 7299–7307. doi:10.1021/la9901581.

[71] a. Scheludko, Thin Liquid Films, Adv. Colloid Interface Sci. 450 (1967) 391–464. doi:10.1016/0001-8686(67)85001-2.

[72] B. V. Toshev, Thermodynamic theory of thin liquid films including line tension effects, Curr. Opin. Colloid Interface Sci. 13 (2008) 100–106. doi:10.1016/j.cocis.2007.11.001.

[73] M. Razi, M.R. Rahimpour, A. Jahanmiri, F. Azad, Effect of a different formulation of demulsifiers on the efficiency of chemical demulsification of heavy crude oil, J. Chem. Eng. Data. 56 (2011) 2936–2945. doi:10.1021/je2001733.

[74] K. Khristov, S.D. Taylor, J. Czarnecki, J. Masliyah, Thin liquid film technique — application to water – oil – water bitumen emulsion films, Colloids Surfaces A Physicochem. Eng. Asp. 174 (2000) 183–196.

[75] S.D. Taylor, J. Czarnecki, J. Masliyah, Disjoining pressure isotherms of water-in-bitumen emulsion films, J. Colloid Interface Sci. 252 (2002) 149–160. doi:10.1006/jcis.2002.8403.

[76] N. Panchev, K. Khristov, J. Czarnecki, D. Exerowa, S. Bhattacharjee, J. Masliyah, A new method for water-in-oil emulsion film studies, Colloids Surfaces A Physicochem. Eng. Asp. 315 (2008) 74–78. doi:10.1016/j.colsurfa.2007.07.013.

[77] J.S. Eow, M. Ghadiri, A.O. Sharif, T.J. Williams, Electrostatic enhancement of coalescence of water droplets in oil: A review of the current understanding, Chem. Eng. J. 84 (2001) 173–192. doi:10.1016/S1385-8947(00)00386-7.

[78] E.D. Manev, C.S. Vassilieff, I.B. Ivanov, Hydrodynamics of thin liquid films Effect of surface diffusion on the rate of thinning of foam films, J. Colloid Polym. Sci. 254 (1976) 99–102. doi:10.1007/BF01526745.

[79] T.Y. Chen, R.A. Mohammed, A.I. Bailey, P.F. Luckham, S.E. Taylor, Dewatering of crude oil emulsions 4. Emulsion resolution by the application of an electric field, Colloids Surfaces A Physicochem. Eng. Asp. 83 (1994) 273–284. doi:10.1016/0927-7757(93)02653-V.

[80] 1-s2.0-S0021979785713409-main.pdf, (n.d.).

[81] W. Wu, H. Fang, F. Yang, S. Chen, X. Zhu, Q. Yuan, W. Gan, Understanding the Di ff erent Steps of Surfactant Adsorption at the Oil − Water Interface with Second Harmonic Generation, J. Phys. Chem. C. (2016). doi:10.1021/acs.jpcc.5b11278.

[82] A. Bumajdad, J. Eastoe, Conductivity of water-in-oil microemulsions stabilized by mixed surfactants, J. Colloid Interface Sci. 274 (2004) 268–276. doi:10.1016/j.jcis.2003.12.050.

[83] R.W. Rennell, D. Ph, Dielectric and conductivity measurements on thin liquid films of n-heptanol, Radio Electron. Eng. 45 (1975) 401–408.

[84] P. Tchoukov, J. Czarnecki, T. Dabros, Study of water-in-oil thin liquid films: Implications for the stability of petroleum emulsions, Colloids Surfaces A Physicochem. Eng. Asp. 372

(2010) 15–21. doi:10.1016/j.colsurfa.2010.09.007.

[85] J. Czarnecki, K. Khristov, J. Masliyah, N. Panchev, S.D. Taylor, P. Tchoukov, Application of Scheludko–Exerowa thin liquid film technique to studies of petroleum W/O emulsions, Colloids Surfaces A Physicochem. Eng. Asp. 519 (2017) 2–10. doi:10.1016/j.colsurfa.2016.04.040.

[86] Shawn David Taylor, Colloidal Interactions in Water-in-Diluted-Bitumen Emulsions, University of Alberta, 2002. doi:10.16953/deusbed.74839.

[87] J. Nguyen, J.G. Underwood, I. Llorente García, Orienting lipid-coated graphitic micro-particles in solution using AC electric fields: A new theoretical dual-ellipsoid Laplace model for electro-orientation, Colloids Surfaces A Physicochem. Eng. Asp. 549 (2018) 237–251. doi:10.1016/j.colsurfa.2018.02.032.

[88] E.A. da Silva, L. Caseli, C. de A. Olivati, Organization of polythiophenes at ultrathin films mixed with stearic acid investigated with polarization-modulation infrared reflection–absorption spectroscopy, Colloids Surfaces A Physicochem. Eng. Asp. 529 (2017) 628–633. doi:10.1016/j.colsurfa.2017.06.035.

[89] M. Knite, A. Linarts, K. Ozols, V. Tupureina, I. Stalte, L. Lapcinskis, A study of electric field-induced conductive aligned network formation in high structure carbon black/silicone oil fluids, Colloids Surfaces A Physicochem. Eng. Asp. 526 (2017) 8–13. doi:10.1016/j.colsurfa.2016.12.032.

[90] H. Er, H. Yasuda, M. Harada, E. Taguchi, M. Iida, Formation of silver nanoparticles from ionic liquids comprising N-alkylethylenediamine: Effects of dissolution modes of the silver(I) ions in the ionic liquids, Colloids Surfaces A Physicochem. Eng. Asp. 522 (2017) 503–513. doi:10.1016/j.colsurfa.2017.03.046.

[91] K. Wattanakul, H. Manuspiya, N. Yanumet, The adsorption of cationic surfactants on BN surface: Its effects on the thermal conductivity and mechanical properties of BN-epoxy composite, Colloids Surfaces A Physicochem. Eng. Asp. 369 (2010) 203–210. doi:10.1016/j.colsurfa.2010.08.021.

[92] J.D. Piper, Thomas D., Dielectric Materials and Applications, John Wiley & Son, New York, 1954.

[93] J. Jia, L.C. Seitz, J.D. Benck, Y. Huo, Y. Chen, J.W.D. Ng, T. Bilir, J.S. Harris, T.F. Jaramillo, Solar water splitting by photovoltaic-electrolysis with a solar-to-hydrogen efficiency over 30%, Nat. Commun. 7 (2016) 1–6. doi:10.1038/ncomms13237.

[94] F. Berny, R. Schurhammer, G. Wipff, Distribution of hydrophilic, amphiphilic and hydrophobic ions at a liquid/liquid interface: A molecular dynamics investigation, Inorganica Chim. Acta. 300–302 (2000) 384–394. doi:10.1016/S0020-1693(99)00561-7.

[95] V.S. Sokolov, V. V Cherny, M. V Simonova, V.S. Markin, Electrical potential distribution over the bilayer lipid membrane due to amphiphilic ion adsorption, J. Electroanal. Chem. Interfacial Electrochem. 298 (1990) 27–44.

[96] P. Debye, E. Huckel, The theory of electrolytes I. The lowering of the freezing point and related occurrences, Phys. Zeitschrift. 24 (1923) 185–206.

[97] L. Onsager, R.M. Fuoss, Irreversible Processes in Electrolytes. Diffusion, Conductance and Viscous Flow in Arbitrary Mixtures of Strong Electrolytes, J. Phys. Chem. 36 (1931) 2689–2778. doi:10.1021/j150341a001.

[98] P.A.L. Wijethunga, Y.S. Nanayakkara, P. Kunchala, D.W. Armstrong, H. Moon, On-chip drop-to-drop liquid microextraction coupled with real-time concentration monitoring technique, Anal. Chem. 83 (2011) 1658–1664. doi:10.1021/ac102716s.

[99] I. Romero-Sanz, R. Bocanegra, J. Fernandez de la Mora, M. Gamero-Castaño, Source of heavy molecular ions based on Taylor cones of ionic liquids operating in the pure ion evaporation regime, J. Appl. Phys. 94 (2003) 3599–3605. doi:10.1063/1.1598281.

[100] D. Garoz, C. Bueno, C. Larriba, S. Castro, I. Romero-Sanz, J.F. De La Mora, Y. Yoshida, G. Saito, Taylor cones of ionic liquids from capillary tubes as sources of pure ions: The role of surface tension and electrical conductivity, J. Appl. Phys. 102 (2007). doi:10.1063/1.2783769.

[101] S. Gmouh, T. Douki, Y. Fouillet, G. Marchand, P. Dubois, J. Berthier, F. Hassine, M. Vaultier, Ionic Liquid Droplet as e-Microreactor, Anal. Chem. 78 (2006) 4909–4917. doi:10.1021/ac060481q.

[102] D.J. Im, J. Noh, D. Moon, I.S. Kang, Electrophoresis of a charged droplet in a dielectric liquid for droplet actuation, Anal. Chem. 83 (2011) 5168–5174. doi:10.1021/ac200248x.

[103] D. Moon, D.W. Lee, D.J. Im, I.S. Kang, B.S. Yoo, M.M. Ahn, Discrete Electrostatic Charge Transfer by the Electrophoresis of a Charged Droplet in a Dielectric Liquid, Langmuir. 28 (2012) 11656–11661. doi:10.1021/la3014392.

[104] H. Nazaripoor, C.R. Koch, S. Bhattacharjee, Electrical perturbations of ultrathin bilayers: Role of ionic conductive layer, Langmuir. 30 (2014) 14734–14744. doi:10.1021/la503839x.

[105] D.W. Lee, D.J. Im, I.S. Kang, Electric Double Layer at the Interface of Ionic Liquid − Dielectric Liquid under Electric Field, Langmuir. 29 (2013) 1875–1884.

[106] P. Gambhire, R. Thaokar, Electrokinetic model for electric-field-induced interfacial instabilities, Phys. Rev. E - Stat. Nonlinear, Soft Matter Phys. 89 (2014) 1–9. doi:10.1103/PhysRevE.89.032409.

[107] H. Nazaripoor, C.R. Koch, M. Sadrzadeh, S. Bhattacharjee, Electrohydrodynamic patterning of ultra-thin ionic liquid films, Soft Matter. 11 (2015) 2193–2202. doi:10.1039/C4SM02477J.

[108] H. Nazaripoor, Electrohydrodynamic and Thermocapillary Instability of Thin Liquid Films, 2016.

[109] J.H. Masliyah, S. Bhattacharjee, Electrokinetic and Colloid Transport Phenomena Electrokinetic and Colloid Transport, JOHN WILEY & SONS, INC., 2006.

[110] O. Schnitzer, E. Yariv, The Taylor-Melcher leaky dielectric model as a macroscale electrokinetic description, J. Fluid Mech. 773 (2015) 1–33. doi:10.1017/jfm.2015.242.

[111] D.A. Saville, ELECTROHYDRODYNAMICS:The Taylor-Melcher Leaky Dielectric Model, Annu. Rev. Fluid Mech. 29 (1997) 27–64. doi:10.1146/annurev.fluid.29.1.27.

# Appendix A- TLF Supporting Information

## Section 1: TLF formation and electrical detection

Formation of thin oil liquid film is electrically characterized using the current density vs time (J-$t$) curve in the potentio-static measurements mode. Under a constant applied voltage, the change in the current density is measured when the TLF is forming. The J shows a decreasing trend as the film begins forming and the TLF is completely formed when the J remained constant over time.

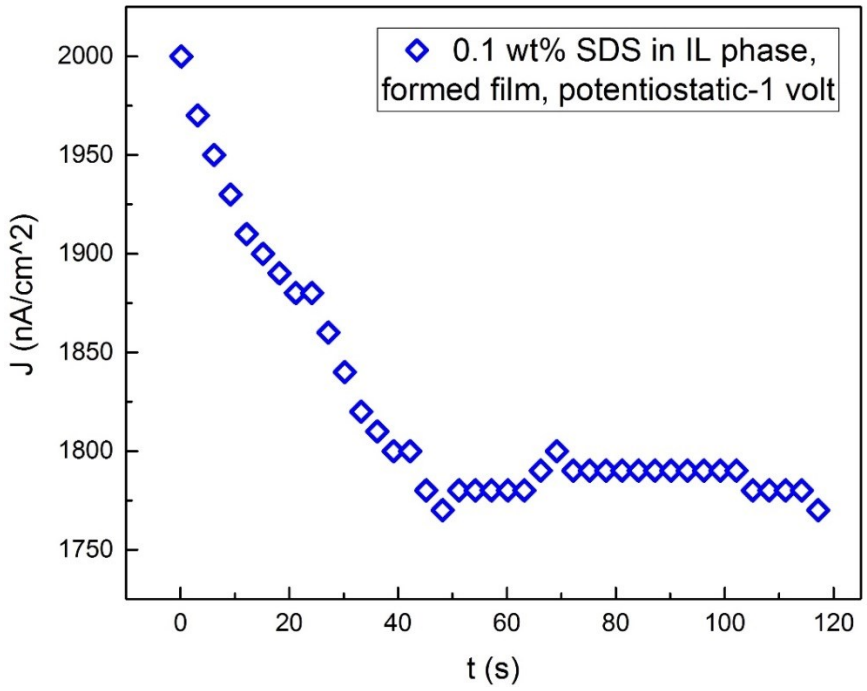


Fig. S1. 1. Current density vs time curve for the system composed of 0.1 wt% SDS concentration in milli-Q water as aqueous phase and n-dodecane as oil phase (TLF phase). The measurement has been done in constant voltage of 1 volt applied to the system. (potentiostatic mode). The film is completely formed after 50 sec of the beginning of the experiment.

# Section 2: Conductivity calculation basics

Three layers of IL phase/n-dodecane/IL phase has been treated each, as a resistor, connected in series to find the induced conductivity in TLF. The electrical behavior of the TLF is modelled in a circuit in which all three phases are linked in series to the electric potential source. As we used DC electric potential in the current experiments and due to the range of the electrical potentials, we have in the current experiments; the capacitance effects in the system are negligible. As Ohm's law needed to be satisfied for the complete circuit of the system, we apply the Ohm's equation as the proportionality of the current through any conductor to the voltage across the conductor at any constant physical conditions. The conductance of the TLF has been obtained using the following sets of equations.

$$V = I_1R_1 + I_2R_2 + I_3R_3 \tag{A2.1}$$

$$R_{equivalent} = R_1 + R_2 + R_3; \;\; R_{equivalent} = \sum R_i \tag{A2.2}$$

$$\frac{1}{g} = \sum \frac{1}{g_i} \tag{A2.3}$$

in which, $g, V, R,$ $I$ are the conductance, applied voltage, resistance and electric current, respectively.

Using the aforementioned equations and the current density-voltage (J-Ψ) characteristics of the system, we were able to obtain the induced conductivity using the following method; by subtracting the inverse of the slope of the (J-Ψ) characteristics curve at BFF (before film formation) from AFF (after film formation) condition, we obtain the resistance of the TLF. Electrical resistivity is successively obtained using the following formula;

$$\rho = \frac{R*L}{A} \quad \text{(A2.4)}$$

in which, $\rho, L, A$ are the electrical resistivity, length and cross-sectional area, respectively.

the electrical conductivity of the TLF is obtained using the following formula;

$$\sigma = \frac{1}{\rho} \quad \text{(A2.5)}$$

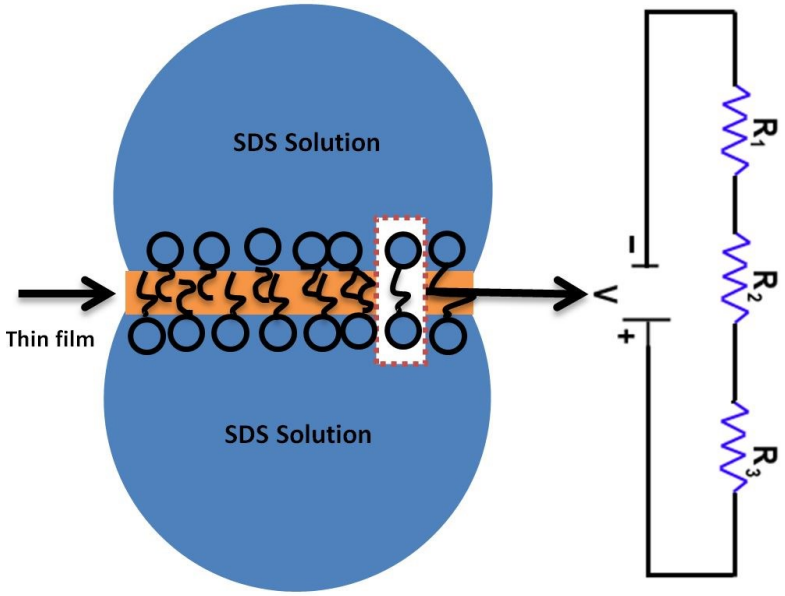


Fig. S2. 1. Schematic representation of formation of n-dodecane and a resistors-in-series modeling of the TLF formation

# Section 3: TLF in deionized water (DI water)

The current density vs electric potential curve for TLF forming in deionized water (without the presence of any charges in the aqueous phase), is found as base-case (results are available in the electrconic supporting information). In AFF condition when there are no additives in the aqueous phase, the quality of the formed TLF is low and it is not stable for the long-time. The TLF had

very high tendency to detach when there was no additive in the deionized water. The instability of TLF is evident in the $J$-$\Psi$ after the film formation and over the electrical detection.

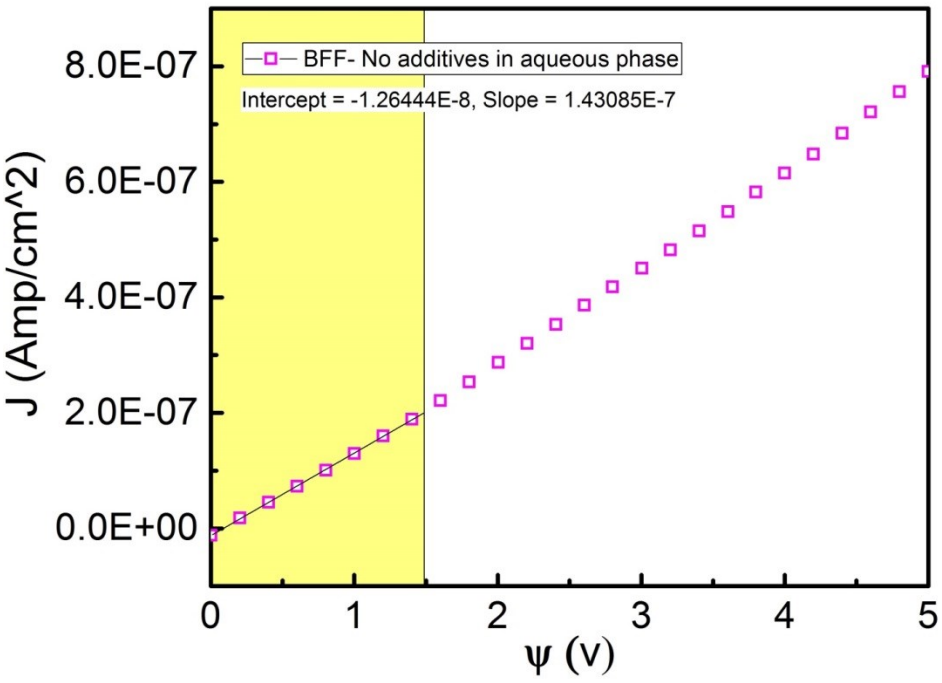


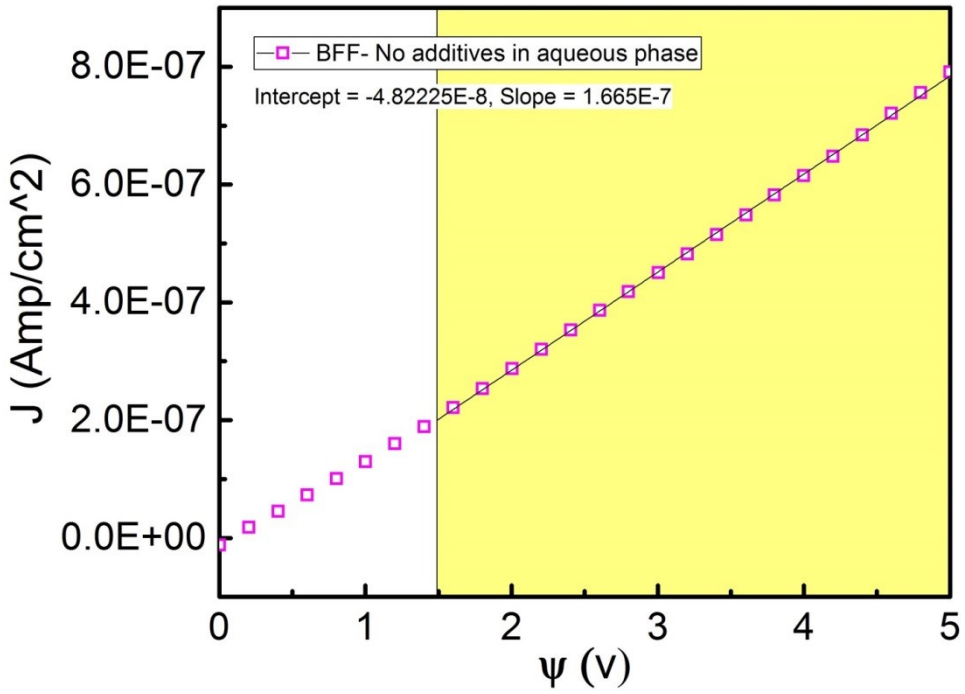

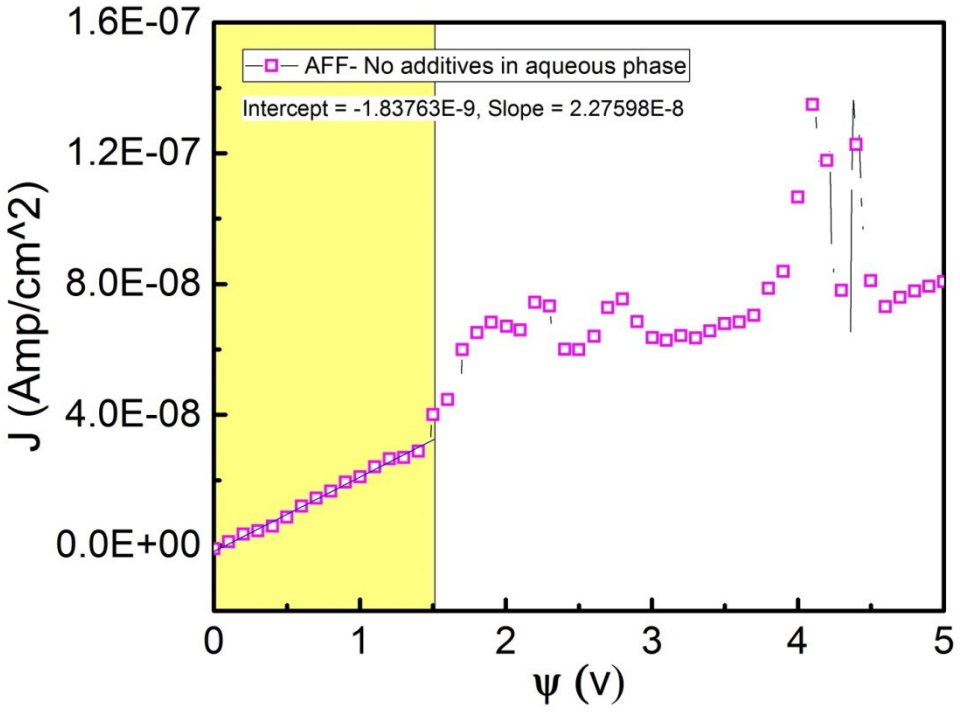


Fig.S3. 1. Current density vs electric potential curve for the TLF formed in deionized water and n-dodecane as TLF phase; before film formation (BFF) and after film formation (AFF)

# Section 4: Rule out the charge leakage within oil phase (PDL phase); experiments and results

As n-dodecane can be considered as LDL medium in different electrical conditions, the charge leakage in the oil phase under the experimental condition has been evaluated in the following experiments. The film-forming hole is filled with TLF medium and the current density of the system by increasing electric potential is monitored as the results are depicted in Figure S3. 1. Current density of n-dodecane in the experimental condition remained constant as the applied potential increased. This ruled out the LDL behavior of the oil film.

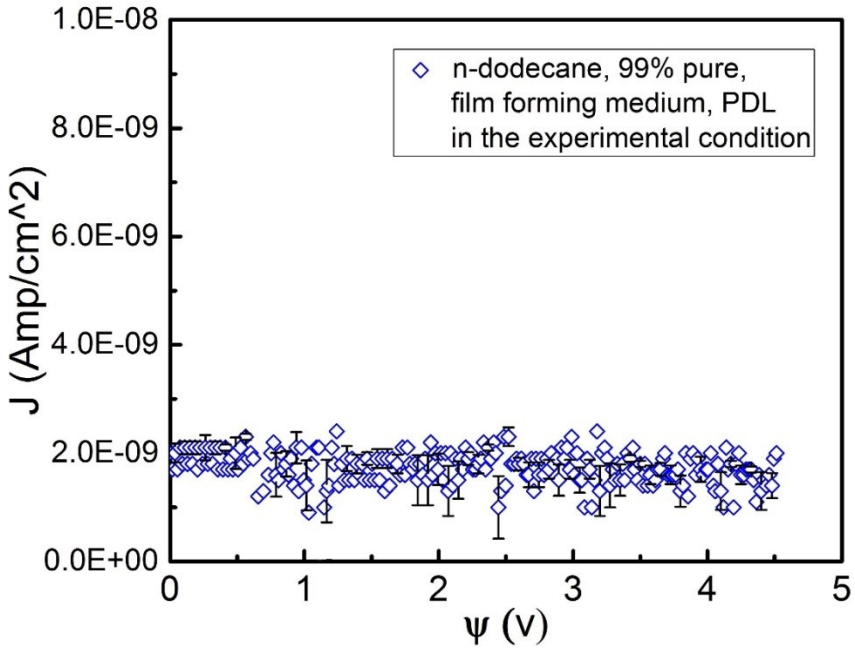


Fig. S4. 1. Current density vs electric potential curve for the system composed of n-dodecane as oil phase.

# Section 5: Dynamic Interfacial Tension (IFT): Measurement and Analysis

Adsorption analysis of SDS surfactants at O/W interface has been carried out using different runs of interfacial tension (IFT) measurement. The dynamic IFT measurements were carried out using a pendant drop tensiometer (KRÜSS GmbH Drop Shape Analyzer, DSA100) which is based on the deformation of a drop depending on the interfacial tension. This method utilizes the time-dependent drop shape analysis for the dynamic interfacial tension measurement. The dynamic interfacial tension between two liquids is determined using a drop shape analysis (DSA) system. The shape of the drop depends on the balance between two counteracting forces of gravity force which tends to elongate the drop and the interfacial tension which minimizes the interface area and tends to sphericalize the drop. The obtained drop profile is then related to the measured interfacial

tension by means of Young-Laplace equation. More details about the measurement technique of interfacial tensiometry are available in the literature [68]; we intentionally include the main equation here for the sake of brevity. Using the following equation, the pressure difference (Laplace pressure) across a curved interface is related to the principal radii of curvature, $R_i$ and the interfacial tension $\gamma$:

$$\gamma\left(\frac{1}{R_1}+\frac{1}{R_2}\right)=\Delta P\equiv\Delta P_0-\Delta\rho gz \tag{A5.1}$$

in which $R_1$ and $R_2$ are the curvature principal radii; $\Delta P = P_{in} - P_{out}$ is the Laplace pressure across the interface and $\Delta\rho = \rho_d - \rho$ is the density difference of two phases. The experimental procedure for measuring the interfacial tension of SDS solution as aqueous phase and n-dodecane as oil phase is as follows; the n-dodecane droplets (ranging from 10-20 μL) were generated at the tip of an inverted needle. The needle tip (20-gauge diameter) is immersed in a cuvette filled with SDS solution. The needle was connected to a Hamilton micro-syringe (500 μL, Hamilton Co., USA) which is mounted in a syringe holder positioned above a cuvette containing 25 mL of the SDS surfactant solution. A CCD camera is used to obtain a clear visualization on the computer screen. As the droplet of the oil phase is generated, dynamic interfacial tension $\gamma_{i(t)}$ measurements were immediately initiated to record the drop shape profile at the rate of 10 frame/s during the experiments. We recorded the drop shape profile until the point that the droplet detached from the needle. The volume of the oil drop was kept constant for the whole duration of the experiment. Temperature was kept constant at 23 °C for all the experiments. The experiments have been repeated three times to ensure the reproducibility of the IFT data.

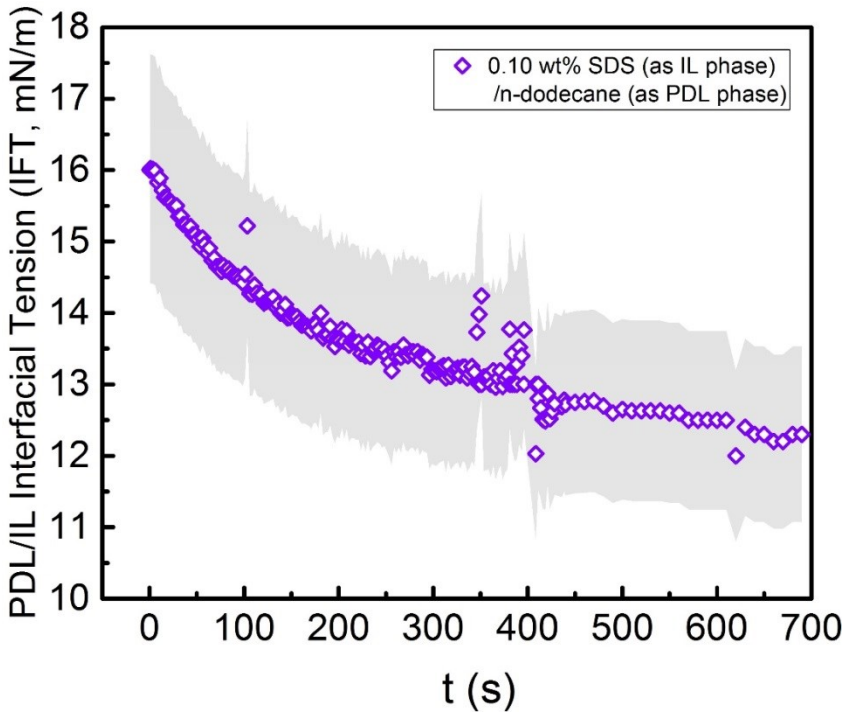


Fig. S5. 1. Dynamic interfacial tension (IFT, mN/m) of 0.1 wt% SDS solution as aqueous phase and n-dodecane as oil phase.

As shown in Fig. S5. 1., the dynamic IFT of 0.1 wt% SDS solution as aqueous phase and n-dodecane as oil phase, there is no significant reduction in IFT after around 600 sec of the experiment. We did not observe further reduction in IFT after around 650-700 sec of the start of the experiment as the oil drop detached from the needle. We correlated the increase in conductivity of the film to the observed reduction in interfacial tension of two phases as a confirmation for the adsorption of SDS moieties at the PDL/IL interface.

# Appendix B- Theoretical Modeling Supporting Information

# Section 1: Curve Fitting Data Using Origin

C=0.01 Molar SDS Surfactant
Equation y = y0 + A1*exp (-(x-x0)/t1) + A2*exp(-(x-x0)/t2)

**********

**Notes**

Description Nonlinear Curve Fit
User Name mrazi
Operation Time 4/19/2017 15:20:54
Iteration Algorithm Levenberg Marquardt
Model ExpDecay2
Number of Parameters 6
Number of Derived Parameters 0
Number of Datasets 1
Equation y = y0 + A1*exp (-(x-x0)/t1) + A2*exp (-(x-x0)/t2)
Report Status New Analysis Report
Special Input Handling
Data Filter No

**Parameters**

| | Value | Standard Error |
|---|---|---|
| y0 | 0.00143 | 8.70994E-5 |
| x0 | -0.3996 | 0 |
| A1 | 0.38373 | 0 |
| t1 | 0.50954 | 0.01204 |
| A2 | 0.03384 | 0 |
| t2 | 6.31661 | 0.25616 |

**********

Reduced Chi-sqr = 5.48405007048E-7
COD(R^2) = 0.99883979212192
Iterations Performed = 16
Total Iterations in Session = 16
Fit converged. Chi-Sqr tolerance value of 1E-9 was reached.

**********

**Statistics**

Number of Points 100
Degrees of Freedom 94
Reduced Chi-Sqr 5.48405E-7
Residual Sum of Squares 5.15501E-5
Adj. R-Square 0.99878
Fit Status Succeeded (100)

**********

**ANOVA**

| | | DF | Sum of Squares | Mean Square | F Value | Prob>F |
|---|---|---|---|---|---|---|
| B | Regression | 6 | 0.04749 | 0.00791 | 14431.47007 | 0 |
| | Residual | 94 | 5.15501E-5 | 5.48405E-7 | | |
| | Uncorrected Total | 100 | 0.04754 | | | |
| | Corrected Total | 99 | 0.04443 | | | |

**********

C=0.001 Molar

| Model | ExpDecay2 | | |
|---|---|---|---|
| Equation | y = y0 + A1*exp(-(x-x0)/t1) + A2*exp(-(x-x0)/t2) | | |
| Reduced Chi-Sqr | 2.1595E-6 | | |
| Adj. R-Square | 0.99672 | | |
| | | Value | Standard Error |
| B | y0 | 0.0039 | 1.88159E-4 |
| B | x0 | -0.4264 | -- |
| B | A1 | 0.30669 | -- |
| B | t1 | 0.69049 | 0.02454 |
| B | A2 | 0.06347 | -- |
| B | t2 | 9.03285 | 0.32067 |

**********

**Notes**

Description Nonlinear Curve Fit
User Name mrazi
Operation Time 4/19/2017 14:45:28
Iteration Algorithm Levenberg Marquardt
Model ExpDecay2
Number of Parameters 6
Number of Derived Parameters 0
Number of Datasets 1
Equation y = y0 + A1*exp(-(x-x0)/t1) + A2*exp(-(x-x0)/t2)
Report Status New Analysis Report
Special Input Handling
Data Filter No

**********

**Parameters**

| | Value | Standard Error |
|---|---|---|
| y0 | 0.0039 | 1.88159E-4 |
| x0 | -0.4264 | -- |
| A1 | 0.30669 | -- |
| t1 | 0.69049 | 0.02454 |
| A2 | 0.06347 | -- |
| t2 | 9.03285 | 0.32067 |

**********

Reduced Chi-sqr = 2.15950370602E-6
COD(R^2) = 0.99688919714347
Iterations Performed = 15
Total Iterations in Session = 15
Fit converged. Chi-Sqr tolerance value of 1E-9 was reached.

**********

**Statistics**

Number of Points 100
Degrees of Freedom 94
Reduced Chi-Sqr 2.1595E-6
Residual Sum of Squares 2.02993E-4
Adj. R-Square 0.99672
Fit Status Succeeded (100)

**********

**ANOVA**

| | | DF | Sum of Squares | Mean Square | F Value | Prob>F |
|---|---|---|---|---|---|---|
| B | Regression | 6 | 0.07882 | 0.01314 | 6083.19086 | 0 |
| | Residual | 94 | 2.02993E-4 | 2.1595E-6 | | |
| | Uncorrected Total | 100 | 0.07902 | | | |
| | Corrected Total | 99 | 0.06525 | | | |

**********

C=0.0001 Molar

**Notes**

Description Nonlinear Curve Fit
User Name mrazi
Operation Time 4/19/2017 15:58:31
Iteration Algorithm Levenberg Marquardt
Model ExpDecay2
Number of Parameters 6
Number of Derived Parameters 0
Number of Datasets 1
Equation y = y0 + A1*exp (-(x-x0)/t1) + A2*exp (-(x-x0)/t2)
Report Status New Analysis Report
Special Input Handling
Data Filter No

**********

**Parameters**

| | Value | Standard Error |
|---|---|---|
| y0 | 0.00969 | 3.23179E-4 |
| x0 | -0.431150 | |
| A1 | 0.2242 | 0 |
| t1 | 0.95078 | 0.04144 |
| A2 | 0.09155 | 0 |
| t2 | 14.74234 | 0.41617 |

**********

| | | DF | Sum of Squares | Mean Square | F Value | Prob>F |
|---|---|---|---|---|---|---|
| B | Regression | 6 | 0.16075 | 0.02679 | 6629.6853 | 0 |
| | Residual | 94 | 3.7987E-4 | 4.04117E-6 | | |
| | Uncorrected Total | 100 | 0.16113 | | | |
| | Corrected Total | 99 | 0.09738 | | | |

**Statistics**

Number of Points 100
Degrees of Freedom 94
Reduced Chi-Sqr 4.04117E-6
Residual Sum of Squares 3.7987E-4
Adj. R-Square 0.99589
Fit Status Succeeded (100)

**********

**ANOVA**

**********

C=0.00001 Molar

**Notes**

Description Nonlinear Curve Fit
User Name mrazi
Operation Time 4/19/2017 16:24:55
Iteration Algorithm Levenberg Marquardt
Model ExpDecay2
Number of Parameters 6
Number of Derived Parameters 0
Number of Datasets 1
Equation y = y0 + A1*exp (-(x-x0)/t1) + A2*exp(-(x-x0)/t2)

Report Status New Analysis Report
Special Input Handling
Data Filter No
**********

**Parameters**

| | Value | Standard Error |
|---|---|---|
| y0 | 0.02224 | 5.39075E-4 |
| x0 | -0.65291 | 1.0804E6 |
| A1 | 0.17923 | 133984.44161 |
| t1 | 1.44526 | 0.06537 |

| | | DF | Sum of Squares | Mean Square | F Value | Prob>F |
|---|---|---|---|---|---|---|
| B | Regression | 6 | 0.38656 | 0.06443 | 15908.74865 | 0 |
| | Residual | 94 | 3.8068E-4 | 4.04978E-6 | | |
| | Uncorrected Total | 100 | 0.38694 | | | |
| | Corrected Total | 99 | 0.12982 | | | |

| | | | |
|---|---|---|---|
| A2 | 0.11088 | 4904.07763 | |
| t2 | 24.42711 | 0.61515 | |

**********

**Statistics**

Number of Points 100
Degrees of Freedom 94
Reduced Chi-Sqr 4.04978E-6
Residual Sum of Squares 3.8068E-4
Adj. R-Square 0.99691
Fit Status Succeeded (100)
**********

**ANOVA**

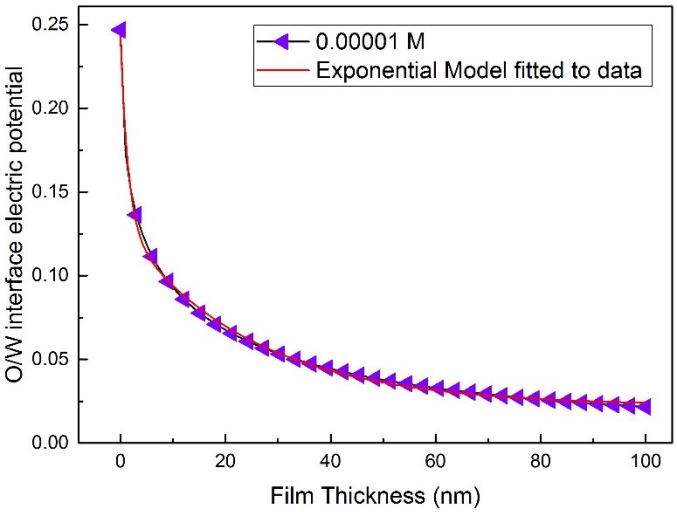


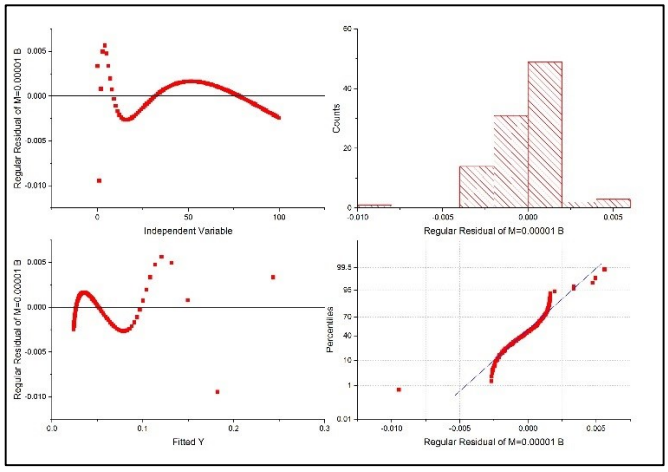

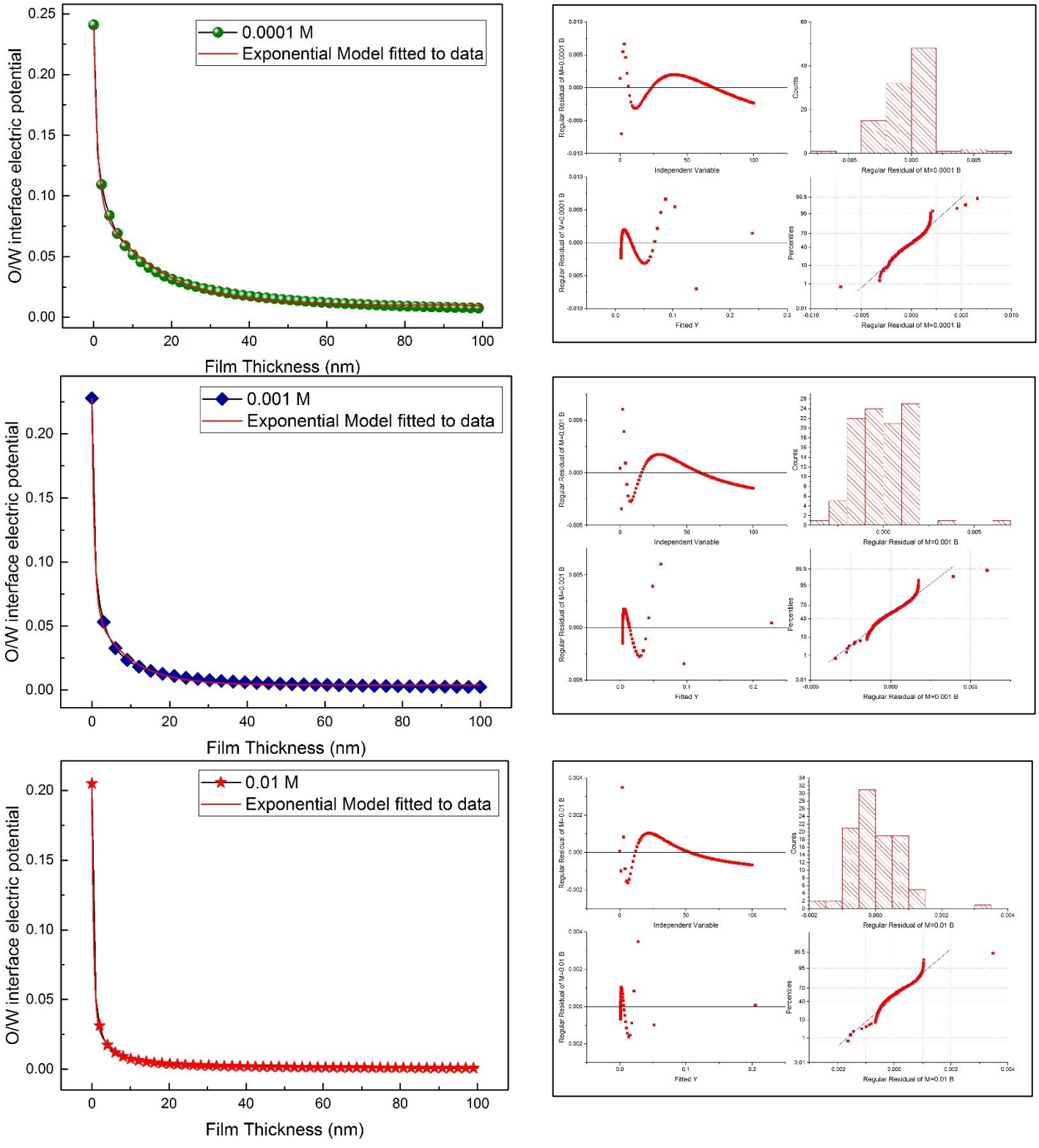


Fig. S1. 1. O/W interface theoretical modeling fitting results

# Section 2: MATLAB Codes for Obtaining the Electric Potential, Electrostatic Conjoining/Disjoining pressure

```
%  first draft of code for Bazant + Gouy-Chapman appproximation.m
%  Using this code, Electric potential, Electrostatic Conjoining/
%  Disjoining pressure is calcultaed while we hve Surface excess charge
%  for a range of h (oil thickness-TLF medium) variation (K Loop)
%          ------------------------------------------------
%            *                          *                  *
%            *    Surfactant Solution, Media 1  *     Oil Media 2      *
%            *                          *                  *
%    Origin ------- positive x direction------------------------
%*********************************************************************
clc
clear all
close all
ePDLr=2;                    % Relative Electrical permitivity of n-dodecane
[ref:https://www.kabusa.com/Dilectric-Constants.pdf]
ePDL=1.7708375634e-11;      % Electrical permitivity of n-dodecane/e0
[ref:https://www.kabusa.com/Dilectric-Constants.pdf]
e0=8.854187817e-12;         % vaccum electric permitivity (c/v.m)
V=1;                        % applied Voltage, in my Experiments (1Volts)
%h=(1e-9)*linspace(0.01,99.99,100);    % TLF (Thin Liquid Film Thickness)
%h=(1e6)*linspace(0.000001,0.0009,100);
z=1;                        % valence of salt or surfactant, here SDS as surfactant
e=1.6e-19;                  % electron charge (c),Electron charge, (symbol e), fundamental
physical constant expressing the naturally occurring unit of electric charge, 1.6021765 × 10?19
coulomb
gr=0.2;                     % mass of salt or surfactant (gram) to prepare wt% solution in 200
ml water, This is the parameter I change to obtain different Molarity of Surfactants
MM=288.372;                 % Molar Mass of surfactant molecule (g/mol)
%M=0.000001;                % Molarity (mol/litre)
NA=6.022e23;                % Avogadro Number
%nINF=2.0882748346e-22;     % nINF=1000*NA (Avogadro Number)*M (Molar Concentration of
ELECTROLYTE)
KT=4.11e-21;
VO=0.2;                     % VOlume of prepared solution of surfactant (Litre)
VT=0.0257025;               % Thermal Voltage, equal to(kB*T/ze)  %KB=1.38e-23;     % Boltzman
constant (J/K)  %T=298; % Temp. (Kelvin)
eIL=710e-12;                % Water  Electrical permitivity
eILr=80;                    % Water relative Electrical permitivity
Lz=100e-9;                  % Domain Length  note that this L is for Z direction
h0=20e-9;
gama=0.1;                   % gama is a factor that represents crowding effect, for a 1 M(molar)
Ionic Liquid,nb=6*10^26/m^3, at 300K, k^-1(Debye Length)
%                            is 0.1 nm  and VT=25*10^-3 VOlts,in this case
%                            the values of gama can be varied as
%                            0.01,0.1,0.5,1 are safe to consider. Can plot
%                            the values of Dimensionless interfacial
%                            potential(si0) versus different crowding effects
%                            and also the plot of Potential Distributions
%                            near the interface (si)for various crowding
%                            effect parameter gama
                            % kappa and Debye, We stick to the definitions
                            % presented at Subir's book ...
                            % chapter 5, equation 5.19
                            %(e0^(-1/2))*
h=0.0009;
%b=0.001303021867096; % b for gr=0.2 gr SDS, which is 3.50 mM, SDS for
%h=99.99e-9
b=1.451597814994982e-13  %b for gr=0.2 gr SDS, which is 3.50 mM, SDS
%for h=900 micro-meter
%b=9.221286145792807e-04; % b for gr=0.4 gr SDS, which is 6.93 mM, SDS
a=(((2*b)-V)/h)
kappa=((eIL*VT)/(2*z*e*nINF))^(-1/2);
```

```
for j=1:100
x=(1e6)*linspace(-0.00045,0,100);
if x(j)<=0
j=j+1;
x1(j)=x(j)
si1G(j)=(a*x1(j))+b
```